The reorganization of human brain networks in the early stages of multiple sclerosis

Ismail Koubiyr

université de BORDEAUX

THÈSE PRÉSENTÉE

POUR OBTENIR LE GRADE DE

DOCTEUR DE

L'UNIVERSITÉ DE BORDEAUX

École doctorale des sciences de la vie et de la santé

Spécialité Neurosciences

Par **Ismail KOUBIYR**

THE REORGANIZATION OF HUMAN BRAIN NETWORKS IN THE EARLY STAGES OF MULTIPLE SCLEROSIS

Sous la direction de Monsieur le Professeur Bruno Brochet

Soutenue publiquement le 17 Septembre 2019

Membres du jury :

Madame la Professeure Iris-Katharina Penner, *Heinrich Heine University, Düsseldorf*.	**Rapporteur, Présidente**
Monsieur le Docteur Menno M. Schoonheim, *VU University Medical Center, Amsterdam*.	**Rapporteur**
Monsieur le Professeur Charles R.G. Guttmann, *Harvard University, Boston*.	**Examinateur**
Madame le Docteur Céline Louapre, *Université Paris-Sorbonne*.	**Examinatrice**
Madame le Docteur Gwenaëlle Catheline, *Université de Bordeaux*.	**Examinatrice**
Madame le Docteur Lucina Q. Uddin, *University of Miami, Miami*.	**Examinatrice invitée**

Titre : Réorganisation des réseaux cérébraux dans les stades précoces de la sclérose en plaques

Résumé : Les troubles cognitifs sont fréquents dans la sclérose en plaques (SEP) mais leurs mécanismes sous-jacents sont encore mal connus. Les techniques d'IRM ont été indispensables pour essayer de mieux comprendre les substrats biologiques des processus cognitifs. L'objectif de cette thèse est de mieux comprendre les mécanismes physiopathologiques du fonctionnement cognitif dans les stades précoces de la SEP. Pour cela, nous avons étudié une cohorte de patients atteints de syndrome cliniquement isolé (SCI) pendant un an, en réalisant une batterie de tests neuropsychologiques ainsi qu'un examen IRM. Nous avons tout d'abord démontré une atteinte précoce de la substance grise, en particulier au niveau de l'hippocampe, se propageant vers le cortex après un an d'évolution. L'atteinte microstructurale précoce de l'hippocampe était capable de prédire sa perte de volume. Ensuite, nous nous sommes intéressés à la réorganisation des réseaux cérébraux fonctionnels à ce stade précoce de la maladie. En utilisant l'IRM fonctionnelle de repos, nous avons démontré une réorganisation cérébrale fonctionnelle précoce impliquant plusieurs régions cérébrales. Cette réorganisation était encore plus prononcée après un an d'évolution. Au même moment, nos patients présentaient un fonctionnement cognitif normal qui était associé au niveau de réorganisation cérébrale présente. Ces résultats suggèrent un mécanisme de compensation aux stades précoces de la pathologie. La relation entre ces modifications fonctionnelles et l'anatomie sous-jacente est inconnue dans la SEP. Nous avons ainsi décidé de combiner l'IRM fonctionnelle de repos et l'imagerie par tenseurs de diffusion pour étudier à la fois la connectivité fonctionnelle et la connectivité structurelle. En utilisant le paramètre de couplage structurel-fonctionnel, nous avons démontré un découplage, un an après l'apparition de la maladie, au niveau de trois réseaux cérébraux du repos (salience, visuel et somato-moteur). Ce découplage était observé alors même que les performances cognitives de nos patients étaient préservées et que la réorganisation fonctionnelle était présente. Ces résultats suggèrent que cette réorganisation fonctionnelle à ce stade, agissant comme un mécanisme de compensation, se produit à travers des connections anatomiques indirectes. Afin de confirmer ces résultats et de suivre l'évolution des réseaux cérébraux et leur impact sur la cognition, nous avons recontacté nos patients SCI pour un suivi à 5 ans.

Mots clés : Sclérose en plaques, IRM, syndrome cliniquement isolé, connectivité, IRM fonctionnelle, imagerie par tenseur de diffusion.

Title: The reorganization of human brain networks in the early stages of multiple sclerosis

Abstract: Cognitive impairment is frequent in multiple sclerosis (MS) but its underlying mechanisms are still poorly understood. MRI techniques have been a valuable tool to investigate the biological substrates of cognitive processes. The objective of this thesis was to better understand the pathophysiological mechanisms of cognitive functioning at the early stage of MS. We followed clinically isolated syndrome (CIS) patients for one year, using neuropsychological tests, conventional and more advanced MRI techniques. We first demonstrated a differential gray matter vulnerability at the beginning of MS with a pathological spread from the hippocampus towards the cortex. We showed that the first microstructural alterations taking place within the hippocampus were able to predict its future volume loss. After that, we were interested in the potential brain functional reorganization at this stage of the disease. Using resting-state functional MRI, we were able to demonstrate very early regional brain functional reorganization starting from the disease onset and becoming more pronounced after one year of evolution. We also noticed a preservation of cognitive performances in CIS patients, which we found was associated to more functional reorganization. These results suggested then a compensation mechanism at the first year after a CIS. However, the relationship between these functional changes and the underlying anatomy was still missing. Thus, we combined resting-state functional MRI and diffusion tensor imaging to represent both functional and structural connectivity. Using the structural-functional coupling parameter, representing the association between structural and functional connections, we showed a decoupling one year after the disease onset in three major networks (salience, visual and somatomotor networks). This decoupling was noticed while cognitive performances were preserved and functional reorganization present. These last results led us to suggest that the functional reorganization at this stage, acting as a compensation mechanism, occurs along indirect anatomical pathways. In order to confirm these results and further follow-up brain networks topology and its impact on cognition, we are currently calling back our CIS patients for their 5-year visit.

Keywords: Multiple sclerosis, MRI, clinically isolated syndrome, connectivity, functional MRI, diffusion tensor imaging.

Unité de recherche

INSERM, Neurocentre Magendie, U1215, Equipe Relations glie-neurone, Bordeaux, France

Acknowledgements

Au Professeur Bruno Brochet,

Je vous remercie de m'avoir fait l'honneur de diriger ce travail. Je tiens à vous remercier pour votre disponibilité, votre soutien et votre confiance au cours de ces trois années. Merci à vous pour votre patience à toutes épreuves lors de la relecture (mais aussi la soumission) de mes papiers. Merci pour toutes les connaissances que vous m'avez apportées et pour votre encadrement qui ont permis d'aboutir à ce résultat. J'aimerais vous témoigner ici de ma gratitude, mon profond respect et mon admiration pour votre carrière et votre implication dans la recherche.

To Professor Iris-Katharina Penner and to Doctor Menno Schoonheim,

Thank you very much for accepting to judge this work. Thank you for taking the time to make the journey to Bordeaux. It is a great honor to present my results in front of international experts in the field of multiple sclerosis. Your professional careers are a model to me.

Au Professeur Charles Guttmann,

Je tiens d'abord à te remercier d'avoir accepté d'être présent au sein de mon jury de thèse. Merci de m'avoir transmis ta passion pour la recherche et plus particulièrement pour la sclérose en plaques. Merci de m'avoir accueilli au sein de ton équipe. J'ai énormément appris lors de ce stage. Merci de m'avoir judicieusement dirigé vers Bordeaux afin de réaliser cette thèse. Enfin je tiens à te remercier pour tous tes conseils et ton soutien lors de ces dernières années.

Au Docteur Gwenaëlle Catheline et au Docteur Céline Louapre,

Vous me faites l'honneur de juger mon travail au regard de vos expertises respectives. Je vous remercie de votre présence aujourd'hui.

To Doctor Lucina Uddin,

Thank you very much for making the journey to join us in Bordeaux and for accepting to judge this thesis work. It is a great honor to present my work in front of an international expert of brain imaging. I have the utmost admiration for your work and your career.

Au Docteur Aurélie Ruet,

Je te remercie pour ton aide, ton soutien infaillible et ta participation à ce travail de thèse. J'ai une profonde admiration pour tes connaissances et ton éthique de travail. Merci aussi de m'avoir fait confiance pour continuer à travailler sur tes cohortes, je suis heureux de pouvoir poursuivre mon travail à tes côtés pendant encore deux années.

Au Professeur Thomas Tourdias,

Je te remercie pour ton aide constante lors de ces trois dernières années, ta bienveillance, la qualité de tes conseils et pour ta disponibilité indéfectible à relire mes papiers et à m'orienter lors de mes travaux. J'ai une admiration pour ton enthousiasme pour la recherche, ta passion pour l'imagerie et ton parcours professionnel.

Au Professeur Vincent Dousset,

Merci pour nos discussions, pour votre soutien, et pour votre accueil au sein de la plateforme de bio-imagerie. Soyez assuré de mon respect et ma gratitude.

Au Docteur Mathilde Deloire,

Merci infiniment pour ton soutien et ton aide dès mon arrivée dans l'équipe. J'aimerais te remercier pour ta disponibilité, ton implication à toute épreuve et tes idées qui m'ont guidées lors de ces travaux de thèse. Enfin, merci pour ta gentillesse et ton humour tout au long de ces années.

Au Docteur Cécile Dulau,

Merci pour ta gentillesse, ta disponibilité, ton soutien et ta bonne humeur. J'ai hâte qu'on puisse avancer ensemble sur SO-COG.

Au Docteur Delphine Lamargue-Hamel,

Merci pour ton soutien, ta disponibilité et ton aide au cours de ces trois années. Nos discussions et tes conseils m'ont beaucoup aidé lors de mon parcours. Enfin, merci d'avoir fait le tour de Carreire avec moi pour trouver une salle de thèse.

Au Docteur Amandine Moroso et au Docteur Vincent Planche,

Merci pour votre soutien, votre gentillesse et votre disponibilité. J'ai énormément appris à partir de vos travaux de thèse respectifs. J'espère qu'on aura l'occasion de collaborer à nouveau.

Au Docteur Pierrick Coupé,

Merci pour ta gentillesse et ta disponibilité pour m'aider et me guider lors de mes travaux de thèse. J'ai une grande admiration pour ta maitrise de l'imagerie cérébrale et ton parcours professionnel.

Au Docteur Aude Panatier et au Docteur Stéphane Oliet,

Merci infiniment de m'avoir accueilli et intégré à votre équipe. Merci pour votre disponibilité, votre gentillesse, votre soutien et votre regard critique sur mon travail. J'ai une fascination pour les travaux que vous menez chez l'animal et j'apprends énormément à chaque réunion de labo.

Merci aussi à tous les membres de l'équipe pour leur sympathie et pour les moments passés autour de bons repas.

A l'équipe du CRMBM de Marseille,

Au **Professeur Jean Pelletier**, au **Professeur Jean-Philippe Ranjeva**, au **Professeur Bertrand Audoin**, au **Docteur Pierre Besson** pour nous avoir accueilli au sein de leur équipe et nous avoir transmis toutes leurs connaissances de l'IRM fonctionnelle. Merci plus particulièrement à **Pierre** pour ton aide précieuse et pour ta participation à ces travaux, en espérant que cette collaboration puisse continuer.

A toute l'équipe du service de Neurologie du CHU de Bordeaux,

A **Katy**, **Dieynaba**, **Timothé**, **Julie**, **Aurore**, **Emeline**, **Nath**, pour m'avoir si bien accueilli dans l'équipe. Merci pour votre gentillesse, votre bonne humeur et tous ces bons moments qui ont fait que ces trois années ont filé à toute vitesse.

A **ma sœur**, **mes amis**, et en particulier **Moncef**, pour les moments passés ensembles et leur soutien tout au long de ces années.

A mes parents,

Pour leur amour, leur générosité, leur soutien inconditionnel, leur éducation et les valeurs qu'ils m'ont inculquées. Je vous dois ce que je suis aujourd'hui et je continuerai à faire de mon mieux pour vous rendre fier. Il n'y a pas assez de mots pour vous exprimer ma gratitude, ma reconnaissance et mon amour.

A ma femme Zineb,

Pour ton amour, ta tendresse, ton soutien et ta patience durant ces dernières années de thèse pas toujours faciles. Tu étais la bouffée d'oxygène qui me ressourçait dans les moments les plus difficiles. Sans toi, cette thèse ne serait pas. Je n'ai pas de mot pour pouvoir te dire ce que tu représentes, ce que tu m'as apporté, et le bonheur d'être à tes côtés.

Enfin, j'aimerais dédier ce travail à la mémoire de **ma grand-mère**. Une femme unique. Pour son amour inconditionnel, sa générosité sans limite, sa bonté et ses encouragements. J'ai eu la chance de grandir à tes côtés. Tu es toujours dans mon cœur et aurais été très fière de me voir arriver jusque-là.

Table of contents

Presentation of the candidate

Ismail Koubiyr
54 Rue El-Alamein, 33000 Bordeaux
ismail.koubiyr@gmail.com
+33(0)7.61.51.36.01

Education

INSERM U1215, Neurocentre Magendie – Bordeaux, France — October 2016 – September 2019
PhD Candidate in Neuroscience - Neuroimaging
The reorganization of human brain networks in the early stages of multiple sclerosis
Supervisor: Pr.Bruno Brochet

Institut National des Sciences Appliquées (INSA) & Université Claude Bernard Lyon I – Lyon, France — *Graduation: September 2016*
Master of Research: Electronics, Power Electronics, Automatism and processes (EEAP)
- Specialized in Digital signal and image processing.

Institut National des Sciences Appliquées (INSA) - Lyon, France — *Graduation: September 2016*
Electrical Engineer
- Specialized in Digital signal and image processing.
- Accomplished the preparatory cycle under the SCAN program (English learning).
- Completed team-management training.

Korean Advanced Institute of Science and Technology (KAIST) - Daejeon, South Korea — *September 2014- June 2015*
- One-year exchange program.
- Specialized in Digital Image processing (Image processing, Image analysis).

Experience

Research Trainee at Center for Neurological Imaging, Brigham and Women's Hospital, Harvard Medical School – Boston, USA
- Transversal characterization of abnormally diffused white matter in multiple sclerosis. — March 2016 - September 2016
- Development of new tools to analyze structural MRI (T1,T2,PD,Diffusion).

Tutor at INSA – Lyon, France — *September 2011 – June 2014*
- Offered Mathematics and Physics support to both freshmen at my school and to middle/high school students. Improving thus, their grades and overall performance by implementing effective and adequate programs.

Teaching Experience

Teaching assistant at the Université de Bordeaux.

Academic year 2018/2019
- Image processing and analysis (L3) — 14h
- Introduction to medical imaging (L1) — 6h

Academic year 2017/2018
- Pathology and MRI: exploring cognitive dysfunction in multiple sclerosis (M2) — 4h
- Image processing and analysis (L3) — 12h
- Introduction to medical imaging (L1) — 6h

Publications

1. **Koubiyr I**, Besson P, Deloire M, Charré-Morin J, Saubusse A, Tourdias T, Brochet B and Ruet A (2019) *Dynamic modular-level alterations of structural-functional coupling in clinically isolated syndrome*. Brain. doi: 10.1093/brain/awz270

2. **Koubiyr I**, Deloire M, Besson P, Coupé P, Dulau C, Pelletier J, Tourdias T, Brochet B, Ranjeva JP and Ruet A (2018) *Longitudinal Study of Functional Brain Network Reorganization in Clinically Isolated Syndrome*. Mult Scler. 1–13. doi: 10.1177/1352458518813108
3. **Koubiyr I**, Deloire M, Coupé P, Dulau C, Besson P, Moroso A, Planche V, Tourdias T, Brochet B and Ruet A (2018) *Differential Gray Matter Vulnerability in the 1 Year Following a Clinically Isolated Syndrome*. Front. Neurol. 9:824. doi: 10.3389/fneur.2018.00824
4. Planche V, **Koubiyr I**, Romero J.E, Manjon J.V, Coupé P, Deloire M, Dousset V, Brochet B, Ruet A and Tourdias T (2018) *Regional hippocampal vulnerability in early multiple sclerosis: dynamic pathological spreading from dentate gyrus to CA1*. Human Brain Mapping. doi: 10.1002/hbm.23970

Talks and posters

1. **Koubiyr I**, Deloire M, Charre-Morin J, Saubusse A, Coupé P, Dulau C, Tourdias T, Besson P, Ranjeva JP, Pelletier J, Audoin B, Brochet B, Ruet A. *Longitudinal study of functional brain networks in clinically isolated syndrome*. European Charcot Foundation (ECF), Baveno, Italy, November 15th-17th 2018
2. **Koubiyr I**, Palotai M, Deloire M, Charre-Morin J, Saubusse A, Tourdias T, Guttmann CRG, Brochet B, Ruet A. *Microstructural damage in cortico-subcortical white matter tracts in patients with clinically isolated syndrome: prediction of cognitive functioning and follow-up of its change for 1 year*. European Committee for Treatment and Research in Multiple Sclerosis (ECTRIMS), Berlin, Germany, October 10th-12th 2018
3. **Koubiyr I**, Deloire M, Ruet A, Charre-Morin J, Saubusse A, Brochet B, Dulau C. *Changes in select resting-state brain functional networks and preservation of social cognitive performances in multiple sclerosis*. European Committee for Treatment and Research in Multiple Sclerosis (ECTRIMS), Berlin, Germany, October 10th-12th 2018
4. Palotai M, **Koubiyr I**, Morales Pinzon A, Makris N, Healy B.C, Glanz B, Weiner H.L, Chitnis T, Guttmann CRG. *Microstructural damage to associative cortico-thalamic tracts play a role in the pathophysiology of fatigue in multiple sclerosis*. European Committee for Treatment and Research in Multiple Sclerosis (ECTRIMS), Berlin, Germany, October 10th-12th 2018
5. **Koubiyr I**, Deloire M, Besson P, Coupé P, Dulau C, Tourdias T, Pelletier J, Audoin B, Brochet B, Ranjeva JP, Ruet A. *Reorganization of functional brain network topology in clinically isolated syndrome: A 1-year longitudinal study*. Organization for Human Brain Mapping (OHBM), Singapore, 17th-21st 2018
6. **Koubiyr I**, Deloire M, Besson P, Coupé P, Dulau C, Tourdias T, Pelletier J, Audoin B, Brochet B, Ranjeva JP, Ruet A. *Reorganization of functional brain network topology in clinically isolated syndrome: A 1-year longitudinal study*. ARSEP Multiple Sclerosis meeting, June 1st 2018
7. **Koubiyr I**, Deloire M, Charre-Morin J, Saubusse A, Coupé P, Dulau C, Tourdias T, Besson P, Ranjeva JP, Pelletier J, Audoin B, Brochet B, Ruet A. *Relationships between reorganization of functional brain network topology and cognition in Clinically Isolated Syndrome: A 1 year Resting state fMRI longitudinal study*. European Committee for Treatment and Research in Multiple Sclerosis (ECTRIMS), October 25th-28th 2017
8. **Koubiyr I**, Deloire M, Charre-Morin J, Saubusse A, Coupé P, Dulau C, Tourdias T, Besson P, Ranjeva JP, Pelletier J, Audoin B, Brochet B, Ruet A. *Microstructural alterations precede deep grey matter volume loss in patients with clinically isolated syndrome*. European Committee for Treatment and Research in Multiple Sclerosis (ECTRIMS), October 25th-28th 2017

Grants and awards

- 2-year post-doctoral grant from LabEx TRAIL, Bordeaux, France (100 000€)
- Best poster presentation award from the European Charcot Foundation (ECF), Baveno, Italy, 2018 (4000€)
- European Charcot Foundation (ECF) Travel grant, Baveno, Italy, 2018
- European Committee for Treatment and Research in Multiple Sclerosis (ECTRIMS) Travel grant, Berlin, Germany, 2018
- European Committee for Treatment and Research in Multiple Sclerosis (ECTRIMS) Travel grant, Paris, France, 2017
- ARSEP (French association for research on multiple sclerosis) Travel grant for internship (5000€)

Glossary

BDI = Beck Depression Inventory
BOLD = Blood Oxygen Level-Dependent
CIS = Clinically Isolated Syndrome
CSF = Cerebrospinal Fluid
Cth = Cortical thickness
DGM = Deep gray matter
DIR = Double Inversion Recovery
DTI = Diffusion Tensor Imaging
EDSS = Expanded Disability Status Scale
FA = Fractional Anisotropy
FC = Functional Connectivity
FDR = False Discovery Rate
FLAIR = Fluid-Attenuated Inversion Recovery
HC = Healthy Controls
HLA = Human Leukocyte Antigen
IPS = Information Processing Speed
MD = Mean Diffusivity
MRI = Magnetic Resonance Imaging
MS = Multiple Sclerosis
MSFC = Multiple Sclerosis Functional Composite
NABT = Normal Appearing Brain Tissue
PPMS = Primary Progressive Multiple Sclerosis
PwCIS = Patients with Clinically Isolated Syndrome
RRMS = Relapsing-Remitting Multiple Sclerosis
SC = Structural Connectivity
SPMS = Secondary Progressive Multiple Sclerosis
TIV = Total Intracranial Volume

Chapter 1

General introduction

MS pathology

Multiple sclerosis (MS) is an inflammatory, demyelinating and neurodegenerative disease of the central nervous system.[1] It is one of the most common neurological disorders among young adults and women are more prone to develop the disease (2.3/1 female-to-male ratio).[2] This chronic disease affects more than 2.3 million people worldwide with approximately 100000 patients in France.[3] Although its exact etiology is currently unknown, the disease is thought to be multifactorial as some genetic and environmental risk factors have been identified, such as Epstein-Barr viral infection, HLA genotype, vitamin D levels (sun exposure), salty diet and smoking.[1]

It is usually accepted that in MS, an autoimmune reaction is initiated in the periphery, where macrophages and leukocytes (e.g. T-cells, B-cells) migrate to the brain due to the leakage of the blood brain barrier. As these lymphocytes and macrophages accumulate, pro-inflammatory cytokines increase the immune response by recruiting microglia. Then, a part of infiltrating T-lymphocytes recognizes myelin, leading to acute demyelination, notoriously known as lesions.[1] These lesions can be partly remyelinated by oligodendrocytes in the early stage of the disease, resulting in the preservation of axons and neurons to a certain degree.[4] Axonal damage becomes more pronounced as the disease progresses, which is thought to be mediated by mitochondrial dysfunction with the production of reactive oxygen species.[5] At this stage, both white and grey matter (cortex and deep grey matter structures) atrophy is observed.[6]

Clinical phenotypes

Multiple sclerosis in characterized by an unpredictable clinical course, as some patients progress rapidly, while others remain relatively stable over the course of the disease. The early phase of MS usually presents acute symptom worsening (also called attacks or exacerbations), followed by partial or complete recovery (relapsing-remitting MS, RRMS) due to demyelination and remyelination processes. With time, recovery from each episode is incomplete and persistent symptoms accumulate. In some patients, symptoms will progressively worsen without relapses or partial recovery, this phase is called secondary progressive MS (SPMS). In some other cases, patients may not present relapse-onset MS, as they show steady worsening of neurologic functioning without any distinct relapses or periods of remission (primary-progressive MS, PPMS) (**Figure 1**).[1]

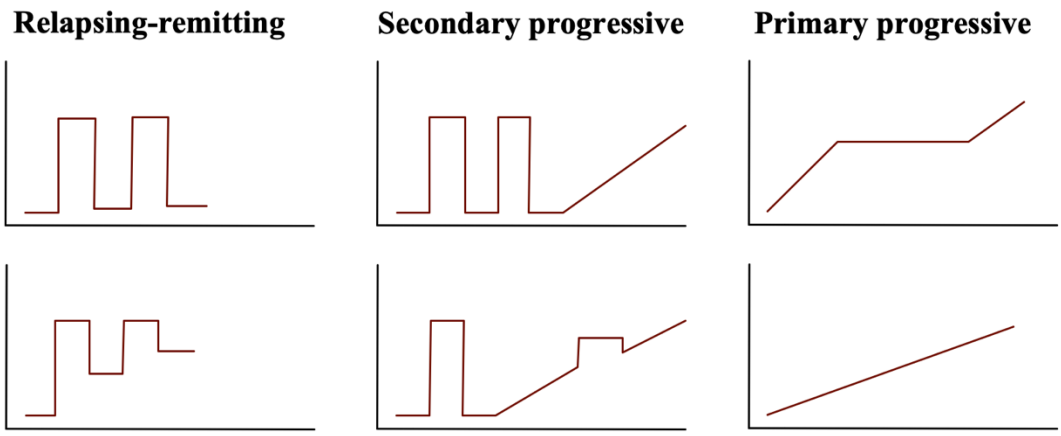

Figure 1. Multiple sclerosis phenotypes

Depending on the location of lesions, RRMS patients may present symptoms including acute unilateral optic neuritis, partial myelitis or a brainstem syndrome,[7] while progressive-onset patients' symptoms tend to progress slowly over the course of months or even years, and include symptoms such as paraparesis, hemiparesis or cerebellar ataxia.[7] Other MS physical symptoms include tingling, body weakness, numbness, imbalance, spasms, gait impairment and vision loss.[1] According to the consensual McDonald criteria based on clinical and/or MRI criteria, MS is diagnosed by the dissemination in time and space of the demyelinating lesions.[8] More recently, the presence of CSF-specific oligoclonal bands may now substitute for dissemination in time even if baseline MRI findings do not meet dissemination in time criteria, and the presence of cortical lesions may now fulfill MRI criteria for dissemination in space (in addition to juxtacortical lesions).[9]

Clinically isolated syndrome

Clinically isolated syndrome (CIS) describes the first monophasic episode of acute or sub-acute onset suggestive of MS.[10] Patients presenting at first with a CIS, may be diagnosed with MS if fulfilling the dissemination in time criteria. Additionally, the long-term risk for clinically definite MS is 60–80% in CIS patients with demyelinating lesions on their first MRI scan.[10] This very early stage of MS is then the perfect window to study the first brain alterations present in MS to obtain a better understanding of the evolving pathogenesis of CIS. This explains our choice to study the evolution of such population in the remainder of the manuscript.

Treatment

During MS relapses, it is usual to treat the patient with high-dose methylprednisolone to immediately relieve the symptoms. However, these corticosteroid treatments have no significant impact on long-term disability and do not prevent future relapses. To this end, patients with RRMS are usually treated with disease modifying treatments with either immunomodulatory or immunosuppressive characteristics to prevent the occurrence of new inflammatory episodes and slow down disease progression. Distinction can be made between first-line therapy and second-line therapy. First-line therapy aims to reduce the inflammatory response by adjusting the immune response (e.g. interferon beta, glatiramer acetate, dimethyl fumarate, teriflunomide). Second-line therapies are more effective, but usually have more potential severe side effects as they interfere more importantly with the immune system (e.g. natalizumab, fingolimod).[11] These current available treatments for MS all target the inflammatory component of the disease. However, new potential therapies aiming at repairing the damaged axons using a remyelination approach are currently undergoing clinical trials.[12]

Cognitive impairment in MS

For many years, cognitive impairment in MS used to be neglected as research and clinical attention mainly focused on the physical problems. However, it is admitted now that it is frequent in MS and appears even early during the course of the disease, from the CIS stage.[13,14] This stage is particularly interesting because it is the critical time when cognitive deficits occur and become detectable. In the years after the CIS, the frequency of these deficits increases notably (from 29% to 54% after 5 years),[15] meaning that there is a strong opportunity to understand the substrate of these deficits and to set up therapeutic strategies. Increasing evidences have shown the pejorative impact of early cognitive impairment in MS affecting quality of life and daily living with vocational impact.[16,17] Cognitive impairment associated with MS concerned several cognitive domains including episodic memory, attention, working memory and executive functions.[13] However, slowness of information processing speed (IPS) is the main cognitive dysfunction observed in MS even at the earlier stages and is associated with poor prognosis, significant consequences on employment status and decreased quality of life.[17] Besides IPS, it is also accepted that episodic memory is frequently and early impaired. Recently an international group of MS

experts has suggested both IPS and episodic memory as the minimal cognitive assessment in patients with MS (Brief International Cognitive Assessment for MS, BICAMS).[18] In addition to BICAMS, several other well-established neuropsychological test batteries are available to assess the performance on different cognitive domains in MS (e.g. the Brief Repeatable Battery of Neuropsychological tests (BRB-N),[19] the Minimal Assessment of cognitive Function in MS (MACFIMS)[20]).

Visualizing brain abnormalities in MS

The advent of magnetic resonance imaging (MRI) has provided a further powerful tool for the in-vivo investigation of diseases of the central nervous system. In MS, MRI has become an invaluable tool for diagnosing the disease as the diagnosis heavily relies on proof of disease dissemination in space and time.[21] As such, MRI can support and substitute clinical information for MS diagnosis, enabling an early and accurate diagnosis and thus, early treatment.

During the last two decades, MRI has been extensively used in the study of MS using a variety of MRI techniques. These MRI techniques used in MS research can vary from conventional MRI sequences visualizing brain lesions or atrophy, usually used in the clinical setting, to advanced sequences quantifying the microstructural integrity of brain tissue and network characteristics. In the following, we will first introduce several of these MRI sequences. Then, we will discuss how these techniques can provide insight into the neural correlates of cognitive impairment.

White/gray matter lesions

White matter lesions represent a typical characteristic of MS and can be visualized using conventional MRI sequences such as T2-weighted or fluid attenuated inverse recovery techniques (FLAIR) (**Box 1**). Both lesion load and lesion counts have been intensively investigated in MS. However, studies showed poor correlation between these parameters and the actual clinical disability of patients. This is called the clinico-radiological paradox of MS.[22] Indeed, some patients showing a large number of white matter lesions can be mildly affected, while others with fewer white matter lesions show a more severe disability. This led MS researchers to investigate gray matter lesions as they may be more prone to play a role in cognitive functioning. In order to do that, the double inversion recovery (DIR) sequence was used as it was shown to improve the detection of intracortical lesions which was verified in post-mortem tissues as well.[23,24] Even

though the DIR sequence still lacks some sensibility in detecting all cortical lesions, active research towards a consensus DIR sequence is currently ongoing.[25] These gray matter lesions were stronger associated to cognitive deficits than white matter lesions, even though correlations were still moderate.[26,27]

Box 1. Conventional MRI sequences

Below, we will describe standard MRI sequences that have been mostly used in the diagnosis of MS and the patient's follow-up.

T1- and T2-weighted imaging

With a T1-weighted sequence, we can easily visualize the anatomy of the brain with a good contrast between white and gray matter. A subset of MS lesions can be seen as focal hypointensities (black holes) (**Figure 2**), indicating axonal and myelin loss. Additionally, this sequence allows the inspection of acute inflammatory processes using a contrast agent (e.g. gadolinium), that can go through the blood brain barrier if disrupted. This results in hyperintense lesions in these images. On the other hand, using a T2-weighted sequence allows to detect MS lesions as focal hyperintensities (**Figure 2**). With that, we can calculate the count and volume of these lesions, which represents an important parameter to monitor the evolution of the disease. Both these sequences are usually included in routine clinical practice. They are also used in research, as T2-weighted images provides the patient's lesion load, while T1-weighted images are mostly used to segment the brain (e.g. white matter, gray matter) and calculate the corresponding volumes.

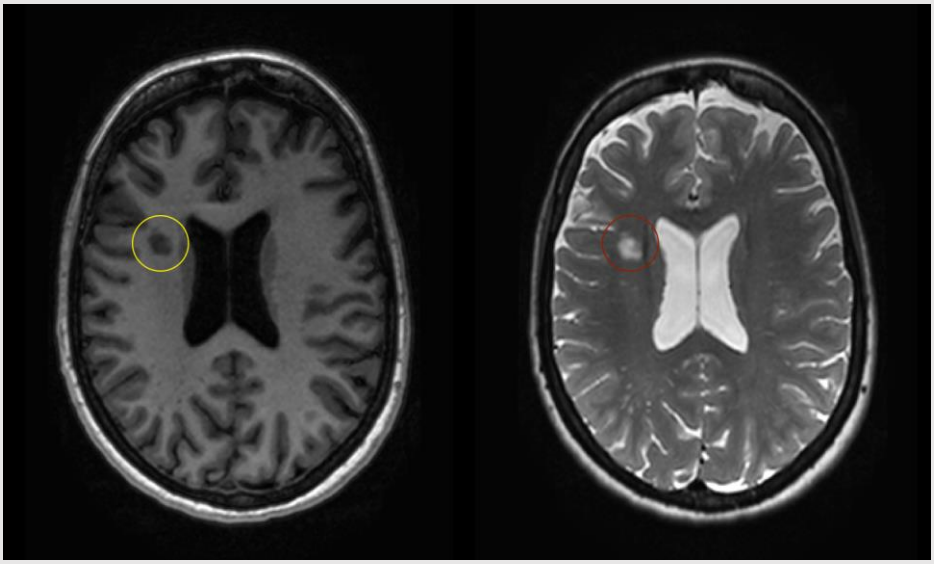

Figure 2. T1- and T2-weighted image of a patient with MS

A T1-weighted image (left) in which black hole is indicated by a yellow circle, and a T2-weighted image (right) in which white matter lesion is indicated by a red circle.

Fluid attenuated inverse recovery sequence

Using a fluid attenuated inverse recovery sequence (FLAIR), we can highlight MS lesions as focal hyperintensities, while suppressing the cerebrospinal fluid's (CSF) signal (**Figure 3**). In this case, lesions are better distinguished from CSF, such as in periventricular lesions for example. FLAIR images are therefore superior to T2-weighted images for detecting MS lesions, and are often used in research settings.

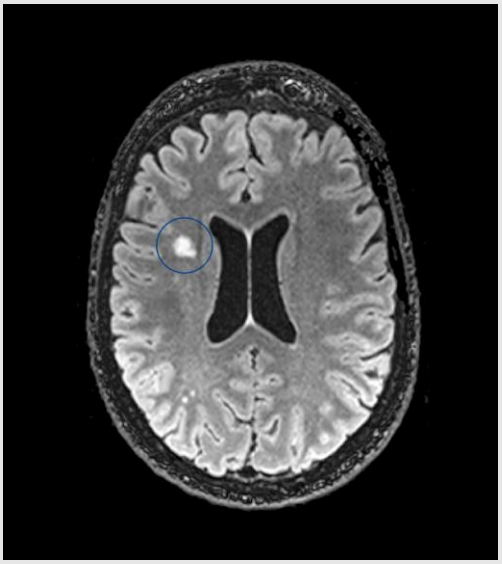

Figure 3. FLAIR image of a patient with MS

A FLAIR image in which white matter lesion is indicated by a blue circle.

Brain atrophy

Brain atrophy in MS was first observed in the first half of the 19th century by Cruveilhier and Carswell when they described the presence of lesions accompanied by atrophy. Later on, with the advent of in-vivo brain imaging, ventricles enlargement was observed in the late 1970s using computerized tomography (CT), indicating central atrophy.[28] Then MRI replaced CT for volumetric measurements as it allows to better distinguish brain tissue types with greater resolution. MS patients usually present a higher yearly whole-brain atrophy (with 0.7% loss per year) compared to healthy controls (0.1% to 0.3% loss per year).[29] This observed whole-brain atrophy is a combination of both white and gray matter volume loss, and it believed to reflect both inflammation-induced axonal loss followed by Wallerian degeneration and post-inflammatory neurodegeneration.[30] As the disease progresses, gray matter volume loss is thought to increase with a higher rate and relates strongly to physical and cognitive deficits.[26,31]

Advanced MRI techniques

It currently well known that macroscopic features such as white/gray matter lesions and atrophy do not provide sufficient information about the extent of tissue, and thus, lack specificity about the more destructive aspects of MS pathology, including diffuse damage in the so-called normal appearing brain tissue (NABT). These more subtle brain alterations can be observed using diffusion tensor imaging (DTI) (**Box 2**). This technique reveals the integrity of white matter tracts which are responsible for inter-region communication, and therefore better relates to cognitive problems.[32]

As the previous sequences allowed us to capture structural brain abnormalities in MS, they did not, however, inform us about brain function alterations in the disease. Functional MRI (fMRI) is therefore a powerful tool to explore activation of brain regions either during a specific task or at rest (**Box 3**), by mapping the change in the level of blood oxygenation.[33] When performing a cognitive task, MS patients showed different levels of activation compared to healthy controls. Indeed, cognitively impaired patients displayed a pattern of decreased brain activation in some regions compared to healthy controls, while cognitively preserved patients showed increased brain activations compared to healthy controls.[34,35] Available fMRI data suggest that cognitive impairment in MS might be a function not only of tissue loss, but also of the progressive failure of

the adaptive capacity of the brain with increasing tissue damage.[36] However, whether these functional changes are beneficial or indicate a maladaptive response to injury is still a matter of debate.[37–39]

Other techniques

Other approaches to assess brain integrity during the course of MS have been used. We propose to briefly introduce some of them, as they have not been used in this thesis.

A more direct approach to investigate myelination is magnetization transfer (MT) imaging. This technique is based on the MT phenomenon in which two or more environments (pools) with distinctly different magnetic resonance properties exchange magnetization. Let us consider two pools of protons with distinctly different MR properties; the liquid protons (i.e. protons associated with water, both intracellular and extracellular), and the macromolecular protons (protons associated with myelin, cell membranes and proteins). To detect the macromolecular protons, an off-resonance radio-frequency pulse (i.e. MT pulse) is used. This pulse preferentially excites the macromolecular protons and is added immediately prior to a conventional MRI sequence (usually a T1-weighted sequence). Adding this pulse induces the transfer of magnetization from the macromolecular protons to nearby liquid protons, resulting in an MRI with intensities that have been modulated by the presence of myelin. Thus, MT imaging is affected by myelin content in MS white matter and has been validated with post-mortem histopathology.[40]

Additionally, positron emission tomography (PET) is an in-vivo imaging technique, allowing to quantitatively investigate the cellular and molecular processes of the disease. PET provides an image of the tissue of interest after the administration of a positron-emitting molecule, ideally binding a selective target.[41] Due to the complexity of MS, different possible radioligands are provided, which can be used in PET imaging with high selectivity. As such, PET imaging is capable of assessing inflammation, demyelination, neuronal damage and astrocyte activation in MS.[42] However, its high cost, its relatively low resolution and the lack of available standardized procedures currently limit its use.

Electroencephalography (EEG) and Magnetoencephalography (MEG) are direct and non-invasive measures of brain function. EEG measures the small electrical currents resulting from postsynaptic potentials, while MEG measures the magnetic fields induced by these currents. They are an important tool to complement other imaging methods such as fMRI, as they have a high temporal

resolution in the range of milliseconds. However, these two techniques have very low spatial resolution and a lack of sensitivity to processes in deep brain areas. Using EEG and MEG acquisitions in MS, studies have shown changes in network topology and slowing of neuronal activity, affecting cognitive performances.[43–46]

Box 2. Diffusion tensor imaging

Diffusion tensor imaging (DTI) is a sequence used to determine the displacements of water molecules (protons) in the brain. This sequence allows to quantify the integrity of both white and gray matter by calculating the water's motion in several directions. When the water's motion is random (i.e. Brownian motion) as in the CSF, the diffusion is called isotropic. However, when water motion is constrained in one direction by neurites, membranes or cell infiltrates, the diffusion is called anisotropic. Thus, water diffusion properties are modified when the microstructural integrity of the tissue is altered. We can express the diffusivity of water molecules using different parameters, such as:
Fractional anisotropy (FA): a summary measure that quantifies the amount of anisotropy (i.e. directionality) in a voxel.
Mean diffusivity (MD): average of diffusion.
Axial diffusivity (AD): diffusivity along the axon.
Radial diffusivity (RD): diffusivity perpendicular to the axon.

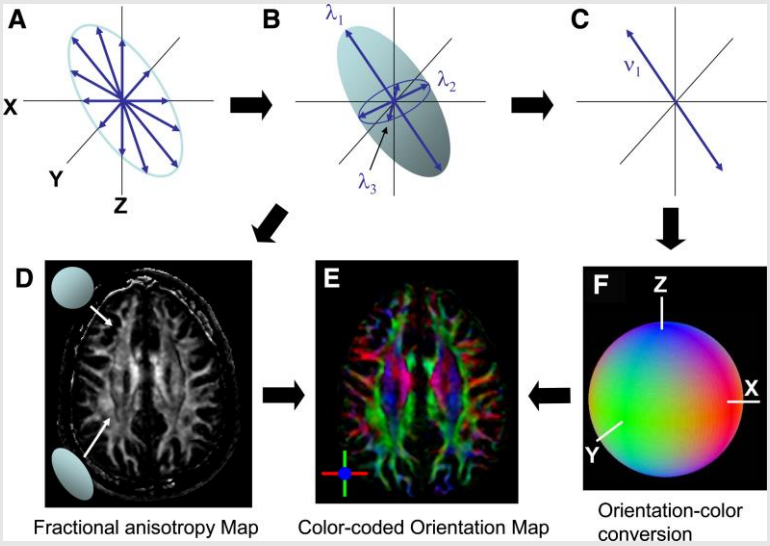

Figure 4. The Principle of DTI and Contrast Generation

From diffusion measurements along multiple axes (A), the shape and the orientation of a "diffusion ellipsoid" is estimated (B). An anisotropy map (D) can be created from the shape, in which dark regions are isotropic (spherical) and bright regions are anisotropic (elongated). From the estimated ellipsoid (B), the orientation of the longest axis can be found (C), which is assumed to represent the local fiber orientation. This orientation information is converted to a color (F) at each pixel. By combining the intensity of the anisotropy map (D) and color (F), a color-coded orientation map is created (E). (Adapted from Mori et al., Neuron, 2006)

Mori S and Zhang J, Principles of diffusion tensor imaging and its applications to basic neuroscience research. Neuron. 2006

Box 3. Functional magnetic resonance imaging

Functional magnetic resonance imaging (fMRI) is a sequence used to measure brain activation during a task or at rest. When a neurons population increase its activity, this region requires an increase in blood flow to deliver enough oxygen. Oxygen is bound in the blood to hemoglobin. Hemoglobin can be found in two forms: hemoglobin with bound oxygen molecules (i.e. oxygenated hemoglobin, with diamagnetic properties), and hemoglobin without bound oxygen molecules (i.e. deoxygenated hemoglobin, with paramagnetic properties). The oxygen brought-in to the specific brain region by the increased blood flow is usually more that the consumed oxygen. This causes a decrease in deoxygenated hemoglobin which can be picked up by the MRI scanner. These changes can be assessed during:
Performance of a cognitive task (i.e. task fMRI), which depicts brain regions activated upon task demands.
Resting-state (resting-state fMRI), which depicts spontaneous brain activity

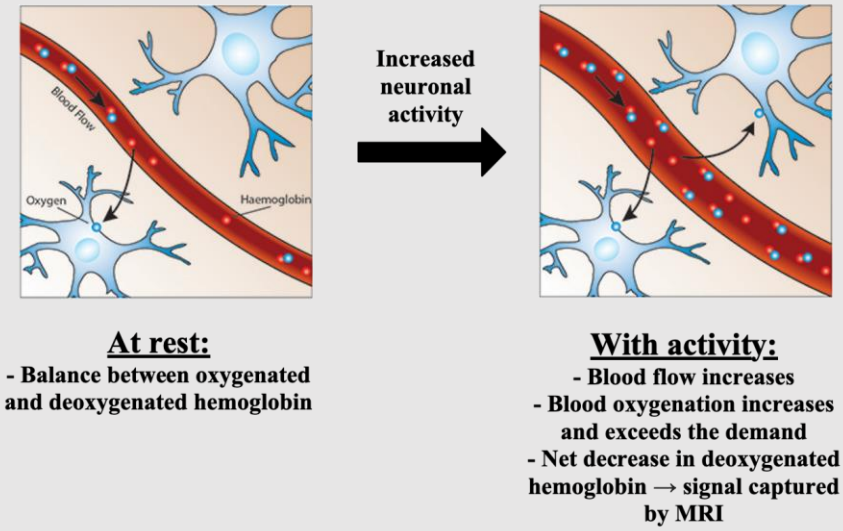

Figure 5. Functional MRI mechanism

Connectomics: Mapping the human brain

For centuries, tracing the human brain's connections has been an important scientific goal for neuroanatomists.[47] Thanks to the advent of MRI, it is now possible to non-invasively capture the intrinsic characteristics of our brain and model connections between different brain regions. This effort to try to map the multiple connections in our brain is referred to as "connectomics". For example, based on DTI data, we can capture the brain's structural organization (i.e. white matter tratcs) using tractography to reveal the trajectories of white matter pathways in vivo.[48] Then, in order to infer the underlying functional connectome of the human brain, we can use resting-state fMRI which identifies synchronization of activity between pairs of gray matter regions.[49] Based on this functional connectome, patterns of simultaneous brain activity have been extracted using independent component analysis, leading to the identification of the so-called "resting-state networks".[50] Alterations to these networks have been shown to be involved in disability and cognitive impairment in patients with MS,[51] especially the default mode network known to intervene across a wide range of cognitive manipulations.[52,53] Both structural and functional networks can be investigated using a mathematical modelling called "graph theory". This model suggests that the brain is represented as a graph with nodes representing brain regions and edges representing connections between them (**Figure 6**).[54]

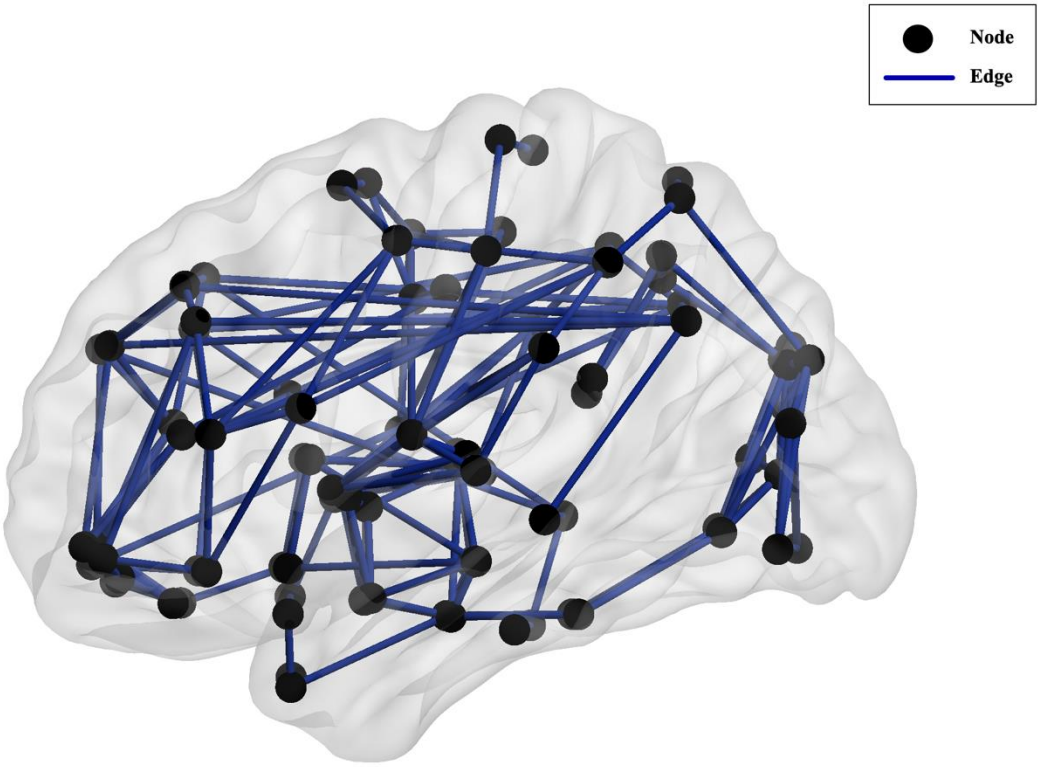

Figure 6. Graph theoretical representation of the brain

For functional networks, connections can be defined as the correlation coefficient between brain regions' activity. Whereas in structural networks, these connections can represent the number of tracts connecting two gray matter regions. A variety of neurobiologically meaningful network measures can be computed to assess its characteristics, such as its efficiency, its centrality and its levels of segregation and integration.[55] We briefly introduce some of the parameters used in this thesis in **Box 4**. Abnormalities in both functional and structural networks have been previously reported in MS patients, showing different topological characteristics compared to HC.[56] Current data on network changes in MS in relation to cognition have led to the introduction of the "network collapse" hypothesis.[57] This hypothesis suggests that as the structural damage progresses, the functional network's efficiency becomes increasingly less efficient, until reaching a certain "threshold point" where the network collapses, leading to important cognitive deficits (**Figure 7**).[57]

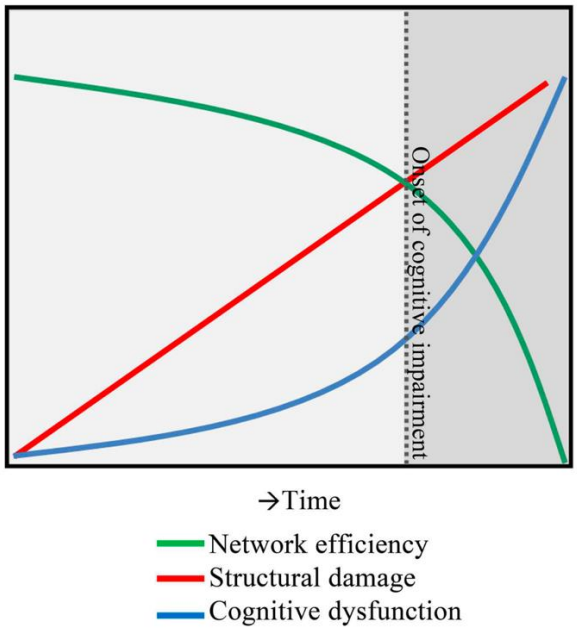

Figure 7. A hypothesis of network collapse as a cause for developing cognitive impairment in MS. In early stages of MS, structural damage is low, leaving network efficiency relatively high. As the structural damage accumulates over time, network efficiency levels drop, inducing a network collapse after a critical threshold (indicated by the dotted line) is exceeded. After this, the network is unable to function normally and cognitive impairment develops. (Adapted from Schoonheim et al., Front Neurol, 2015)

Aims of the thesis

The overall aim of this thesis was to tackle some neural substrates of cognitive functioning in the early phase of MS. This was achieved using advanced MRI techniques and a comprehensive neuropsychological battery in a homogeneous cohort of CIS patients, followed over 1-year after their first episode. First, we were interested in looking into the differential gray matter vulnerability at this early stage of the disease. Then, we investigated the evolution of topological network properties (both structural and functional) in our patients related to their cognitive performances.

Box 4. Network measures of brain connectivity

In the following, we will briefly introduce and describe some important network measures used in our analyses. First, let us recall that a node indicates a brain region, and an edge (i.e. link) indicates the connection between a pair of brain regions.

Table 1. Network measures definition

Measure	Definition
Degree	Number of links connected to a node
Global efficiency	The average inverse shortest path length between all pairs of nodes. It estimates the ease with which brain regions communicate
Local efficiency	Represents the short-range connectivity and is related to the density of the short-distance connections of the network. It shows the information transfer in the immediate neighborhood of each node
Betweenness centrality	Represents a measure of *hubness*, and generally speaking corresponds to brain areas that have the highest connectivity and form the core of the brain network
Clustering coefficient	Represents the fraction of the node's neighbors that were also neighbors of each other
Participation coefficient	Represents the diversity of inter-modular connectivity for each node. It ranges from 0 to 1. Participation coefficient is close to 1 if a node had a homogeneous connection distribution with all the modules, and 0 if a node is exclusively linked to other nodes in its own module.
Within-module degree z-score	Represents the intra-modular connectivity of a node. Within-module degree is large for a node that has many intra-module connections relative to other nodes in the same module.

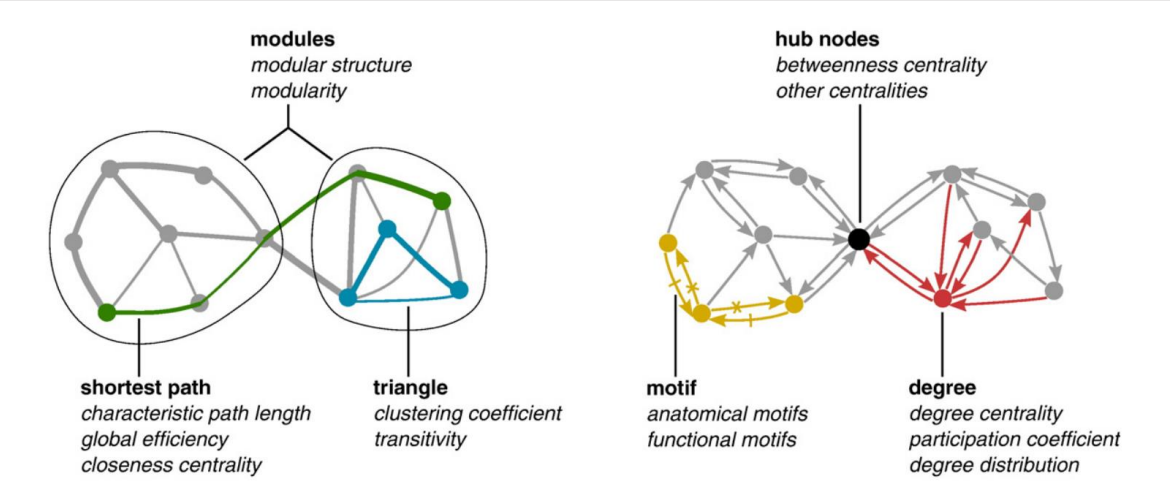

Figure 8. Measures of network topology
(Adapted from Rubinov and Sporns, NeuroImage, 2010)

Rubinov M and Sporns O, Complex network measures of brain connectivity: Uses and interpretations. NeuroImage. 2010

Thesis outline

In order to answer our previous objectives, we broke down our studies into multiple chapters. In **chapter 2**, we investigated whether some gray matter regions are differentially vulnerable at the early stage of MS. By quantifying deep gray matter and cortical volumes, along with their microstructural integrity using DTI metrics, we found that hippocampus was the first structure showing microstructural alterations since baseline. Then after 1-year, hippocampus volume was decreased along with damage spreading to the cortex. Hippocampus microstructural alterations at baseline were also predictive of its future volume loss.

In **chapter 3**, we explored the evolution of functional brain networks reorganization at rest in patients with CIS. Based on fMRI data, and using graph theoretical measures, we observed brain reorganization from the onset of the disease, by depicting a combination of underconnected and overconnected brain regions. This reorganization was even more pronounced after 1-year of evolution. Importantly, these changes were present while global brain efficiency was normal compared to HC, and correlated with the preservation of cognitive performances, suggesting a compensatory mechanism at this stage.

In **chapter 4**, we will analyze both structural and functional connectivity, and how they relate to each other in the early phase of MS. Structural connectivity was extracted from white matter tractography using DTI data, while functional connectivity was based on resting-state fMRI. By introducing a novel concept of structural-functional coupling in MS, we will look at brain regions directly connected and how the function evolves with the structure. Our analysis revealed that structural damage precedes functional reorganization during the first year following a clinically isolated syndrome along with normal cognitive performance, suggesting a compensatory mechanism at this stage of the disease. Importantly, structural–functional decoupling observed for the first time in MS suggests that functional reorganization occurs along indirect anatomical pathways.

In **chapter 5**, we will finally summarize and discuss the main findings of this thesis, and we will state the limitations of this work as well as the perspectives we intend to further develop.

References

1. Compston A, Coles A. Multiple sclerosis. *Lancet* 2008; 372: 1502–1517.
2. Kalincik T, Vivek V, Jokubaitis V, et al. Sex as a determinant of relapse incidence and progressive course of multiple sclerosis. *Brain* 2013; 136: 3609–3617.
3. Fromont A, Binquet C, Sauleau EA, et al. Geographic variations of multiple sclerosis in France. *Brain* 2010; 133: 1889–1899.
4. Popescu BFG, Lucchinetti CF. Pathology of Demyelinating Diseases. *Annu Rev Pathol Mech Dis* 2012; 7: 185–217.
5. Mahad DJ, Ziabreva I, Campbell G, et al. Mitochondrial changes within axons in multiple sclerosis. *Brain* 2009; 132: 1161–1174.
6. Lassmann H. Pathology and disease mechanisms in different stages of multiple sclerosis. *J Neurol Sci* 2013; 333: 1–4.
7. Brownlee WJ, Hardy TA, Fazekas F, et al. Diagnosis of multiple sclerosis: progress and challenges. *Lancet* 2017; 389: 1336–1346.
8. Polman CH, Reingold SC, Banwell B, et al. Diagnostic criteria for multiple sclerosis: 2010 Revisions to the McDonald criteria. *Ann Neurol* 2011; 69: 292–302.
9. Thompson AJ, Banwell BL, Barkhof F, et al. Diagnosis of multiple sclerosis: 2017 revisions of the McDonald criteria. *Lancet Neurol* 2018; 17: 162–173.
10. Miller DH, Chard DT, Ciccarelli O. *Clinically isolated syndromes*. Epub ahead of print 2012. DOI: 10.1016/S1474-4422(11)70274-5.
11. Ciccarelli O, Thompson A. Managing the complexity of multiple sclerosis. *Nat Rev Neurol* 2016; 12: 70–72.
12. Plemel JR, Liu W-Q, Yong VW. Remyelination therapies: a new direction and challenge in multiple sclerosis. *Nat Rev Drug Discov* 2017; 16: 617–634.
13. Chiaravalloti ND, Deluca J. Cognitive impairment in multiple sclerosis. *Lancet Neurol* 2008; 7: 1139–1151.
14. Feuillet L, Reuter F, Audoin B, et al. Early cognitive impairment in patients with clinically isolated syndrome suggestive of multiple sclerosis. *Mult Scler* 2007; 13: 124–7.
15. Reuter F, Zaaraoui W, Crespy L, et al. Frequency of cognitive impairment dramatically increases during the first 5 years of multiple sclerosis. *J Neurol Neurosurg Psychiatry* 2011; 82: 1157–1159.
16. Morrow SA, Drake A, Zivadinov R, et al. Predicting loss of employment over three years in multiple sclerosis: Clinically meaningful cognitive decline. *Clin Neuropsychol* 2010; 24: 1131–1145.
17. Ruet A, Deloire M, Hamel D, et al. Cognitive impairment, health-related quality of life and vocational status at early stages of multiple sclerosis: a 7-year longitudinal study. *J Neurol* 2013; 260: 776–784.
18. Langdon D, Amato M, Boringa J, et al. Recommendations for a Brief International Cognitive Assessment for Multiple Sclerosis (BICAMS). *Mult Scler J* 2012; 18: 891–898.
19. Rao S., Society and the CFSG of the NMS. A manual for brief repeatable battery of the neuropsychological tests in multiple sclerosis. *Med Coll Wisconsin, Milwaukee, WI*.
20. Benedict RHB, Fischer JS, Archibald CJ, et al. Minimal Neuropsychological Assessment of MS Patients: A Consensus Approach. *Clin Neuropsychol* 2002; 16: 381–397.
21. Filippi M, Rocca MA, Ciccarelli O, et al. MRI criteria for the diagnosis of multiple sclerosis: MAGNIMS consensus guidelines. *Lancet Neurol* 2016; 15: 292–303.

22. Barkhof F. The clinico-radiological paradox in multiple sclerosis revisited. *Curr Opin Neurol* 2002; 15: 239–45.
23. Geurts JJG, Pouwels PJW, Uitdehaag BMJ, et al. Intracortical Lesions in Multiple Sclerosis: Improved Detection with 3D Double Inversion-Recovery MR Imaging. *Radiology* 2005; 236: 254–260.
24. Seewann A, Kooi EJ, Roosendaal SD, et al. Postmortem verification of MS cortical lesion detection with 3D DIR. *Neurology* 2012; 78: 302–308.
25. Geurts JJG, Roosendaal SD, Calabrese M, et al. Consensus recommendations for MS cortical lesion scoring using double inversion recovery MRI. *Neurology* 2011; 76: 418–424.
26. Geurts JJG, Calabrese M, Fisher E, et al. Measurement and clinical effect of grey matter pathology in multiple sclerosis. *The Lancet Neurology* 2012; 11: 1082–1092.
27. Harrison DM, Peper JS, Dahl RE. Association of Cortical Lesion Burden on 7-T Magnetic Resonance Imaging With Cognition and Disability in Multiple Sclerosis. 2015; 22: 134–139.
28. Cala LA, Mastaglia FL, Black JL. Computerized tomography of brain and optic nerve in multiple sclerosis. Observations in 100 patients, including serial studies in 16. *J Neurol Sci* 1978; 36: 411–26.
29. Vollmer T, Signorovitch J, Huynh L, et al. The natural history of brain volume loss among patients with multiple sclerosis: A systematic literature review and meta-analysis. *J Neurol Sci* 2015; 357: 8–18.
30. Miller DH, Barkhof F, Frank JA, et al. Measurement of atrophy in multiple sclerosis: pathological basis, methodological aspects and clinical relevance. *Brain* 2002; 125: 1676–95.
31. van Munster CEP, Jonkman LE, Weinstein HC, et al. Gray matter damage in multiple sclerosis: Impact on clinical symptoms. *Neuroscience* 2015; 303: 446–461.
32. Dineen RA, Vilisaar J, Hlinka J, et al. Disconnection as a mechanism for cognitive dysfunction in multiple sclerosis. *Brain* 2009; 132: 239–249.
33. Friston KJ, Holmes AP, Poline J-B, et al. Analysis of fMRI Time-Series Revisited. *Neuroimage* 1995; 2: 45–53.
34. Hulst HE, Schoonheim MM, Roosendaal SD, et al. Functional adaptive changes within the hippocampal memory system of patients with multiple sclerosis. *Hum Brain Mapp* 2012; 33: 2268–2280.
35. Rocca MA, Valsasina P, Hulst HE, et al. Functional correlates of cognitive dysfunction in multiple sclerosis: A multicenter fMRI Study. *Hum Brain Mapp* 2014; 35: 5799–5814.
36. Rocca MA, De Meo E, Filippi M. Functional MRI in investigating cognitive impairment in multiple sclerosis. *Acta Neurol Scand* 2016; 134: 39–46.
37. Rocca MA, Filippi M. Functional reorganization is a maladaptive response to injury – YES. *Mult Scler J* 2017; 23: 191–193.
38. Penner IK, Aktas O. Functional reorganization is a maladaptive response to injury - NO. *Multiple Sclerosis Journal* 2017; 23: 194–196.
39. Schoonheim MM. Functional reorganization is a maladaptive response to injury – Commentary. *Mult Scler J* 2017; 23: 194–196.
40. Schmierer K, Scaravilli F, Altmann DR, et al. Magnetization transfer ratio and myelin in postmortem multiple sclerosis brain. *Ann Neurol* 2004; 56: 407–415.
41. de Paula Faria D, Copray S, Buchpiguel C, et al. PET imaging in multiple sclerosis. *J Neuroimmune Pharmacol* 2014; 9: 468–482.

42. Moccia M, Ciccarelli O. Molecular and Metabolic Imaging in Multiple Sclerosis. *Neuroimaging Clin N Am* 2017; 27: 343–356.
43. Schoonheim MM, Geurts JJG, Landi D, et al. Functional connectivity changes in multiple sclerosis patients: A graph analytical study of MEG resting state data. *Hum Brain Mapp* 2013; 34: 52–61.
44. Tewarie P, Schoonheim MM, Schouten DI, et al. Functional brain networks: Linking thalamic atrophy to clinical disability in multiple sclerosis, a multimodal fMRI and MEG Study. *Hum Brain Mapp* 2015; 36: 603–618.
45. Schoonhoven DN, Fraschini M, Tewarie P, et al. Resting-state MEG measurement of functional activation as a biomarker for cognitive decline in MS. *Mult Scler J* 2018; 135245851881026.
46. Keune PM, Hansen S, Weber E, et al. Exploring resting-state EEG brain oscillatory activity in relation to cognitive functioning in multiple sclerosis. *Clin Neurophysiol* 2017; 128: 1746–1754.
47. Sporns O. The human connectome: Origins and challenges. *Neuroimage* 2013; 80: 53–61.
48. Maier-Hein KH, Neher PF, Houde JC, et al. The challenge of mapping the human connectome based on diffusion tractography. *Nat Commun*; 8. Epub ahead of print 2017. DOI: 10.1038/s41467-017-01285-x.
49. Smith SM, Fox PT, Miller KL, et al. Correspondence of the brain's functional architecture during activation and rest. *Proc Natl Acad Sci* 2009; 106: 13040–13045.
50. van den Heuvel MP, Hulshoff Pol HE. Exploring the brain network: A review on resting-state fMRI functional connectivity. *Eur Neuropsychopharmacol* 2010; 20: 519–534.
51. Rocca MA, Valsasina P, Leavitt VM, et al. Functional network connectivity abnormalities in multiple sclerosis: Correlations with disability and cognitive impairment. *Mult Scler J* 2017; 135245851769987.
52. Rocca MA, Valsasina P, Absinta M, et al. Default-mode network dysfunction and cognitive impairment in progressive MS. *Neurology* 2010; 74: 1252–1259.
53. Smith V, Mitchell DJ, Duncan J. Role of the Default Mode Network in Cognitive Transitions. *Cereb Cortex* 2018; 28: 3685–3696.
54. Bullmore E, Sporns O. Complex brain networks: graph theoretical analysis of structural and functional systems. *Nat Rev Neurosci* 2009; 10: 312–312.
55. Rubinov M, Sporns O. Complex network measures of brain connectivity: Uses and interpretations. *Neuroimage* 2010; 52: 1059–1069.
56. Fleischer V, Radetz A, Ciolac D, et al. Graph theoretical framework of brain networks in multiple sclerosis: A review of concepts. *Neuroscience*. Epub ahead of print 2017. DOI: 10.1016/j.neuroscience.2017.10.033.
57. Schoonheim MM, Meijer KA, Geurts JJG. Network collapse and cognitive impairment in multiple sclerosis. *Front Neurol*; 6. Epub ahead of print 2015. DOI: 10.3389/fneur.2015.00082.

Chapter 2

Differential gray matter vulnerability in the early course of MS

Summary page

Rationale: Differential vulnerability of gray matter regions at the early stage of multiple sclerosis (MS) is still unknown. We aimed to investigate whether deep and cortical gray matter are differentially vulnerable after a clinically isolated syndrome (CIS) suggestive of MS.

Summary of the methods: We measured volume and diffusion tensor imaging (DTI) metrics within deep gray matter structures and the cortex in patients with CIS (PwCIS) and healthy controls (HC) at both baseline and after 1-year of follow-up.

Main results: Hippocampus was the only structure altered at baseline with microstructural abnormalities measured by DTI, while no gray matter atrophy was noticed at this stage. After 1-year, gray matter damage was more widespread with putamen and hippocampus volumes decreasing in PwCIS, and cortical thinning in different parts of the cortex along with microstructural abnormalities. Furthermore, hippocampus volume loss could be predicted by its microstructural abnormalities at baseline.

Comments: This study shows a differential gray matter vulnerability at the onset of MS spreading from hippocampus to the cortex. Additionally, we could detect early structural abnormalities in the hippocampus which were predictive of its subsequent volume loss. However, gray matter abnormalities in MS could also be studied by investigating the functional networks topology in patients.

Differential gray matter vulnerability in the one year following a clinically isolated syndrome

Ismail Koubiyr[1,2]; Mathilde Deloire[3]; Pierrick Coupé[4]; Cécile Dulau[3]; Pierre Besson[5]; Amandine Moroso[1,3]; Vincent Planche[1,2,3]; Thomas Tourdias[1,2,3]; Bruno Brochet[1,2,3*]; Aurélie Ruet[1,2,3]

[1] Univ. Bordeaux, F-33000 Bordeaux, France

[2] Inserm U1215 - Neurocentre Magendie, F-33000 Bordeaux, France

[3] CHU de Bordeaux, F-33000 Bordeaux, France

[4] Laboratoire Bordelais de Recherche en Informatique, UMR CNRS 5800, PICTURA, F-33405 Talence, France

[5] AixMarseille Univ, CNRS, CRMBM UMR 7339, Marseille

Front Neurol. (2018) doi: 10.3389/fneur.2018.00824.

Abstract

Background and purpose: Whether some gray matter (GM) regions are differentially vulnerable at the early stages of MS is still unknown. The objective of this study is to investigate whether deep and cortical GM are differentially vulnerable after a clinically isolated syndrome (CIS) suggestive of multiple sclerosis (MS).

Methods: Fifty-six patients with CIS (PwCIS) and 38 healthy controls (HC) had conventional and diffusion tensor imaging (DTI) at baseline and 46 PwCIS and 20 HC were rescanned after one year. Deep GM (DGM) volumes, cortical thickness (CTh) and DTI metrics (FA: fractional anisotropy; MD: mean diffusivity) within these structures were calculated for each participant at each time-point and compared between PwCIS and HC. Linear regression models were used to investigate whether baseline DTI parameters could predict GM volume loss over time.

Results: At baseline, GM volumes did not differ between PwCIS and HC, but hippocampal MD was higher in PwCIS than HC ($p<0.01$). Over one year, GM alterations became more widespread with putamen and hippocampus volumes decreasing in PwCIS ($p<0.01$), and cortical thinning in different parts of the cortex along with a significant increase of MD. Hippocampus MD at baseline could predict its volume loss ($R^2=0.159$; $p<0.05$) and cortical thinning was associated to microstructural damage (Spearman's rho ranging from -0.424 to -0.603 with $p<0.003$).

Conclusion: Along with MS being a diffuse inflammatory disease, GM showed a differential vulnerability at the early stage spreading from hippocampus to the cortex. Hippocampus volume loss could be predicted by its MD at baseline.

Introduction

Multiple sclerosis (MS) is an inflammatory, demyelinating and neurodegenerative disease of the central nervous system, leading to physical deterioration and cognitive impairment. At the clinical onset of the disease, approximately 85% of patients experience a monophasic neurological episode, known as a clinically isolated syndrome (CIS).[1] Gray matter (GM) atrophy has been found to occur in different phenotypes of MS associating deep GM (DGM) atrophy and cortical atrophy.[2] GM atrophy has been shown to progress in the first years after the CIS,[3,4] but conflicting results have been reported at the initial time of CIS, which questions whether or not the disease induces tissue loss from this very early stage.[2,5–7] Especially, DGM atrophy has been inconsistently found in CIS,[8–10] while cortical atrophy seems to be absent.[10] The dynamics of GM vulnerability at the early stages remain unclear, and the mechanisms leading to atrophy are not well understood.

A relationship has been suggested between atrophy in some GM nuclei and lesions in the related white matter tracts through Wallerian degeneration as this has been shown for the thalamus.[11] However, a direct injury of the GM by inflammation is also possible,[12] as suggested by recent studies using magnetic resonance-positron emission tomography.[13] Either mechanism could lead to some differential vulnerability of the GM as some structures might be more connected than others, or some types of neurons might be more fragile than others. This selective vulnerability has been shown in Alzheimer's disease particularly, as the pathology seems to spread from entorhinal cortex to hippocampus.[14]

In order to study the selective vulnerability of GM, diffusion tensor imaging (DTI) allows to explore the microstructural integrity of the structures. A few studies used this technique in CIS, showing abnormal results in the thalamus,[15] hippocampus[16] and the cerebellum[17] suggesting microstructural changes from the early stages of MS. In the other hand, cortex has been investigated in patients with MS with fractional anisotropy (FA) and mean diffusivity (MD).[18–20] Results of these studies presented some discrepancies, as FA in the normal appearing gray matter (NAGM) was found to be increased[19] or decreased,[18,20] while MD either increased[18,20] or showed no difference compared to healthy volunteers.[19] Also, the majority of these findings was cross-sectional and could not infer about the dynamics of the microstructural damage spreading. Thus, gray matter microstructural damage that may be leading to irreversible atrophy is not well assessed in MS yet, and this even more for CIS patients.

The objective of this 1-year longitudinal study is to investigate the differential vulnerability of GM

(both DGM and cortical GM) at the very early stages of MS. Both microstructural and macrostructural damage were assessed and we have investigated whether microstructural damage is able to predict future GM volume loss in PwCIS.

Materials and Methods

Standard protocol, approvals, registration and patient consent

Each participant gave written informed consent. Patients were included in a prospective study analyzing cognition in PwCIS (SCI-COG, ClinicalTrials.gov Identifier: NCT01865357). This study was approved by the local ethics committee.

Participants

- Patients

Fifty-Six PwCIS were recruited less than 6 months after a first neurological episode suggestive of MS as defined by Thompson et al. (2017),[21] including optic neuritis, partial myelitis, supratentorial syndrome, brainstem or cerebellar syndrome. The presence of at least two asymptomatic cerebral lesions on fast fluid-attenuated inversion recovery (FLAIR) images was required to confirm central nervous system involvement. Data were collected from December 2012 through January 2017. Each participant underwent an MRI scan. Forty-Six PwCIS were rescanned 1 year after the first assessment. Others patients declined to be rescanned. Exclusion criteria were age under 18, history of other neurological or psychiatric disorders, MS attack or corticosteroid pulse therapy within 2 months preceding screening, severe cognitive deficits (Mini-Mental State Examination < 27), and severe depressive symptoms (Beck Depression Inventory score (BDI) > 27). Clinical assessment and the Expanded Disability Status Scale (EDSS) scores were determined by expert neurologists.

- Healthy controls

Thirty-eight healthy controls (HC) matched for age, sex and educational level were also included and underwent an MRI scan. Twenty of these individuals were rescanned after one year.

MRI acquisition

MRI acquisition was performed on a 3T MRI system at our MS center (Achieva TX system, Philips Healthcare, Best, The Netherlands; Signa, GE Healthcare, Discovery MR 750w, Milwaukee, Wisconsin). Seventeen patients (out of 46, i.e., 37%) were not scanned on the same machine at baseline and after one year (Philips Achieva at baseline and GE Discovery after 1 year). The acquisition protocol was harmonized between magnets and consisted of a three-dimensional (3D)

T1-weighted sequence using magnetization prepared rapid gradient echo (MP-RAGE) imaging (TR=8.2 ms, TE=3.5 ms, TI=982 ms, α=7°, FOV=256 mm, voxel size=1 mm^3, 180 slices), a two-dimensional (2D) FLAIR sequence (TR=11000 ms, TE=140 ms, TI=2800 ms, FOV=230 mm, 45 axial slices, 3-mm thick) and a diffusion tensor echo-planar-imaging (EPI) pulse sequence (TR=11676 ms, TE=60 ms, FOV=230 mm, an isotropic resolution of 1.6x1.6x1.6 mm^3 and b=1000 s/mm^2) in 21 non-colinear directions and one b=0 s/mm^2.

MRI analyses

Lesions were segmented by the lesion growth algorithm as implemented in the Lesion Segmentation Tool (LST) version 2.0.15 (http://www.applied-statistics.de/lst.html) in Statistical Parametric Mapping (SPM12). It segments T1 images into 3 main tissue classes (cerebrospinal fluid (CSF), GM and WM). This information is then combined with the coregistered FLAIR to calculate lesion belief maps. An initial binary lesion map is first obtained by thresholding these maps with a prechosen initial threshold (kappa=0.3). This map is subsequently grown along voxels that appear hyperintense in the FLAIR image. This results in a lesion probability map that is thresholded to 50% to obtain a lesions binary map. Finally, these maps were manually corrected by two blinded experts. Using these maps, a lesion filling algorithm[22] was applied to the T1-weighted images to avoid lesions that affect brain tissue segmentations.

For volumetric analyses of whole brain, total WM, total GM, total CSF and DGM structures, T1-weighted images were processed using volBrain (http://volbrain.upv.es). The segmentation procedure is described in detail elsewhere.[23] Briefly, after denoising and inhomogeneity correction, images were affine-registered into the Montreal Neurological Institute (MNI) space using Advanced Neuroimaging Tools (ANTs),[24] and the total brain volume was estimated. The hippocampus, caudate, putamen, thalamus, amygdala, accumbens and globus pallidus were automatically segmented with a patch-based multi-templates method described in detail elsewhere[25] that uses expert manual segmentations in MNI space as priors. Every mask was then blindly checked and manually corrected if needed. To control for variations in head size, each structure's volume was assessed as a fraction of total intracranial volume (TIV). Cortical thickness (CTh) evaluation was performed with the Freesurfer 5.3[26,27] image analysis suite, which is documented and freely available online (http://surfer.nmr.mgh.harvard.edu). We performed the longitudinal stream[28] using an unbiased within-subject template space and image obtained by robust, inverse consistent registration.[29] To detect possible misclassification of white and gray

matter, all images were visually inspected. Cortical ribbon masks of the different lobes (frontal, temporal, parietal, occipital, cingulate, insula) were also extracted. Diffusion data were processed using the Oxford Centre for Functional MRI of the Brain (FMRIB) Software Library (FSL, version 5.0.9, fsl.fmrib.ox.ac.uk/fsl). Eddy current distortions and motion artifacts were first corrected (using the eddy_correct function), and the diffusion tensor was calculated. Scalar maps of fractional anisotropy (FA) and mean diffusivity (MD) were then extracted. Since no preferential water molecular motion is expected to occur in the GM, fractional anisotropy was used as a secondary metrics that is expected to be less sensitive.

To bring the GM masks and the scalar maps to the same space, we registered the T1-weighted images to the B0 image as a reference. This was done to keep the scalar maps in their native space, where the tensor was computed. To do that, we first used the FSL Brain Extraction Tool BET[30] (fsl.fmrib.ox.ac.uk/fsl/fslwiki/BET) to extract the brain from both the T1-weighted and the B0 images. Then, we resampled our B0 to 1x1x1 mm^3. After that, we used a rigid registration followed by a non-rigid registration of the T1-weighted image to the subject's B0 space using ANTs.[24] We then applied the transform obtained to our previous masks of GM (subcortical and cortical) and extracted DTI scalar parameters for each label. To avoid partial volume effect and the inclusion of cortical lesions, this cortical segmentation was masked by both the gray matter mask from volBrain and the segmented cortical lesions.

Statistical analysis

Statistical analysis was performed using SPSS software version 23.0 (IBM SPSS Statistics for Macintosh, Version 23.0. Armonk, NY: IBM Corp).

All MRI measures analyses were statistically adjusted for the scanner. Normality of the distribution was assessed using the Shapiro-Wilk test. Parametric and non-parametric tests were used according to the distribution of the variables. Categorical variables were investigated with χ^2 tests. At baseline, volumes, CTh and DTI scalars comparisons between PwCIS and HC were performed by general linear models (GLM) where gender, age and level of education were entered as covariates. For the longitudinal comparisons of baseline and 1-year characteristics of our subjects, paired t-tests or Wilcoxon tests were used as appropriate. Relationships between imaging variables were assessed using correlation coefficients (Pearson or Spearman according to statistical distribution). To investigate whether baseline DTI parameters could predict volume loss during one year in DGM, DGM volume loss (dependent variable) was predicted with hierarchical

regression models, including two hierarchical blocks. In the first block, age, gender, level of education and scanner also known as nuisance variables were systematically forced into the model. In the second block, the abnormal DTI metrics were added to the variables of the first block. Considering the issue of multiple comparisons, all the following results are Bonferroni corrected to reduce the risk of type I errors. A p-value <0.05 was considered significant.

Results

Demographic and clinical characteristics

Clinical phenotypes of PwCIS were summarized in **Table 1**. PwCIS and HC groups were matched for age, gender and educational level at both time points. EDSS was not significantly different in the CIS group between the two time-points (**Table 1**).

In this cohort of patients, after one year, 65.2% of PwCIS were diagnosed with MS according to the 2010 McDonald criteria.

Conventional MRI

T2-Lesion load (T2-LL) did not differ in the CIS group between the two time-points (**Table 1**).

At baseline, there was no difference between the two groups in whole normalized brain volume, WM, GM and total CSF. However, over 1 year, PwCIS showed a global brain atrophy as the whole brain volume and WM decreased ($p<0.05$), (**Table 1**) and total CSF volume increased ($p<0.05$).

Table 1. **Demographic, Clinical, and Conventional MR Imaging Characteristics**

	Baseline		Year 1	
Clinical features	**HC** *(n=38)*	**CIS** *(n=56)*	**HC** *(n=20)*	**CIS** *(n=46)*
Mean age, years *(SD)*[a]	38.1 (9.3)	36.5 (11.2)	37.9 (8.4)	38.1 (11.5)
Sex ratio *(F/M)*[b]	26/12	46/10	14/6	36/10
Education level *(high/low*[c]*)*[b]	27/11	39/17	11/9	30/16
Symptoms at clinical onset: *Brain* *Optic neuritis* *Brainstem/Cerebellar* *Spinal cord*	-	5 (9%) 12 (21%) 11 (20%) 28 (50%)	-	-
Median EDSS score *[range]*[d]	-	1.0 [0-4]	-	1.0 [0-5]
Median T2-Lesion volume *(ml)*[d]	-	0.73 [0.23-63.12]	-	1.09 [0.61-67.74]
Normalized Brain fraction *(%)*[d,e,f]	86.36 ± 3.12	85.06 ± 3.93	86.39 ± 2.94	83.91 ± 4.03*†
Normalized WM fraction *(%)*[g,e,f]	37.02 ± 2.48	35.67 ± 3.17	37.32 ± 3.06	34.65 ± 3.33†
Normalized GM fraction *(%)*[g,e,f]	49.34 ± 2.64	49.40 ± 2.70	49.07 ± 2.26	49.26 ± 2.91
Normalized CSF fraction *(%)*[d,e,f]	13.64 ± 3.12	14.94 ± 3.93	13.61 ± 2.94	16.09 ± 4.03*†
Mean CTh *(mm)*[d,e]	2.55 ± 0.10	2.54 ± 0.12	2.54 ± 0.10	2.49 ± 0.12†††

[a] Mann-Whitney test
[b] χ^2 test
[c] Education level was considered as high or low according to a French baccalaureate.
[d] Wilcoxon test to compare PwCIS at baseline and year 1.
[e] GLM comparing PwCIS to HC with age, sex and level of education as covariates.
[f] Percentage: (structure's volume/TIV)*100.
[g] Paired t-test.
Differences between PwCIS and HC: *: p<0.05; **: p<0.01; ***: p<0.001
Differences in PwCIS between baseline and year 1: †: p<0.05; ††: p<0.01; †††: p<0.001
TIV: Total Intracranial Volume; EDSS: Expanded Disability Status Scale; WM : White Matter ; GM : Gray Matter ; CSF : Cerebrospinal fluid (includes liquid in subarachnoid space and ventricular system); CTh: Cortical Thickness.

Baseline findings

We wanted to assess whether some GM regions are more vulnerable at the onset of the disease than others.

- Volumetric measures

We found no significant atrophy in DGM structures and no cortical thinning when comparing

PwCIS to HC.

- DTI

However, when looking at the microstructural integrity of the GM, hippocampus was the only structure altered at this stage as its MD was significantly higher in PwCIS compared to HC (**Fig 1**), indicating a differential vulnerability of this structure compared to the rest of the GM.

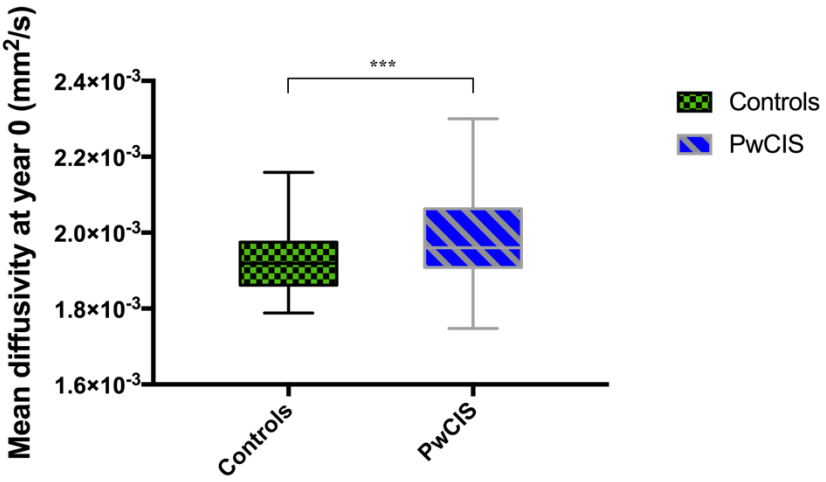

Figure 1. Hippocampus mean diffusivity at baseline
PwCIS: patients with clinically isolated syndrome. p-values indicate significant differences after multiple comparisons correction.
***: p<0.001

Longitudinal findings

To study the evolution of GM damage, we compared these structures between year 0 and year 1.

- Volumetric measures

No differences were noticed in HC. However, in PwCIS, lateral ventricles volumes increased ($p<0.01$) reflecting deep brain atrophy, whereas putamen and hippocampus volumes significantly decreased (**Fig 2**).

The mean CTh significantly decreased in one year ($p<0.001$). Regionally, multiple brain areas of significant cortical thinning in both hemispheres were observed. This cortical thinning was noticed

in the bilateral frontal and temporal lobes, left insula and right parietal lobe (**Table 2**).

- DTI

Regarding microstructural changes, PwCIS showed significantly higher MD in the left frontal ($p<0.006$), left temporal ($p<0.003$), left cingulate ($p<0.003$) and bilateral parietal lobes ($p<0.002$) (**Table 3**). No changes were noticed for the FA.

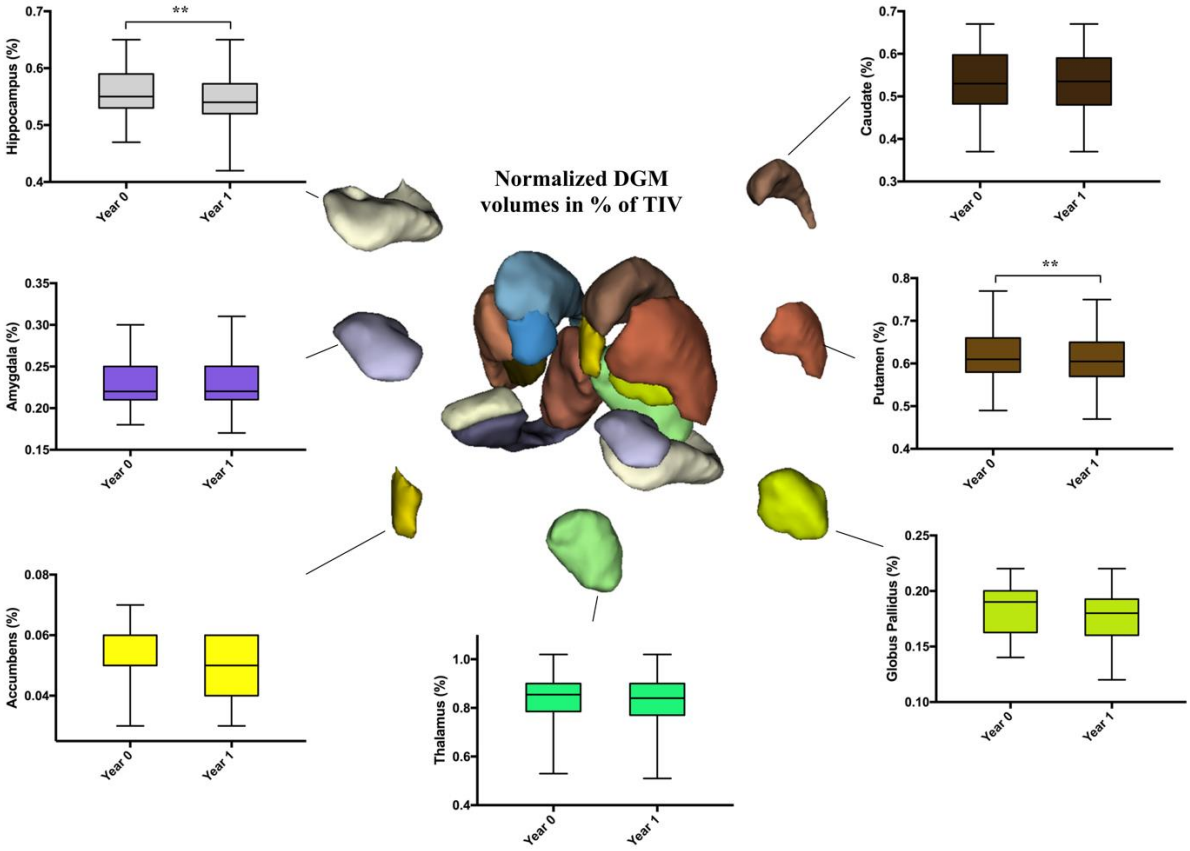

Figure 2. Longitudinal comparison of DGM structures volume fractions in PwCIS

Volumes are percentages calculated as: (structure's volume/TIV)*100.

DGM: Subcortical deep gray matter; PwCIS: patients with clinically isolated syndrome. p-values indicate significant differences after multiple comparisons correction.

**: $p<0.01$

Table 2. Cortical thinning in a longitudinal comparison of PwCIS between baseline and 1 year of follow-up

Regions	Baseline thickness *(mm)*	1-year thickness *(mm)*
Frontal_L	2.52 ± 0.14	2.45 ± 0.14 ***
Cingulate_L	2.62 ± 0.23	2.66 ± 0.19
Occipital_L	2.01 ± 0.14	1.97 ± 0.12
Temporal_L	2.74 ± 0.20	2.67 ± 0.14
Parietal_L	2.31 ± 0.18	2.23 ± 0.13 **
Insula_L	3.05 ± 0.18	2.99 ± 0.19 **
Frontal_R	2.48 ± 0.15	2.37 ± 0.14 ****
Cingulate_R	2.57 ± 0.21	2.55 ± 0.17
Occipital_R	2.03 ± 0.17	1.99 ± 0.13
Temporal_R	2.79 ± 0.19	2.75 ± 0.13 **
Parietal_R	2.31 ± 0.15	2.25 ± 0.12 **
Insula_R	3.02 ± 0.18	2.94 ± 0.19

L: Left hemisphere; R: Right hemisphere. p-values indicate significant differences after multiple comparisons correction.
**: p<0.01; ***: p<0.001; ****: p<0.0001

Table 3. Cortical mean diffusivity changes over one year of follow-up in PwCIS

Regions	Baseline MD *(10^{-3} mm^2/s)*	1-year MD *(10^{-3} mm^2/s)*
Frontal_L	1.05 ± 0.13	1.11 ± 0.16 **
Cingulate_L	0.93 ± 0.10	0.98 ± 0.11 **
Occipital_L	0.89 ± 0.06	0.90 ± 0.07
Temporal_L	0.90 ± 0.05	0.92 ± 0.06 **
Parietal_L	0.95 ± 0.11	1.01 ± 0.12 ***
Insula_L	1.03 ± 0.08	1.04 ± 0.10
Frontal_R	1.05 ± 0.12	1.11 ± 0.14
Cingulate_R	0.96 ± 0.09	0.99 ± 0.11
Occipital_R	0.90 ± 0.07	0.92 ± 0.07
Temporal_R	0.91 ± 0.06	0.92 ± 0.06
Parietal_R	0.96 ± 0.11	1.02 ± 0.13 **
Insula_R	1.02 ± 0.08	1.03 ± 0.10

MD: Mean diffusivity. L: Left hemisphere; R: Right hemisphere. p-values indicate significant differences after multiple comparisons correction.
**: p<0.01; ***: p<0.001

Relationship between volume loss and microstructural damage

While trying to assess whether microstructural damage at baseline could predict volume loss, we found that baseline hippocampus MD was able to predict hippocampus volume loss after 1 year (adjusted R^2=0.16, p<0.05) (**Table 4**). T2-LL was taken into account in this model and was not responsible for the volume loss.

We then investigated whether the microstructural abnormalities appearing over 1 year in the cortical ribbon could be related to the cortical thinning over the same period of time. Therefore, we found that the mean diffusivity change from year 0 to year 1 was strongly correlated to the cortical thinning in the left frontal lobe (rho= -0.603; p<0.0001), the right parietal lobe (rho= -0.424; p<0.003) and the left temporal lobe (rho= -0.427; p<0.003).

We also investigated the relationship between EDSS and MRI (volumetric and DTI) abnormalities, but no correlation was found. These abnormalities were not able to predict the conversion to MS after 1-year.

Table 4. Hierarchical regression model between hippocampus volume loss over 1 year and demographical and baseline MD

Dependent variable		Explanatory variables	Univariate analysis (*r*)	Multivariate analysis (*ß*)	Adjusted multivariate model (R^2)
Hippocampus volume loss over 1 year	**Block 1**	*Age*	0.12	ns	ns
		Educational level	0.19	ns	
		Gender	0.05	ns	
		Scanner	0.05	ns	
	Block 2	*Age*	0.12	ns	0.16*
		Educational level	0.19	ns	
		Gender	0.05	ns	
		Scanner	0.05	ns	
		Hippocampus MD at year 0	-0.40**	-0.45**	

MD: Mean diffusivity; ns: non significant.
* : p<0.05 ; ** : p<0.01.

Discussion

The present study showed differential GM vulnerability as microstructural damage spread from the deep gray matter (hippocampus) to the cortex one year after the CIS. This microstructural

damage occurred before irreversible gray matter atrophy. At baseline, there was no sign of GM atrophy in PwCIS compared to HC. However, microstructural damage was already present and the hippocampus was the first and only GM structure altered. The hippocampus showed increased MD in PwCIS compared to controls, confirming preliminary findings in a previous paper[16] that compared cross-sectionally a subgroup of this population with a group of MS patients. The damage occurring to the hippocampus was further confirmed by a significant volume loss after 1 year of follow-up. The putamen showed also a significant volume loss at follow-up. Since microstructural damage appears to precede volume loss, we investigated whether the former could predict the latter. We then showed that hippocampus MD was able to predict its volume loss independently of lesion volume. Microstructural abnormalities, as detected by DTI in the hippocampus, preceding volume loss and predicting it suggested that a primary tissue alteration within this structure is involved in the neurodegenerative process. Activation of microglia/macrophages, associated with demyelination and neuro degeneration, has been pathologically observed in DGM, including the hippocampus in MS.[31–33] In experimental auto-immune encephalomyelitis, microglial activation within the hippocampus has been observed in association with neuronal dysfunction and memory impairment independently of demyelination.[34] DTI was able to detect microstructural abnormalities in the hippocampus in this model. According to the pathological and experimental data discussed above, we hypothesized that neuro-inflammation that results in microglial activation, for example, could occur at the very early stages of the disease in the hippocampus. However, a role for lesions within the tracts connected to the hippocampus cannot be ruled out, but the persistence of the prediction after adjustment on lesion load suggests an independent mechanism.

Brain atrophy measured on MRI is considered as a hallmark of long lasting MS. It reflects the net effect of the pathology on the brain; it is correlated with physical and cognitive disability and increasingly used as an end-point in clinical trials. It is well-established that GM atrophy, including cortical and DGM atrophy, is mainly responsible for the development of the whole brain atrophy.[35] The dynamics of GM atrophy remain, however, not well known and the mechanisms of GM alterations remain hypothetical. One possible mechanism is a consequence of distant lesions by dying back axonopathy, leading to atrophy of the cortical gray matter. However, it has also been suggested that meningeal inflammation and microglial activation could lead to direct pathology of the GM[36,37] and some evidence of this mechanism has been observed in progressive MS.[38]

We hypothesized that early structural abnormalities could be detected in some nuclei of DGM in CIS and could predict the subsequent development of atrophy in the same structures.

The different results between studies concerning the presence of DGM volume loss in CIS could be explained by different sample size, disease duration and selection bias toward CIS with higher or lower burden of the disease. The disease duration in our sample was less than 6 months, and PwCIS must have only at least two lesions on the brain MRI; in fact, their lesion load was very low (0.7 cm^3). For example, in one study showing some level of DGM atrophy[8], lesion volume was superior to 2 cm^3. In another study, CIS patients with lesion load superior to 4.49 cm^3 had lower DGM volumes than those with a median lesion load inferior to 4.49 cm^3.[10] This suggests that in the CIS samples with lower lesion load, the pre-clinical stage before CIS was shorter, explaining why atrophy was not developed.

In our sample, we did not observe significant cortical thinning at baseline, in agreement with the absence of cortical atrophy in previous studies,[9] but we observed some cortical thinning during the follow-up period in bilateral frontal lobes, bilateral temporal lobes and left insular and right parietal lobes. These results are in line with the study by Rocca et al[4] showing GM atrophy of frontal, temporal and parietal lobes in CIS patients 1 year after the onset of the disease. Microstructural abnormalities in the cortex appeared only after 1 year of follow-up as opposed to hippocampus. MD of bilateral parietal lobes, left frontal, left temporal and left cingulate lobes was significantly increased after 1 year in PwCIS. This result did not only reflect atrophy because of CSF contamination. First, we found an altered MD in hippocampus before any atrophy. Second, if an increase of MD in cortical GM was due to partial volume, we would also find a decrease of FA which was not the case. Moreover, these microstructural abnormalities were found to correlate with the presence of cortical thinning in left frontal and temporal lobes, as well as in the right parietal lobe. A recent study using 7 Tesla MRI showed the existence of a gradient of pathology in the cortex of MS patients, suggesting that the pathological process was driven from the pial surface[39] and supported the role of inflammation within the cortex in relation with meningeal inflammation. Cortical volume loss seems to parallel DGM volume loss at these very early stages of MS, however, microstructural damage starts within the hippocampus first.

The present study is not without limitations. First, our patients did not have double inversion recovery sequences, thus some cortical lesions may have been missed in the FLAIR sequence and included in the cortical gray matter mask. Second, we are aware that the follow-up time (one year)

is too short to observe more damage in our patients, thus we will follow them at a longer period of time. However, this short follow-up period was used to detect very early changes occurring at the onset of MS.

Conclusion

The current study allowed us to explore the whole GM integrity and to detect differential vulnerability of the hippocampus at the earliest stage of MS, showing a pathological spread towards the cortex after 1 year of the disease.

Since the respective role of atrophy of cortical and DGM in clinical, physical and cognitive disability remains an important question, this cohort of CIS patients will be followed-up to explore this question.

Abbreviations: CIS = clinically isolated syndrome; DGM = deep gray matter; PwCIS = patients with CIS; HC = healthy controls; FA = fractional anisotropy; MD = mean diffusivity; CTh = cortical thickness

Data availability: The datasets generated during and/or analyzed during the current study are available from the corresponding author on reasonable request.

Acknowledgments: The authors thank the neurologists of the AQUISEP network for their involvement in recruiting patients. The authors thank Dr. JC Ouallet and Dr. P Louiset
for referring patients to the study. This work has been performed with the help of the French Observatoire of Multiple Sclerosis (OFSEP).

Funding: This study was supported by ANR-10-LABX-57 Translational Research and Advanced Imaging Laboratory (TRAIL), laboratory of excellence. The SCICOG study was also supported by a grant from Teva.

Author contributions:

IK and BB were involved in drafting the manuscript. All authors revised the manuscript for important intellectual content. MD, CD, AM, VP, TT, AR and BB were involved in study concept and design. IK, MD, PC, CD, PB, AR and BB were involved in analysis and interpretation of the data. IK, MD, CD, AM, VP, TT, AR and BB were involved in acquisition of the data. IK and MD were involved in statistical analysis. BB, AR and TT were involved in study supervision and coordination. All authors approved the final version to be published and agreed to be accountable

for all aspects of the work in ensuring that questions related to the accuracy or integrity of any part of the work are appropriately investigated and resolved.

Conflict of Interest: The authors have nothing to disclose in direct link with the work submitted. Other potential conflict of interest:

Ismail Koubiyr, Dr Deloire, Dr Coupé, Dr Besson, Dr Moroso and Pr Tourdias have nothing to disclose. Dr. Dulau reports personal fees from Biogen, outside the submitted work. Dr. Planche reports non-financial support from Teva, non-financial support from Biogen Idec, personal fees and non-financial support from Merck-Serono, outside the submitted work. Dr. Ruet reports grants from TEVA, during the conduct of the study; personal fees and non-financial support from Novartis, personal fees and non-financial support from Biogen, grants, personal fees and non-financial support from TEVA, grants and non-financial support from Roche, grants and non-financial support from Merck, grants and non-financial support from Genzyme, non-financial support from Medday, grants from Bayer, outside the submitted work. Dr. Brochet reports grants from French Ministry of Health, during the conduct of the study; personal fees and non-financial support from biogen-idec, grants from merck-serono, personal fees and non-financial support from novartis, personal fees and non-financial support from genzyme, grants, personal fees and non-financial support from teva, grants and non-financial support from bayer, outside the submitted work.

References

1. Polman CH, Reingold SC, Banwell B, et al. Diagnostic criteria for multiple sclerosis: 2010 Revisions to the McDonald criteria. *Ann Neurol*. 2011;69(2):292-302. doi:10.1002/ana.22366
2. Ceccarelli A, Rocca MA, Pagani E, et al. A voxel-based morphometry study of grey matter loss in MS patients with different clinical phenotypes. *Neuroimage*. 2008;42(1):315-322. doi:10.1016/j.neuroimage.2008.04.173
3. Pérez-Miralles F, Sastre-Garriga J, Tintoré M, et al. Clinical impact of early brain atrophy in clinically isolated syndromes. *Mult Scler*. 2013;19(14):1878-1886. doi:10.1177/1352458513488231
4. Rocca MA, Preziosa P, Mesaros S, et al. Clinically Isolated Syndrome Suggestive of Multiple Sclerosis: Dynamic Patterns of Gray and White Matter Changes-A 2-year MR Imaging Study. *Radiology*. 2015;000(0):150532. doi:10.1148/radiol.2015150532
5. Cappellani R, Bergsland N, Weinstock-Guttman B, et al. Subcortical deep gray matter pathology in patients with multiple sclerosis is associated with white matter lesion burden and atrophy but not with cortical atrophy: A diffusion tensor MRI study. *Am J Neuroradiol*. 2014;39(5):912-919. doi:10.3174/ajnr.A3788
6. Raz E, Cercignani M, Sbardella E, et al. Clinically Isolated Syndrome Suggestive of Multiple Sclerosis: Voxelwise Regional Investigation of White and Gray Matter 1. *Radiology*. 2010;254. http://pubs.rsna.org.gate2.inist.fr/doi/pdf/10.1148/radiol.2541090817. Accessed March 29, 2017.
7. Chard DT, Griffin CM, Rashid W, et al. Progressive grey matter atrophy in clinically early relapsing-remitting multiple sclerosis. *Mult Scler*. 2004;10(4):387-391. doi:10.1191/1352458504ms1050oa
8. Audoin B, Zaaraoui W, Reuter F, et al. Atrophy mainly affects the limbic system and the deep grey matter at the first stage of multiple sclerosis. *J Neurol Neurosurg Psychiatry*. 2009;81:690-695. doi:10.1136/jnnp.2009.188748
9. Henry RG, Shieh M, Okuda DT, Evangelista A, Gorno-Tempini ML, Pelletier D. Regional grey matter atrophy in clinically isolated syndromes at presentation. *J Neurol Neurosurg Psychiatry*. 2008;79(11):1236-1244. doi:10.1136/jnnp.2007.134825
10. Bergsland N, Horakova D, Dwyer MG, et al. Subcortical and cortical gray matter atrophy in a large sample of patients with clinically isolated syndrome and early relapsing-remitting multiple sclerosis. *Am J Neuroradiol*. 2012;33(8):1573-1578. doi:10.3174/ajnr.A3086
11. Henry RG, Shieh M, Amirbekian B, Chung S, Okuda DT, Pelletier D. Connecting white matter injury and thalamic atrophy in clinically isolated syndromes. *J Neurol Sci*. 2009;282(1-2):61-66. doi:10.1016/j.jns.2009.02.379
12. Lucchinetti CF, Popescu BFG, Bunyan RF, et al. Inflammatory Cortical Demyelination in Early Multiple Sclerosis. *N Engl J Med*. 2011;365(23):2188-2197. doi:10.1056/NEJMoa1100648
13. Herranz E, Giannì C, Louapre C, et al. Neuroinflammatory component of gray matter pathology in multiple sclerosis. *Ann Neurol*. 2016;80(5):776-790. doi:10.1002/ana.24791
14. Du AT, Schuff N, Kramer JH, et al. Higher atrophy rate of entorhinal cortex than hippocampus in AD. *Neurology*. 2004;62(3):422-427. doi:10.1212/01.WNL.0000106462.72282.90

15. Deppe M, Krämer J, Tenberge JG, et al. Early silent microstructural degeneration and atrophy of the thalamocortical network in multiple sclerosis. *Hum Brain Mapp*. 2016;37(5):1866-1879. doi:10.1002/hbm.23144
16. Planche V, Ruet A, Coupé P, et al. Hippocampal microstructural damage and memory impairment in clinically isolated syndrome. *Mult Scler J*. 2015;21:363. doi:10.1177/1352458516675750
17. Moroso A, Ruet A, Lamargue-Hamel D, et al. Microstructural analyses of the posterior cerebellar lobules in relapsing-onset multiple sclerosis and their implication in cognitive impairment. *PLoS One*. 2017;12(8). doi:10.1371/journal.pone.0182479
18. Poonawalla AH, Hasan KM, Gupta RK, et al. Diffusion-Tensor MR Imaging of Cortical Lesions in Multiple Sclerosis: Initial Findings. *Radiology*. 2008;246(3):880-886. doi:10.1148/radiol.2463070486
19. Calabrese M, Rinaldi F, Seppi D, et al. Cortical Diffusion-Tensor Imaging Abnormalities in Multiple Sclerosis: A 3-year Longitudinal Study. *Radiology*. 2011;261(3):891-898. doi:10.1148/radiol.11110195
20. Filippi M, Preziosa P, Pagani E, et al. Microstructural magnetic resonance imaging of cortical lesions in multiple sclerosis. *Mult Scler J*. 2013;19(4):418-426. doi:10.1177/1352458512457842
21. Thompson AJ, Banwell BL, Barkhof F, et al. Diagnosis of multiple sclerosis: 2017 revisions of the McDonald criteria. *Lancet Neurol*. 2018;17(2):162-173. doi:10.1016/S1474-4422(17)30470-2
22. Prados F, Cardoso MJ, Kanber B, et al. A multi-time-point modality-agnostic patch-based method for lesion filling in multiple sclerosis. *Neuroimage*. 2016;139:376-384. doi:10.1016/j.neuroimage.2016.06.053
23. Manjón J V, Coupé P. volBrain: An Online MRI Brain Volumetry System. *Front Neuroinform*. 2016;10. doi:10.3389/fninf.2016.00030
24. Avants BB, Tustison NJ, Song G, Cook PA, Klein A, Gee JC. A Reproducible Evaluation of ANTs Similarity Metric Performance in Brain Image Registration. *Neuroimage*. 2011. doi:10.1016/j.neuroimage.2010.09.025
25. Coupé P, Manjón J V., Fonov V, Pruessner J, Robles M, Collins DL. Patch-based segmentation using expert priors: Application to hippocampus and ventricle segmentation. *Neuroimage*. 2011;54(2):940-954. doi:10.1016/j.neuroimage.2010.09.018
26. Dale AM, Fischl B, Sereno MI. Cortical surface-based analysis: I. Segmentation and surface reconstruction. *Neuroimage*. 1999;9(2):179-194. doi:10.1006/nimg.1998.0395
27. Fischl B, Dale AM. Measuring the Thickness of the Human Cerebral Cortex from Magnetic Resonance Images. *PNAS*. Vol 97.; 2000. doi:10.1073/pnas.200033797
28. Reuter M, Schmansky NJ, Rosas HD, Fischl B. Within-subject template estimation for unbiased longitudinal image analysis. *Neuroimage*. 2012;61(4):1402-1418. doi:10.1016/j.neuroimage.2012.02.084
29. Reuter M, Rosas HD, Fischl B. Highly accurate inverse consistent registration: A robust approach. *Neuroimage*. 2010;53(4):1181-1196. doi:10.1016/j.neuroimage.2010.07.020
30. Smith SM. Fast robust automated brain extraction. *Hum Brain Mapp*. 2002;17(3):143-155. doi:10.1002/hbm.10062
31. Haider L, Simeonidou C, Steinberger G, et al. Multiple sclerosis deep grey matter: the relation between demyelination, neurodegeneration, inflammation and iron. *J Neurol Neurosurg Psychiatr*y. 2014;85(12):1386-1395. doi:10.1136/jnnp-2014-307712

32. Geurts JJG, Bö L, Roosendaal SD, et al. Extensive hippocampal demyelination in multiple sclerosis. *J Neuropathol Exp Neurol*. 2007;66(9):819-827. doi:10.1097/nen.0b013e3181461f54
33. Dutta R, Chang A, Doud MK, et al. Demyelination causes synaptic alterations in hippocampi from multiple sclerosis patients. *Ann Neurol*. 2011;69(3):445-454. doi:10.1002/ana.22337
34. Planche V, Panatier A, Hiba B, et al. Selective dentate gyrus disruption causes memory impairment at the early stage of experimental multiple sclerosis. *Brain Behav Immun*. 2017;60:240-254. doi:10.1016/j.bbi.2016.11.010
35. Geurts JJG, Calabrese M, Fisher E, Rudick RA. Measurement and clinical effect of grey matter pathology in multiple sclerosis. *Lancet Neurol*. 2012;11(12):1082-1092. doi:10.1016/S1474-4422(12)70230-2
36. Magliozzi R, Howell O, Vora A, et al. Meningeal B-cell follicles in secondary progressive multiple sclerosis associate with early onset of disease and severe cortical pathology. *Brain*. 2007;130(4):1089-1104. doi:10.1093/brain/awm038
37. Howell OW, Reeves CA, Nicholas R, et al. Meningeal inflammation is widespread and linked to cortical pathology in multiple sclerosis. *Brain*. 2011;134(9):2755-2771. doi:10.1093/brain/awr182
38. Choi SR, Howell OW, Carassiti D, et al. Meningeal inflammation plays a role in the pathology of primary progressive multiple sclerosis. *Brain*. 2012;135(10):2925-2937. doi:10.1093/brain/aws189
39. Mainero C, Louapre C, Govindarajan ST, et al. A gradient in cortical pathology in multiple sclerosis by in vivo quantitative 7 T imaging. *Brain*. 2015;138(4):932-945. doi:10.1093/brain/awv011

Chapter 3

Longitudinal functional brain network reorganization in early MS

Summary page

Rationale: We have demonstrated structural gray matter alterations present from the early course of multiple sclerosis (MS) with a pathological spread from hippocampus to the cortex (**Chapter 2**). However, the topological organization of functional brain networks at the early stage of MS and how it relates to cognitive performance needs to be characterized. This is why we intend to assess potential brain functional reorganization at rest in patients with clinically isolated syndrome (CIS) and to characterize the dynamics of functional brain networks at the early stage of the disease.

Summary of the methods: Using resting-state functional MRI data and graph theory, we explored topological metrics for each brain region in patients with CIS (PwCIS) and healthy controls (HC) at baseline and after 1-year of follow-up.

Main results: By using a novel graph metric called Hub disruption index, we demonstrated early brain networks reorganization with some overconnected and underconnected regions in PwCIS. This reorganization became even more pronounced after 1-year of follow-up. Importantly, PwCIS showed preserved global brain efficiency and cognitive performances compared to HC. We then showed that these cognitive performances were getting better as the brain networks reorganization was more pronounced.

Comments: These results demonstrate dynamic changes in functional brain networks from the early stages of MS, which are associated with the maintenance of normal cognitive performances, suggesting a compensatory effect at this stage of the disease. However, it remains unknown how these functional changes are related to the underlying anatomy.

Longitudinal study of functional brain network reorganization in clinically isolated syndrome

Ismail Koubiyr[1,2]; Mathilde Deloire[3]; Pierre Besson[5,6]; Pierrick Coupé[4]; Cécile Dulau[3]; Jean Pelletier[5,6,7]; Thomas Tourdias[1,2,3]; Bertrand Audoin[5,6,7]; Bruno Brochet[1,2,3]; Jean-Philippe Ranjeva[5,6]; Aurélie Ruet[1,2,3]

[1] Univ. Bordeaux, F-33000 Bordeaux, France

[2] Inserm U1215 - Neurocentre Magendie, F-33000 Bordeaux, France

[3] CHU de Bordeaux, F-33000 Bordeaux, France

[4] Laboratoire Bordelais de Recherche en Informatique, UMR CNRS 5800, PICTURA, F-33405 Talence, France

[5] AixMarseille Univ, CNRS, CRMBM UMR 7339, Marseille, France

[6] AixMarseille Univ, APHM, Hopital la Timone, CEMEREM, Marseille, France

[7] APHM, Hopital la Timone, service de Neurologie, Marseille, France

Mult Scler. (2018) doi: 10.1177/1352458518813108

Abstract

Background: There is a lack of longitudinal studies exploring the topological organization of functional brain networks at the early stages of multiple sclerosis (MS).

Objectives: This study aims to assess potential brain functional reorganization at rest in patients with CIS (PwCIS) after one year of evolution and to characterize the dynamics of functional brain networks at the early stage of the disease.

Methods: We prospectively included 41 PwCIS and 19 matched healthy controls (HC). They were scanned at baseline and after 1 year. Using graph theory, topological metrics were calculated for each region. Hub disruption index was computed for each metric.

Results: Hub disruption indexes of degree and betweenness centrality were negative at baseline in patients ($p<0.05$), suggesting brain reorganization. After 1 year, hub disruption indexes for degree and betweenness centrality were still negative ($p<0.00001$), but such reorganization appeared more pronounced than at baseline. Different brain regions were driving these alterations. No global efficiency differences were observed between PwCIS and HC either at baseline or at 1 year.

Conclusion: Dynamic changes in functional brain networks appear at the early stages of MS and are associated with the maintenance of normal global efficiency in the brain, suggesting a compensatory effect.

Introduction

Patients with a first neurological episode of the type seen in multiple sclerosis (MS), so-called clinically isolated syndrome (CIS) are at a high risk of progressing to MS.[1] Multiple sclerosis pathology is characterized by inflammation, demyelination, axonal injury and axonal loss.[2] This pathology induces disruptions in brain connectivity, which can lead to sensory [3], motor[4] or cognitive[5,6] dysfunction. Some studies have shown that functional compensatory mechanisms occurring at the early stages of the disease can limit these clinical manifestations.[7–9] Resting-state functional imaging studies in MS have shown the potential to non-invasively map the intrinsic functional brain networks and to detect early functional brain changes.[6,10–12] Furthermore, graph theory has proved to depict the topological organization of the brain by visualizing the overall connectivity patterns and by characterizing the brain's global organization.[13] Recent studies investigated brain network topology at the CIS stage. Liu et al. (2016)[14] showed decreased nodal efficiency in the superior temporal gyrus, left rolandic operculum and left insula, while Shu et al. (2016)[15] did not notice any local changes in the functional connectome of CIS patients. This lack of network changes was then thought to be due to subtle functional changes during this very early stage of the disease. To the best of our knowledge, these graph-based functional studies of CIS were only performed cross-sectionally; therefore, they did not provide answers regarding the dynamics of the functional brain networks at this stage.[16] In MS, both increased and decreased centrality have been observed in different parts of the brain.[6,11,17] Faivre et al. (2016)[18] studied the evolution of network topology over 2 years of follow-ups in relapsing-remitting MS (RRMS) patients after on average 10 years of evolution of the disease. At baseline, the local and nodal efficiencies were higher in patients compared to controls, while after 2 years, these values were decreased and were no longer different from controls. Thus, the authors hypothesized that the compensatory mechanisms failed after reaching a maximal level. In this context, one may wonder whether such compensatory mechanisms (or failure of compensation) could be involved as early as at the stage of CIS.

For such needs, we aimed to study resting-state functional brain network topology longitudinally, few months after CIS and one year after using both global and local graph-based measures to assess functional brain network reorganization.

Materials and methods

Standard protocol, approvals, registration and patient consent

Each participant gave written informed consent. The patients were included in a prospective study without intervention, analyzing early brain damage in patients with CIS (PwCIS) (SCI-COG, ClinicalTrials.gov Identifier: NCT01865357). This study was approved by the local ethics committee.

Participants

Fifty-two PwCIS were prospectively recruited less than 6 months after a first neurological episode of the type seen in MS and presented with at least two clinically silent cerebral lesions on fast fluid-attenuated inversion recovery (FLAIR) images characteristic of MS. All patients underwent an MRI scan at baseline, and forty-one PwCIS were rescanned 1 year after the first assessment. The exclusion criteria included under 18 years of age, the inability to perform the MRI, a history of other neurological or psychiatric disorders, an MS attack within the 2 months prior to the screening, corticosteroid pulse therapy within the 2 months prior to the screening and severe depression (Beck Depression Inventory score (BDI) > 27). Clinical assessments and the Expanded Disability Status Scale (EDSS) scores were determined by expert neurologists.

Twenty healthy controls (HC) matched for age, sex and educational level were also included and underwent the same MRI protocol. Nineteen of these HC were rescanned within one year of the first assessment. Because our aim was to study the longitudinal evolution of brain network topology, only participants with longitudinal follow-ups were considered for the current analyses. Therefore, the 41 patients and the 19 HC followed over 1 year are referred to as PwCIS and HC, respectively.

All participants were also evaluated using a large neuropsychological (NP) battery detailed in supplementary material.

MRI acquisition

The MRI acquisition was performed on a 3T MRI system (Achieva TX system, Philips Healthcare, Best, The Netherlands; Signa, GE Healthcare, Discovery MR 750w, Milwaukee, Wisconsin). The acquisition protocol was harmonized between the magnets and consisted of a three-dimensional (3D) T1-weighted sequence using magnetization prepared rapid gradient echo (MP-RAGE) imaging, a two-dimensional (2D) FLAIR sequence, and resting-state functional MRI was obtained with an echo-planar imaging (EPI) sequence. See supplementary material for technical details.

fMRI preprocessing

Using Statistical Parametric Mapping (SPM12, www.fil.ion.ucl.ac.uk/spm), we followed the same fMRI preprocessing that was used in a previous study [19]. Preprocessing steps are detailed in supplementary material.

Structural preprocessing and regions of interest

Briefly, lesions were segmented on FLAIR data and lesion filling was applied to T1-weighted images. Structural data were preprocessed with FreeSurfer (v5.3) leading to a custom-made atlas of 83 regions per hemisphere. Details are available in supplementary material.

Network construction

Interactions between brain regions can be described by graph theoretical methods [20]. These methods represent interactions consisting of nodes (brain regions) and links/edges between the nodes (functional interaction). To construct functional connectivity networks, for each participant, the average BOLD time courses were extracted from each one of the 166 regions defined by our final atlas. Then, Pearson's linear correlation coefficients were computed between the signals from all pairs of regions. It led to an individual-level square 166x166 correlation matrix. We created an adjacency matrix with the same number of edges among participants. To do this, we performed proportional thresholding so that each correlation was retained and set to 1 if superior to that threshold or set to 0 otherwise. We assessed the networks over a wide range of density thresholds (5-20%). Our results were considered robust when they were identical across these different densities. To simplify, we only show the results for a 15% density threshold. This choice was based on priors relative to the known sparsity of the anatomical connections in the human nervous systems [18,20]. The brain connectivity toolbox (brain-connectivity-toolbox.net) [21] was used to calculate the following connectivity measures:

Degree (Deg) represents the number of links connected to a node

$$k_i = \sum_{j \in N} a_{ij}$$

where a_{ij} is the connection status between i and j: $a_{ij} = 1$ when link (i, j) exists (when i and j are neighbors); $a_{ij} = 0$ otherwise.

Local efficiency (Eloc) [22] represents the short-range connectivity and is related to the density of the short-distance connections of the network. Eloc shows the information transfer in the immediate neighborhood of each node

$$Eloc_i = \frac{1}{n}\sum_{i\in N}\frac{\sum_{j,h\in N, j\neq i} a_{ij}a_{ih}\left[d_{jh}(N_i)\right]^{-1}}{k_i(k_i-1)}$$

where $Eloc_i$ is the local efficiency of node i, and $d_{jh}(N_i)$ is the length of the shortest path between j and h that contains only neighbors of i.

Global efficiency (Eglob) [22] of the network

$$E_{glob} = \frac{1}{n}\sum_{i\in N}\frac{\sum_{j\in N, j\neq i} d_{ij}^{-1}}{n-1}$$

where d_{ij} is the shortest path length between nodes i and j.

Betweenness centrality (BCN) [23] represents a measure of 'hubness', and generally speaking corresponds to brain areas that have the highest connectivity and form the core of the brain network

$$BCN_i = \frac{1}{(n-1)(n-2)}\sum_{h,j\in N, h\neq j, h\neq i, j\neq i}\frac{\rho_{hj}(i)}{\rho_{hj}}$$

where ρ_{hj} is the number of shortest paths between h and j, and $\rho_{hj}(i)$ is the number of shortest paths between h and j that pass through i.

We first assessed the global brain reorganization using the hub disruption indexes (κ) [24,25] for Deg, Eloc and BCN. The hub disruption indexes measured the way the network's nodes were radically reorganized in comparison with healthy volunteers, with increased hubness in some regions and decreased hubness in others. To compute κ, we first subtracted the HC group mean network metric of the same node from a patient before we plotted the difference against the HC group mean. κ is the gradient of a straight line fitted to these data. In other words, for each subject and each measure, this gradient was estimated as the slope of the following graph:

$$(Measure_{subject} - Measure_{\mu Controls}) = f(Measure_{\mu Controls})$$

where $\mu Controls$ is the mean value across the whole HC group. Figure 1 illustrates the hub disruption index calculation for both a representative patient and a healthy volunteer. In other words, this metric can be used to compare the behavior of the network of a single subject with respect to a referential network topology (the normative network topology of a healthy control group).

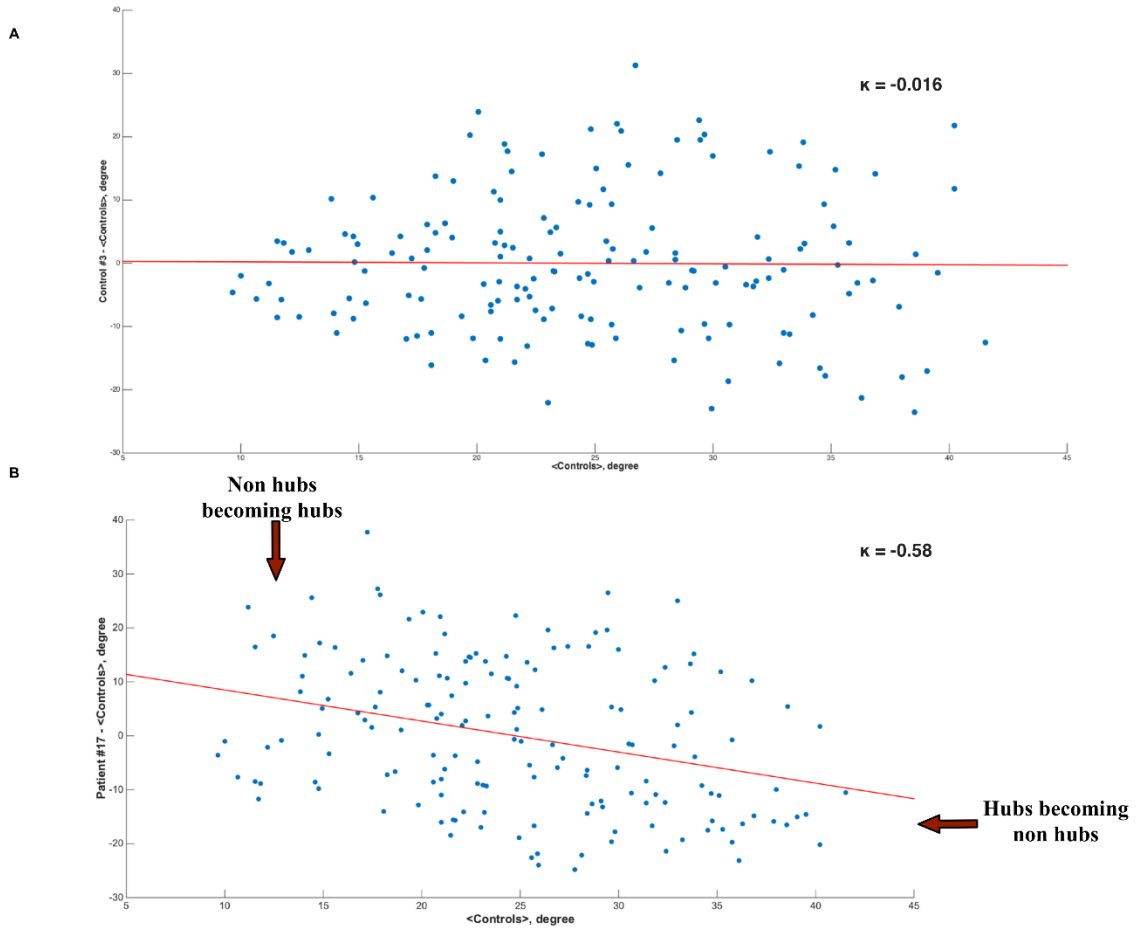

Figure 1. Hub disruption index calculation

Hub disruption index calculation method (of degree) of an individual subject relative to the healthy control group mean for (A) a healthy control subject and (B) a CIS patient subject. To construct the hub disruption index (κ) for the degree, we subtracted the mean degree of the healthy control group for each node from the degree of the corresponding node in an individual subject before plotting this individual difference against the healthy group mean. Each point on this scatterplot represents a node. (κ) is the slope of the red fitted regression line computed on this scatterplot.

Statistical analysis

The statistical analyses were performed using SPSS software version 23.0 (SPSS, Chicago, IL, USA).

Parametric and non-parametric tests were used according to the variables distribution. Normality of the distribution was assessed using the Shapiro-Wilk test. The categorical variables were investigated with χ^2 tests. Cross-sectional comparisons were performed using two sample t-tests (normally distributed data) and Mann-Whitney U tests (non-normal data), while longitudinal comparisons used paired t-tests (normally distributed data) or Wilcoxon tests (non-normal data).

The hub disruption indexes for each metric were investigated using one-sample t-tests. If it was significantly different from zero indicating a global reorganization, a region-wise comparison for the correspondent metric was used to look for the major regions driving this reorganization. This comparison was done using a Mann-Whitney U test and was corrected for multiple comparisons using the false discovery rate (FDR).

The p-value < 0.05 was considered statistically significant.

Results

Clinical and conventional MRI characteristics

The characteristics of PwCIS and HC at both time-points are reported in **Table 1**.

The groups were matched for age, gender and educational level.

In patients, EDSS scores did not change significantly between baseline (median EDSS = 1, range = 0-3) and year 1 (median EDSS = 1, range = 0-5), and T2 lesion volumes (T2 LV) did not differ significantly between baseline (median T2 LV = 0.98 ml, range = 0.02-63.12) and year 1 (median T2 LV = 1.32 ml, range = 0.07-67.74).

Only a moderate cognitive impairment was noticed at baseline, as only the computerized speed cognitive test (CSCT) and the brief visual memory test revised (BVMTR) were altered (see **Table S.1**). This cognitive impairment was no longer observed after 1-year as PwCIS showed no significant differences compared to HC (see **Table S.2**).

Brain network reorganization at baseline

The PwCIS showed significant brain network reorganization, in that the hub disruption indexes for degree and betweenness centrality were significantly negative ($p<0.001$ and $p<0.05$, respectively) (**Figure 2**). However, their global efficiencies were not different compared to the HC (0.525 ± 0.013 vs 0.533 ± 0.012). The hub disruption index of the local efficiency was not significantly different from 0.

Table 1. **Demographic, Clinical, and Conventional MR Imaging Characteristics**

	Baseline		Year 1	
Clinical features	**HC** *(n=19)*	**CIS** *(n=41)*	**HC** *(n=19)*	**CIS** *(n=41)*
Mean age, years *(SD)*[a]	37.8 (8.6)	38.3 (11.2)	-	
Sex ratio *(F/M)*[b]	14/5	32/9		
Converters to clinically definite MS *(%)*	-	-	-	27/41 (66%)
Treatment *Interferon* *Glatiramer acetate* *Dimethyl fumarate* *Fingolimod* *None*	-	-	-	 10 (24%) 5 (12%) 2 (5%) 2 (5%) 22 (54%)
Education level *(high/low*[c]*)*[b]	10/9	26/15	-	
Mean disease duration *(SD) in months*	-	4.12 (1.85)		
Median EDSS score *[range]*[d]	-	1.0 [0-3]	-	1.0 [0-5]
Median T2 Lesion volume *(ml)*[d]	-	0.98 [0.02-63.12]	-	1.32 [0.07-67.74]

[a] Mann-Whitney U test
[b] χ^2 test
[c] Education level was considered as high or low according to a French baccalaureate.
[d] Wilcoxon test to compare PwCIS at baseline and year 1.

Brain network reorganization at 1 year

Functional brain reorganization was still present at the 1-year follow-up in PwCIS, as the hub disruption indexes for degree and betweenness centrality were still significantly negative ($p<0.00001$ for both comparisons) (**Figure 3**). Patients were still able to maintain their global efficiency, as it was not different compared to the controls (0.525 ± 0.017 vs 0.522 ± 0.025). As was the case at baseline, the hub disruption index for local efficiency was not significantly different from 0. When comparing these network parameters between converters to MS and CIS, no significant differences were noticed.

To assess the longitudinal evolution of these hub disruption indexes, a paired t-test comparison was used for degree and betweenness centrality at both time-points. The hub disruption indexes of degree and betweenness centrality were both significantly lower at year 1 compared to baseline (-0.30 ± 0.55 at baseline vs -0.65 ± 0.60 at year 1 for degree, $p < 0.001$; -0.00005 ± 0.00014 at baseline vs -0.0002 ± 0.00014 at year 1 for betweenness centrality, $p < 0.00001$, respectively).

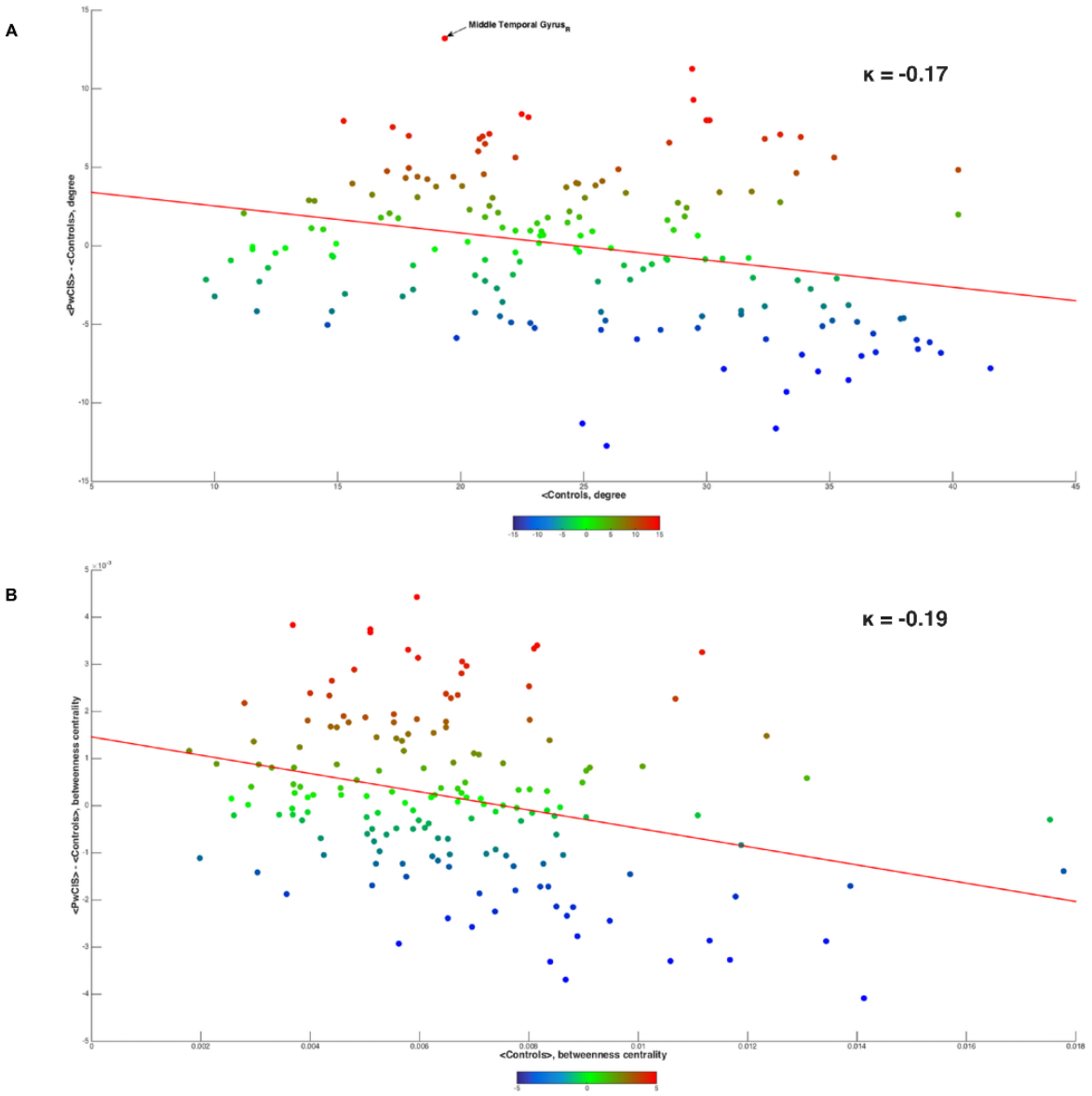

Figure 2. Hub disruption index of PwCIS at baseline

(A) Degree (B) Betweenness centrality

Red denotes increased connectivity measures in the PwCIS compared to HC on average; blue denotes decreased connectivity measures in the PwCIS compared to HC on average.

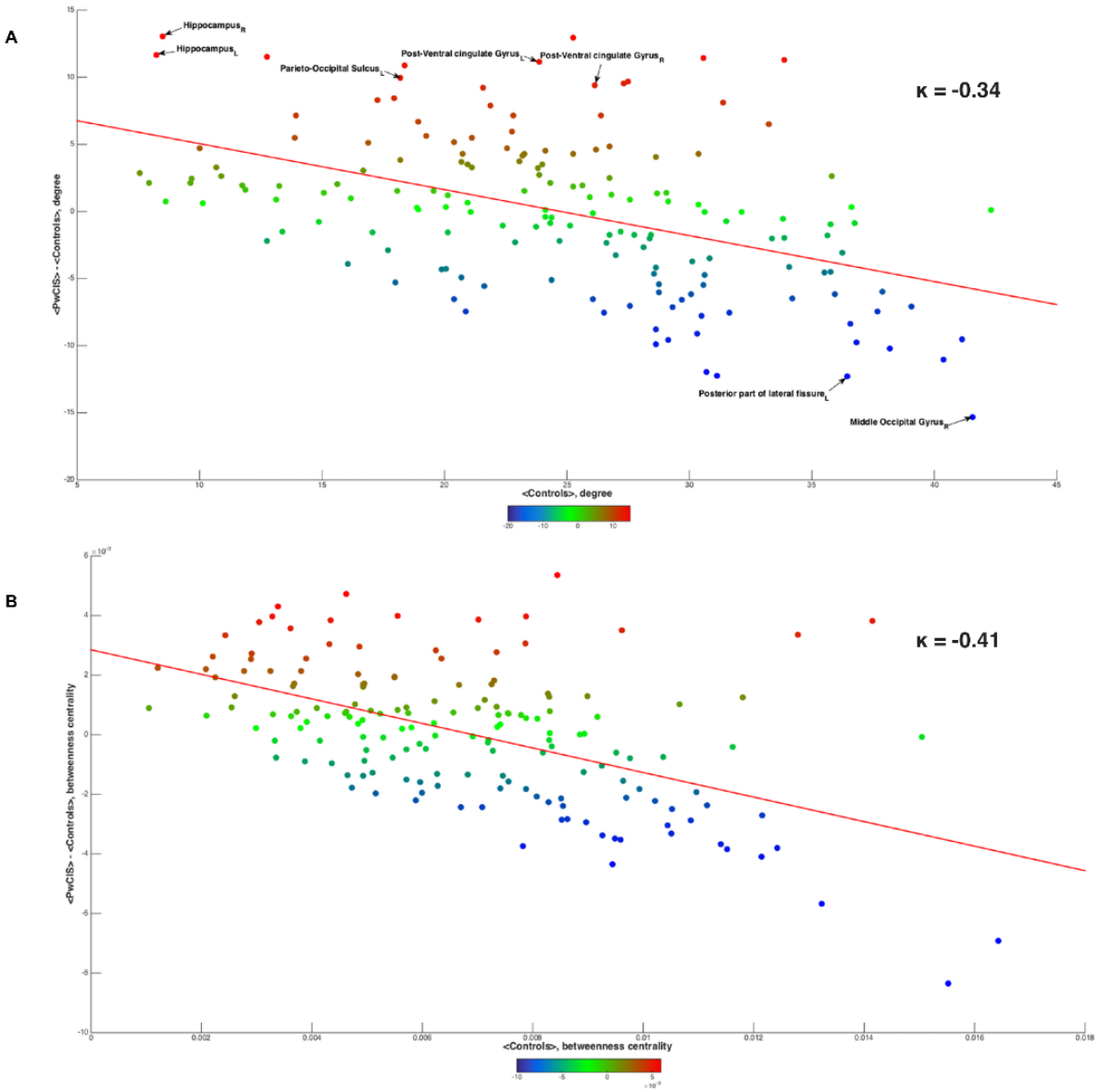

Figure 3. Hub disruption index of PwCIS at 1-year follow-up

(A) Degree (B) Betweenness centrality

Red denotes increased connectivity measures in the PwCIS compared to HC on average; blue denotes decreased connectivity measures in the PwCIS compared to HC on average.

Regional modifications

Both the degree and betweenness centrality showed significantly negative hub disruption indexes at both time-points in PwCIS, indicating global brain reorganization. To assess the major regions driving this reorganization, region-wise comparisons were performed for these two metrics.

To qualitatively assess the topography of the brain network reorganization in PwCIS for both the degree and betweenness centrality, we displayed on surface renderings the regions showing

abnormal connectivity compared to the HC before multiple comparison correction (**Figures 4, 5** and **Table 2**).

In regard to betweenness centrality, no region survived the multiple comparison correction at either time-points.

In regard to degree, the right middle temporal gyrus showed significantly more connections in PwCIS compared to HC at baseline. One year after, the bilateral hippocampus and the post-ventral cingulate gyrus, as well as the left parieto-occipital sulcus, exhibited significantly higher degrees in PwCIS than in controls, while the right middle occipital gyrus and the left posterior segment of the lateral fissure had lower connections.

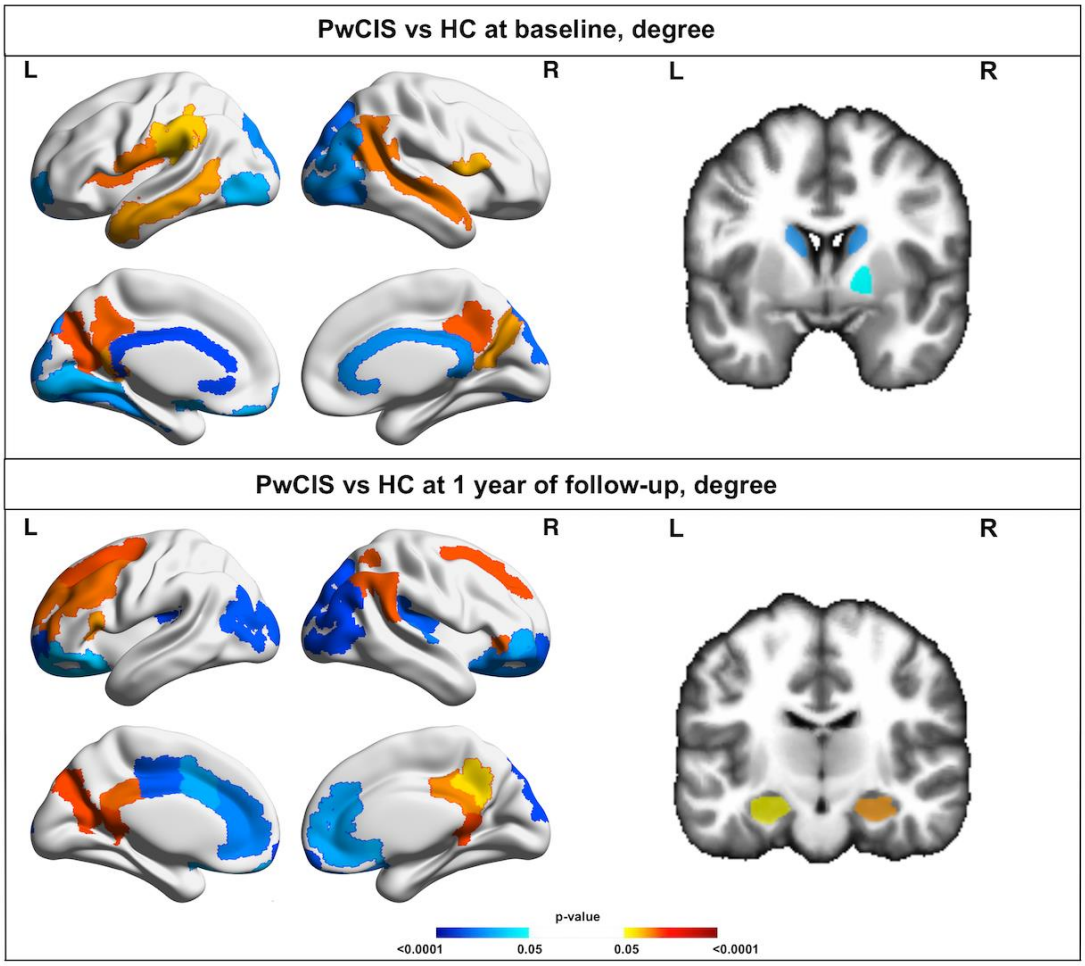

Figure 4. Regional differences in the nodal degree between PwCIS and HC at baseline and 1 year
Red denotes an increased degree in the PwCIS compared to HC; blue denotes a decreased degree in the PwCIS compared to HC.

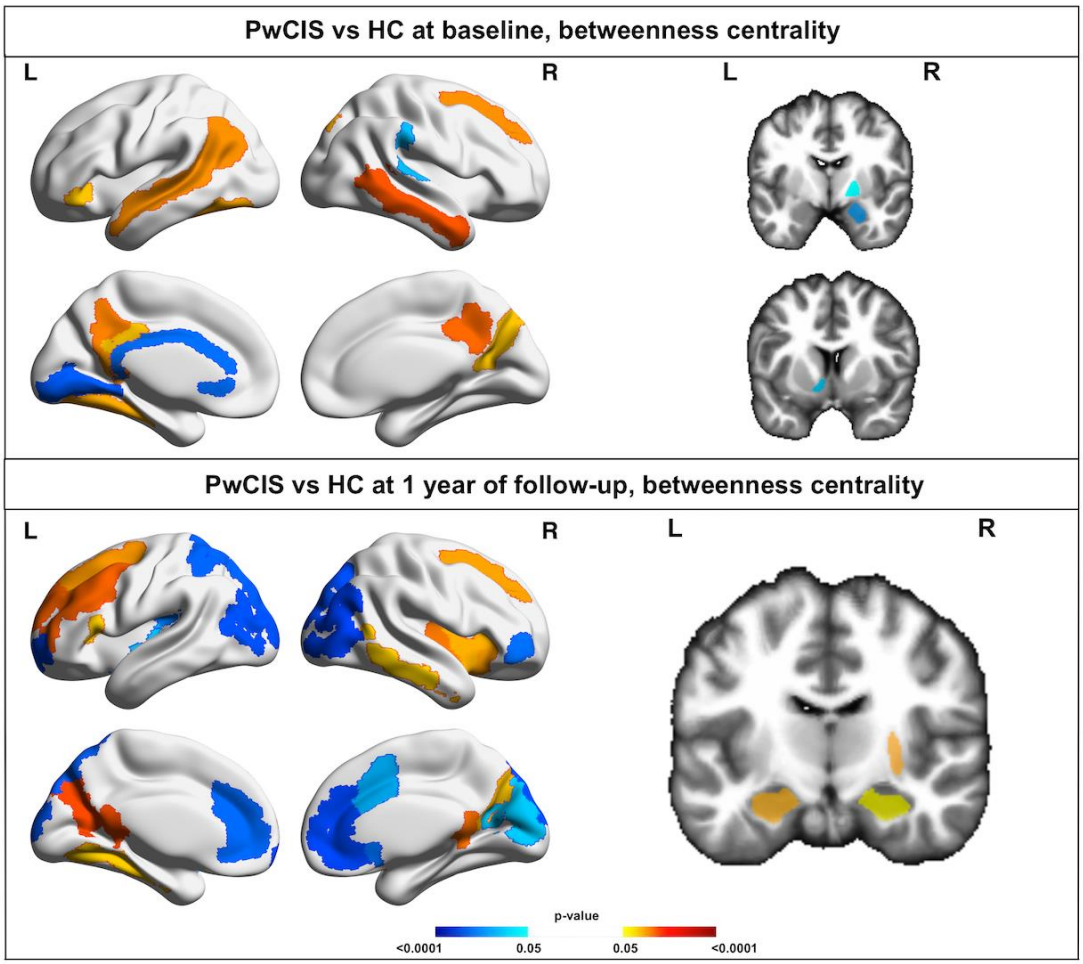

Figure 5. Regional differences of betweenness centrality between the PwCIS and HC at baseline and 1 year

Red denotes increased betweenness centrality in the PwCIS compared to HC; blue denotes decreased betweenness centrality in the PwCIS compared to HC.

Hub disruption index and clinical outcomes

To assess whether brain reorganization at this stage of the disease is related to disability (EDSS) or to the patient's lesion load (LL), the hub disruption indexes of degree and betweenness centrality were correlated to EDSS scores and LL using the Spearman rank correlation coefficient. Both the EDSS scores and LL did not show any significant correlations with the altered hub disruption indexes, either at baseline or 1-year after.

Then, Pearson correlation was used between altered cognitive tests and corresponding hub disruption indexes. Hub disruption index of betweenness centrality was observed to be correlated to delayed recall of the BVMTR (BVMTR-DR) as $r = -0.32$ and $p<0.05$ at 1-year. This indicates a more pronounced brain network reorganization as the cognitive performances are getting better.

Discussion

In the current study, we investigated, for the first time, the longitudinal topological reorganization of functional brain networks in PwCIS. We found that brain network reorganization began at the onset of the disease and evolved over the first year. However, global brain function preservation and normal cognitive performances indicate here a compensatory mechanism that is effective over this one year follow-up.

At baseline, we noticed the first hubness reorganization as the hub disruption indexes for both degree and betweenness centrality were significantly negative in PwCIS, which indicated a combination of underconnected and overconnected brain regions. This was mainly driven by an increased degree, which indicated the development of new connections, in the right middle temporal gyrus in PwCIS compared to HC. At this stage, the global efficiency of the brain in the PwCIS was still normal compared to HC, and PwCIS had only a moderate cognitive alteration at this stage. One year later, this brain network reorganization was even more pronounced. The hub disruption indexes for degree and betweenness centrality were significantly negative in the PwCIS but were also significantly lower than their baseline values, indicating an increased reorganization. Regionally, this reorganization was characterized by an increased degree in the bilateral hippocampus, the bilateral posterior cingulate gyrus and the left parieto-occipital sulcus. On the other hand, a decreased degree was observed in the right middle occipital gyrus and the left posterior segment of the lateral fissure. A preserved global efficiency with normal cognitive performances suggests a compensatory mechanism at this early stage, a hypothesis which was also sustained by the association of better visuo-spatial episodic memory performances with more pronounced brain network reorganization.

A few cross-sectional studies have assessed functional brain reorganization in CIS. Using a relatively small population of 14 CIS with a median disease duration of 1.4 years, Roosendaal et al. (2010)[27] observed increased functional synchronization in the posterior cingulate gyrus in CIS patients, as well as in other resting-state networks (the executive function network, attention system and sensorimotor function network). Recently, Liu et al. (2016)[14] investigated a population of 34 CIS with shorter disease duration (median disease duration of 1 month) and found a decrease in the nodal efficiency of the left rolandic operculum in CIS, which was in line with our findings of a decrease in the degree in the left posterior part of the lateral fissure. They also showed a

decrease in the nodal efficiency of the insula and the superior temporal gyrus. These heterogeneous findings may be due to the inclusion of different sample sizes, disease durations or disability levels. In clinically definite MS after years of evolution, increased functional connectivity was detected as a possible compensatory mechanism,[4,6,10,11,17,28] while, decreased functional connectivity as a probable consequence of maladaptive reorganization due to acute or chronic inflammation, was also detected.[6,11,17]

All together, these results suggested network alterations predominantly in the sensorimotor cortex, cingulate and fronto-temporal regions, as well as in the thalamus.[6,10,11,17]

Furthermore, most studies have been performed cross-sectionally, which limits the understanding of the dynamics of brain network reorganization in MS and, more specifically, at the first stages of the disease. In the only longitudinal study performed in RRMS patients, Faivre et al. (2016)[18] reported higher nodal and local efficiencies in patients than in controls at baseline. Two years later, these values decreased and were no longer different from controls, suggesting a primary compensatory mechanism followed by a brain functional connectivity depletion as the disease progresses.

Functional connectivity changes can be associated with a compensatory mechanism, as well as with maladaptive network rearrangements due to the loss of different large-scale cortical dynamics or the expression of between-network vulnerability.[29–31] A recent study showed the complex involvement of functional connectivity alterations, as they can be seen as compensatory but are not limited to that.[32] For example, an attempt to compensate after an acute lesion was shown,[33] while increased functional connectivity in CIS without conventional brain lesions was also associated to a high risk to develop MS.[34] In our case, the global efficiency preservation of our CIS population relative to HC and their normal cognitive performances, indicating normal brain functioning, suggest a compensatory mechanism at this early stage of the disease. This finding is in line with a task fMRI study in PwCIS, showing improvements in the patients' PASAT scores depending on their ability to recruit more compensatory mechanisms involving the right lateral prefrontal cortices (LPFC) [35].

This current study was not without limitations. The examination of network characteristics might have been influenced by the choice in the parcellation scheme.[36] Even though the organizational principles of functional brain networks seem to be independent of the selected parcellation method, our quantitative measures might have been modulated. Also, nonstationarity of brain connections

is often disregarded as it is the case in our study, only the most robust effects in the steady state are captured. This leaves unknown transient states in network connectivity that may better explain how brain networks adapt to challenge and disruption.[37]

In conclusion, the current study demonstrated, longitudinal brain network reorganization in patients with CIS. The pattern of functional connectivity reorganization remains the same during the first year after CIS but tends to be more pronounced at one year. In patients, regional reorganization of the connectivity was associated with the maintenance of normal global efficiency in the brain and normal cognitive and functional (EDSS) performances suggesting a compensatory effect. These findings provided new insights into the understanding of the underlying mechanisms and evolution of the disease. Further follow-ups with this cohort will be analyzed in order to generate a long-term model of brain network reorganization in MS.

Acknowledgments: The authors thank the neurologists of the AQUISEP network for their involvement in recruiting patients. The authors thank Dr. JC Ouallet, Dr. A Moroso and Dr. P Louiset for referring patients to the study. This work has been performed with the help of the French Observatoire of Multiple Sclerosis (OFSEP), which is supported by a grant provided by the French State and handled by the "AgenceNationale de la Recherche," within the framework of the "Investments for the Future" program, under the reference ANR-10-COHO-002.

Funding: This study was supported by ANR-10-LABX-57 Translational Research and Advanced Imaging Laboratory (TRAIL), laboratory of excellence. The SCICOG study was also supported by a grant from Teva and ARSEP (Fondation ARSEP pour la recherche sur la sclérose en plaques).

Disclosures:

Ismail Koubiyr – PhD grant from TRAIL.

Mathilde Deloire – Nothing to disclose.

Pierre Besson – Nothing to disclose.

Pierrick Coupé – Nothing to disclose.

Cécile Dulau – received a speaker fee from BIOGEN.

Jean Pelletier – reports consulting fees and travels from Biogen, Sanofi-Genzyme, Novartis, Teva, Merck-Serono, Roche, Medday and unconditional research grants from Biogen, Novartis, Roche and Merck-Serono.

Thomas Tourdias – Nothing to disclose.

Bertrand Audoin – Nothing to disclose.

Bruno Brochet – Pr Brochet has received consultancy fees, speaker fees, research grants (non-personal), or honoraria from Novartis, BiogenIdec, Merck, Bayer Schering, Roche, Medday, Bayer, Actelion, Teva and Genzyme Sanofi outside the submitted study.

Jean Philippe Ranjeva – Nothing to disclose.

Aurélie Ruet – has received consultancy fees, speaker fees, research grants (nonpersonal), or honoraria from Novartis, BiogenIdec, Roche, Teva and Merck outside the submitted study.

References

1. Polman CH, Reingold SC, Banwell B, et al. Diagnostic criteria for multiple sclerosis: 2010 Revisions to the McDonald criteria. *Ann Neurol* 2011; 69: 292–302.
2. Zipp F, Gold R, Wiendl H. Identification of Inflammatory Neuronal Injury and Prevention of Neuronal Damage in Multiple Sclerosis. *JAMA Neurol*. Epub ahead of print 21 October 2013. DOI: 10.1001/jamaneurol.2013.4391.
3. Basile B, Castelli M, Monteleone F, et al. Functional connectivity changes within specific networks parallel the clinical evolution of multiple sclerosis. *Mult Scler J* 2014; 20: 1050–1057.
4. Dogonowski AM, Siebner HR, Soelberg Sørensen P, et al. Resting-state connectivity of pre-motor cortex reflects disability in multiple sclerosis. *Acta Neurol Scand* 2013; 128: 328–335.
5. Gamboa OL, Tagliazucchi E, Von Wegner F, et al. Working memory performance of early MS patients correlates inversely with modularity increases in resting state functional connectivity networks. *Neuroimage* 2014; 94: 385–395.
6. Rocca MA, Valsasina P, Meani A, et al. Impaired functional integration in multiple sclerosis: a graph theory study. *Brain Struct Funct* 2016; 221: 115–131.
7. Pantano P, Iannetti GD, Caramia F, et al. Cortical motor reorganization after a single clinical attack of multiple sclerosis. *Brain* 2002; 125: 1607–1615.
8. Mainero C, Caramia F, Pozzilli C, et al. fMRI evidence of brain reorganization during attention and memory tasks in multiple sclerosis. *Neuroimage* 2004; 21: 858–867.
9. Audoin B, Van Au Duong M, Ranjeva JP, et al. Magnetic resonance study of the influence of tissue damage and cortical reorganization on PASAT performance at the earliest stage of multiple sclerosis. *Hum Brain Mapp* 2005; 24: 216–228.
10. Faivre A, Rico A, Zaaraoui W, et al. Assessing brain connectivity at rest is clinically relevant in early multiple sclerosis. *Mult Scler J* 2012; 18: 1251–1258.
11. Schoonheim MM, Geurts JJG, Wiebenga OT, et al. Changes in functional network centrality underlie cognitive dysfunction and physical disability in multiple sclerosis. *Mult Scler J* 2014; 20: 1058–1065.
12. Meijer KA, Eijlers AJC, Geurts JJG, et al. Staging of cortical and deep grey matter functional connectivity changes in multiple sclerosis. *J Neurol Neurosurg Psychiatry* 2017; 0: jnnp-2017-316329.
13. Bullmore E, Sporns O. Complex brain networks: graph theoretical analysis of structural and functional systems. *Nat Rev Neurosci* 2009; 10: 312–312.
14. Liu Y, Wang H, Duan Y, et al. Functional Brain Network Alterations in Clinically Isolated Syndrome and Multiple Sclerosis: A Graph-based Connectome Study. *Radiology* 2016; 000: 152843.
15. Shu N, Duan Y, Xia M, et al. Disrupted topological organization of structural and functional brain connectomes in clinically isolated syndrome and multiple sclerosis. *Sci Rep* 2016; 6: 29383.
16. Fleischer V, Radetz A, Ciolac D, et al. Graph theoretical framework of brain networks in multiple sclerosis: A review of concepts. *Neuroscience*. Epub ahead of print 2017. DOI: 10.1016/j.neuroscience.2017.10.033.
17. Eijlers AJC, Meijer KA, Wassenaar TM, et al. Increased default-mode network centrality in cognitively impaired multiple sclerosis patients. *Neurology* 2017; 88: 952–960.

18. Faivre A, Robinet E, Guye M, et al. Depletion of brain functional connectivity enhancement leads to disability progression in multiple sclerosis: A longitudinal resting-state fMRI study. *Mult Scler J* 2016; 22: 1695–1708.
19. Yeo T, Buckner R. The organization of the human cerebral cortex estimated by intrinsic functional connectivity. *J Neurophysiol*. 2011.
20. Achard S, Salvador R, Whitcher B, et al. A Resilient, Low-Frequency, Small-World Human Brain Functional Network with Highly Connected Association Cortical Hubs. *J Neurosci* 2006; 26: 63–72.
21. Rubinov M, Sporns O. Complex network measures of brain connectivity: Uses and interpretations. *Neuroimage* 2010; 52: 1059–1069.
22. Latora V, Marchiori M. Efficient Behavior of Small-World Networks. *Phys Rev Lett* 2001; 87: 198701.
23. Freeman LC. Centrality in social networks conceptual clarification. *Soc Networks* 1978; 1: 215–239.
24. Termenon M, Achard S, Jaillard A, et al. The 'Hub Disruption Index', a reliable index sensitive to the brain networks reorganization. A study of the contralesional hemisphere in stroke. *Front Comput Neurosci* 2016; 10: 84.
25. Achard S, Delon-Martin C, Vertes PE, et al. Hubs of brain functional networks are radically reorganized in comatose patients. *Proc Natl Acad Sci* 2012; 109: 20608–20613.
26. Roosendaal SD, Schoonheim MM, Hulst HE, et al. Resting state networks change in clinically isolated syndrome. *Brain* 2010; 133: 1612–1621.
27. Roosendaal SD, Schoonheim MM, Hulst HE, et al. Resting state networks change in clinically isolated syndrome. *Brain* 2010; 133: 1612–1621.
28. Tewarie P, Schoonheim MM, Schouten DI, et al. Functional brain networks: Linking thalamic atrophy to clinical disability in multiple sclerosis, a multimodal fMRI and MEG Study. *Hum Brain Mapp* 2015; 36: 603–618.
29. Schoonheim MM, Geurts JJG, Barkhof F. The limits of functional reorganization in multiple sclerosis. *Neurology* 2010; 74: 1246–1247.
30. Tona F, Petsas N, Sbardella E, et al. Multiple sclerosis: Altered Thalamic Resting-State Functional Connectivity and Its Effect on Cognitive Function 1. *Radiology*. 2014
31. Hawellek DJ, Hipp JF, Lewis CM, et al. Increased functional connectivity indicates the severity of cognitive impairment in multiple sclerosis. *Proc Natl Acad Sci* 2011; 108: 19066–19071.
32. Castellazzi G, Debernard L, Melzer TR, et al. Functional Connectivity Alterations Reveal Complex Mechanisms Based on Clinical and Radiological Status in Mild Relapsing Remitting Multiple Sclerosis. *Front Neurol* 2018; 9: 1–15.
33. Droby A, Yuen KSL, Muthuraman M, et al. Changes in brain functional connectivity patterns are driven by an individual lesion in MS: a resting-state fMRI study. *Brain Imaging Behav* 2016; 10: 1117–1126.
34. Liu Y, Dai Z, Duan Y, et al. Whole brain functional connectivity in clinically isolated syndrome without conventional brain MRI lesions. *Eur Radiol* 2016; 26: 2982–2991.
35. Audoin B, Reuter F, Duong MVA, et al. Efficiency of cognitive control recruitment in the very early stage of multiple sclerosis: A one-year fMRI follow-up study. *Mult Scler* 2008; 14: 786–792.
36. de Reus MA, van den Heuvel MP. The parcellation-based connectome: Limitations and extensions. *Neuroimage* 2013; 80: 397–404.

37. Hillary FG, Roman CA, Venkatesan U, et al. Hyperconnectivity is a fundamental response to neurological disruption. *Neuropsychology* 2015; 29: 59–75.

Supplementary material

Neuropsychological assessment

We evaluated each cognitive domain with the following tests:

- Attention: Test of Attentional Performance (TAP)[1] consisting of subtests for reaction times (RT) of visual scanning, auditory attention and visual and auditory divided attention. For divided attention, reaction time ratios of the double task (auditory and visual divided attention) to the simple task (auditory or visual attention) was considered.
- Working memory: Paced-Auditory Serial Addition Test-3 s (PASAT).[2]
- Episodic memory: Selective Reminding Test (SRT),[3] which tested verbal memory (three subscores: SRT-LTS=long-term storage; SRT-CLTR=consistent long-term retrieval; SRT-DR=delay recall). Brief Visual Memory Test Revised (BVMTR)[4] for episodic visuo-spatial memory (two subscores: BVMTR=learning; BVMTR-DR=delay recall).
- Executive functions: Stroop test[3] (inhibition task scores) and Word List Generation test[3] (verbal fluency assessment).
- Information processing speed (IPS): Computerised Speed Cognitive Test (CSCT)[5] which is an IPS, a computerised digit-symbol substitution task [6] and alertness (with and without warning).

Cognitive status was assessed by z-scores for each test and for both groups (PwCIS and HC) at each time-point to avoid test-retest effect. In order to have a more powerful approach, norms from two in-house studies involving large datasets of HC (N=404 and N=276) were used. Sixteen groups were established according to four age categories (18–34, 34–44, 45–54 and ≥ 55), gender and level of education (low education level (LEL) was below secondary education, which is usually 12 years of schooling; high education level (HEL) was above secondary education, or graduated at least at a “baccalauréat” level of college degree).

For the cognitive comparison, all of our patients (41 patients) were compared to the initial healthy control group (55 healthy controls) as they all had the neuropsychological assessment.

Table S1: Cognitive performances of clinically isolated syndrome patients and healthy controls at baseline

	HC	CIS	P-value
CSCT	**0.25 (0.87)**	**-0.25 (1.1)**	**0.04**
BVMTR	**0.53 (0.8)**	**0.01 (0.97)**	**0.006**
BVMTR-DR	**0.53 (0.53)**	**-0.11 (1.04)**	**0.003**
PASAT	0.16 (0.94)	0.12 (1.05)	0.93
SRT-LTS	0.42 (1.02)	0.29 (0.93)	0.48
SRT-CLTR	0.34 (1.05)	0.23 (1.07)	0.59
SRT-DR	0.32 (0.69)	0.20 (0.92)	0.95
WLG	-0.30 (0.73)	-0.58 (0.76)	0.07
Alertness	0.49 (0.69)	0.21 (2.55)	0.29
RT_Simple_Visual_Attention	0.24 (0.97)	-0.13 (1.21)	0.43
RT_Simple_Auditory_Attention	0.15 (1.03)	0.16 (1.04)	0.52
RT_Divided_Visual_Attention	-0.51 (1.54)	-0.15 (1.18)	0.28
RT_Divided_Auditory_Attention	-0.04 (1.26)	-0.26 (1.23)	0.31
Stroop	0.03 (0.88)	0.23 (0.84)	0.28

HC: healthy controls; CIS: clinically isolated syndrome; CSCT: computerized speed cognitive test; BVMTR: brief visual memory test revised; DR: delay recall; PASAT: paced auditory serial addition test; SRT: selective reminding test; LTS: long-term storage; CLTR: consistent long-term retrieval; WLG: word list generation; RT: reaction time.

Table S2: Cognitive performances of clinically isolated syndrome patients and healthy controls at 1-year

	HC	CIS	P-value
CSCT	0.43 (1.18)	0.02 (1.04)	0.09
BVMTR	0.44 (0.72)	0.39 (0.89)	0.91
BVMTR-DR	0.22 (0.77)	0.15 (0.89)	0.69
PASAT	0.39 (0.8)	0.36 (0.91)	0.94
SRT-LTS	0.38 (0.75)	0.26 (1.16)	0.65
SRT-CLTR	0.27 (0.98)	0.31 (1.1)	0.85
SRT-DR	0.15 (0.88)	-0.04 (1.06)	0.84
WLG	-0.24 (0.96)	-0.19 (0.98)	0.81
Alertness	0.68 (0.61)	0.25 (1.2)	0.17
RT_Simple_Visual_Attention	0.27 (1.01)	-0.05 (1.1)	0.16
RT_Simple_Auditory_Attention	0.30 (0.91)	-0.07 (1.16)	0.13
RT_Divided_Visual_Attention	0.08 (1.22)	-0.09 (1.27)	0.80
RT_Divided_Auditory_Attention	-0.11 (1.17)	-0.003 (1.33)	0.96
Stroop	0.19 (0.99)	0.35 (1.1)	0.46

HC: healthy controls; CIS: clinically isolated syndrome; CSCT: computerized speed cognitive test; BVMTR: brief visual memory test revised; DR: delay recall; PASAT: paced auditory serial addition test; SRT: selective reminding test; LTS: long-term storage; CLTR: consistent long-term retrieval; WLG: word list generation; RT: reaction time.

MRI acquisition

The MRI acquisition was performed on a 3T MRI system (Achieva TX system, Philips Healthcare, Best, The Netherlands; Signa, GE Healthcare, Discovery MR 750w, Milwaukee, Wisconsin). Resting-state fMRI has been shown to be a reliable imaging marker in multicenter imaging studies as it showed good inter-vendor reliabilities.[7] The acquisition protocol was harmonized between the magnets and consisted of a three-dimensional (3D) T1-weighted sequence using magnetization prepared rapid gradient echo (MP-RAGE) imaging (TR=8.2 ms, TE=3.5 ms, TI=982 ms, α=7°, FOV=256 mm, voxel size=1 mm^3, and 180 slices), a two-dimensional (2D) FLAIR sequence (TR=11000 ms, TE=140 ms, TI=2800 ms, FOV=230 mm, 45 axial slices, and 3-mm thick). Additionally, resting-state functional MRI was obtained with an echo-planar imaging (EPI) sequence (250 volumes, 40 axial slices, TR=2200 ms, TE=30 ms, 3x3-mm in-plane resolution, and slice thickness=3 mm). The first four volumes of the functional run were discarded to achieve steady-state magnetization.

fMRI preprocessing

Using Statistical Parametric Mapping (SPM12, www.fil.ion.ucl.ac.uk/spm), we followed the same fMRI preprocessing that was used in a previous study [8]. Briefly, the constant offset and linear trend over each run were removed and a low-pass temporal filter with a 0.08 Hz cut-off was used, and data were slice time corrected. Sources of spurious variance, as well as their temporal derivatives, were removed through linear regression, including the following: 1) six parameters obtained via correction of rigid body head motion, 2) the signal averaged over the whole brain, 3) the signal averaged over the ventricles, and 4) the signal averaged over the deep cerebral white matter. This regression procedure contributes to the minimization of signal contributions of non-neuronal origin, including respiration-induced signal fluctuations [9]. Registration between the fMRI and the 3D T1 sequences was performed through the use of boundary-based registration and visually checked.

Structural preprocessing and regions of interest

Lesions were segmented on FLAIR data using the Lesion Segmentation Tool (LST) version 2.0.15 (http://www.applied-statistics.de/lst.html) in SPM12. Then, they were manually corrected by two

blinded experts (IK and CD). Using these maps, a lesion filling algorithm[10] was applied to the T1-weighted images in order to avoid that the lesions affect brain tissue segmentations.

The structural data were preprocessed with the FreeSurfer (v5.3) image analysis suite, which is documented and freely available online (http://surfer.nmr.mgh.harvard.edu) [11]. The brain was separated into regions of interest (ROIs) using a custom-made atlas. The cortical atlas was derived from the Destrieux cortical atlas [12], which is based on a parcellation scheme that first divides the cortex into gyral and sulcal regions, the limit between both being given by the curvature value of the surface. Deep gray matter (DGM) structures (i.e., the thalamus, hippocampus, pallidus, accumbens, putamen, caudate and amygdala), the cerebellar cortex and the ventral diencephalon (DC), as segmented by FreeSurfer, were also included as ROIs. The complete atlas was then coregistered to each participant's fMRI scan with the inverted boundary-based registration matrix and nearest-neighbor interpolation. The final atlas then segmented the fMRI scan into 83 regions per hemisphere, of which the mean time series were derived.

References

1. Zimmermann P, Fimm B. Test for attentional performance (TAP). *PsyTest, Herzogenrath*. 1995:76-77. doi:10.1017/CBO9781107415324.004
2. Gronwall DMA. Paced Auditory Serial-Addition Task: A Measure of Recovery from Concussion. *Percept Mot Skills*. 1977;44(2):367-373. doi:10.2466/pms.1977.44.2.367
3. Ruet A, Deloire M, Charre-Morin J, Hamel D, Brochet B. Cognitive impairment differs between primary progressive and relapsing-remitting MS. *Neurology*. 2013;80(16):1501-1508. doi:10.1212/WNL.0b013e31828cf82f
4. Benedict RHB. The Brief Visuospatial Memory Test - Revised. *Psychol Assess*. 1997;(2):145-153. doi:10.1037/1040-3590.8.2.145
5. Ruet A, Deloire MS, Charré-Morin J, Hamel D, Brochet B. A new computerised cognitive test for the detection of information processing speed impairment in multiple sclerosis. *Mult Scler J*. 2013;19(12):1665-1672. doi:10.1177/1352458513480251
6. Smith A. The Symbol-Digit Modalities Test: A neuropsychologic test for economic screening of learning and other cerebral disorders. *Learn Disord*. 1968;3:83-91.
7. An HS, Moon WJ, Ryu JK, et al. Inter-vender and test-retest reliabilities of resting-state functional magnetic resonance imaging: Implications for multi-center imaging studies. *Magn Reson Imaging*. 2017;44:125-130. doi:10.1016/j.mri.2017.09.001
8. Yeo T, Buckner R. The organization of the human cerebral cortex estimated by intrinsic functional connectivity. *J Neurophysiol*. 2011. http://jn.physiology.org.gate2.inist.fr/content/jn/106/3/1125.full.pdf. Accessed May 23, 2017.
9. Van Dijk KRA, Hedden T, Venkataraman A, Evans KC, Lazar SW, Buckner RL. Intrinsic Functional Connectivity As a Tool For Human Connectomics: Theory, Properties, and Optimization. *J Neurophysiol*. 2010;103(1):297-321. doi:10.1152/jn.00783.2009

10. Prados F, Cardoso MJ, Kanber B, et al. A multi-time-point modality-agnostic patch-based method for lesion filling in multiple sclerosis. *Neuroimage*. 2016;139:376-384. doi:10.1016/j.neuroimage.2016.06.053
11. Dale AM, Fischl B, Sereno MI. Cortical surface-based analysis: I. Segmentation and surface reconstruction. *Neuroimage*. 1999;9(2):179-194. doi:10.1006/nimg.1998.0395
12. Destrieux C, Fischl B, Dale A, Halgren E. Destrieux C, et al 2010 Automatic parcellation of human cortical gyri and sulci using standard anatomical nomenclature supplemental. *Neuroimage*. 2010;53(1):1-15. doi:10.1016/j.neuroimage.2010.06.010

Chapter 4

Dynamic structural-functional coupling alterations in early MS

Summary page

Rationale: We have demonstrated in Chapter 3 early dynamic brain functional reorganization following a clinically isolated syndrome (CIS). These modifications were associated with the preservation of cognitive performances. However, little is known about how these functional alterations are related to structural connectivity. In this chapter, we aim to investigate the association between structural and functional connectivity to better understand the pathophysiological changes underlying cognitive functioning in early MS.

Summary of the methods: Patients with CIS (PwCIS) and healthy controls (HC)were followed for 1 year and underwent both resting-state functional MRI and diffusion tensor imaging (DTI), along with an extensive neuropsychological battery. Graph theory measures were used to characterize both structural and functional networks, and structural-functional coupling was used to represent the association between these two modalities. This analysis was done at both the whole-brain and the modular level.

Main results: We first showed structural reorganization at baseline with an increase in the clustering coefficient in PwCIS compared to HC, as well as modular-level alterations. After one year of follow-up, both structural and functional reorganization was present with abnormal modular-level connections and a global increase of the functional betweenness centrality in patients compared to controls. Moreover, structural–functional decoupling was observed in the salience, visual, and somatomotor networks. These alterations were present along with preserved cognitive performances at this stage.

Comments: We demonstrated structural damage preceding functional reorganization at a global and modular level during the first year following CIS. Preserved cognitive performances were present along global brain functional reorganization (as it was also shown in Chapter 3) suggesting

a compensation mechanism at this stage of the disease. Importantly, the structural–functional decoupling observed for the first time in MS suggests that this functional reorganization occurs along indirect anatomical pathways.

Dynamic modular-level alterations of structural–functional coupling in clinically isolated syndrome

Ismail Koubiyr[1,2], Pierre Besson[3,4], Mathilde Deloire[5], Julie Charre-Morin[5], Aurore Saubusse[5], Thomas Tourdias[1,2,5], Bruno Brochet[1,2,5], Aurélie Ruet[1,2,5]

[1] Univ. Bordeaux, F-33000 Bordeaux, France

[2] Inserm U1215 - Neurocentre Magendie, F-33000 Bordeaux, France

[3] Department of Radiology, Northwestern University, Feinberg School of Medicine, Chicago, IL

[4] Department of Neurological Surgery, Northwestern University, Feinberg School of Medicine, Chicago, IL

[5] CHU de Bordeaux, F-33000 Bordeaux, France

Brain (2019) doi: 10.1093/brain/awz270

Abstract

Structural and functional connectivity abnormalities have been previously reported in multiple sclerosis. However, little is known about how each modality evolution relates to the other. Recent studies in other neurological disorders have suggested that structural–functional coupling may be more sensitive in detecting brain alterations than any single modality. Accordingly, this study aimed to investigate the longitudinal evolution of structural–functional coupling, both at the global and modular levels, in the first year following clinically isolated syndrome. We hypothesized that during the course of multiple sclerosis, patients exhibit a decoupling between functional and structural connectivity due to the disruptive nature of the disease.

Forty-one consecutive patients with clinically isolated syndrome were prospectively enrolled in this study, along with 19 age-, sex- and educational level-matched healthy controls. These participants were followed for one year and underwent resting-state functional magnetic resonance imaging and diffusion tensor imaging at each time-point, along with an extensive neuropsychological assessment.

Graph theory analysis revealed structural reorganization at baseline that appeared as an increase in the clustering coefficient in patients compared to controls ($P < 0.05$), as well as modular-specific alterations. After one year of follow-up, both structural and functional reorganization was depicted with abnormal modular-specific connectivity and an increase of the functional betweenness centrality in patients compared to controls ($P < 0.01$). More importantly, structural–functional decoupling was observed in the salience, visual, and somatomotor networks. These alterations were present along with preserved cognitive performance at this stage.

These results depict structural damage preceding functional reorganization at a global and modular level during the first year following clinically isolated syndrome along with normal cognitive performance, suggesting a compensation mechanism at this stage of the disease. Principally, structural–functional decoupling observed for the first time in multiple sclerosis suggests that functional reorganization occurs along indirect anatomical pathways.

Key words: multiple sclerosis, clinically isolated syndrome, functional MRI, diffusion tensor imaging, graph theory

Introduction

Clinically isolated syndrome (CIS) is a single neurological episode that may be suggestive of multiple sclerosis (MS).[1] Most patients with CIS (PwCIS) will further progress to definite MS.[2] The underlying pathology of MS is characterized by inflammation, demyelination, axonal injury, and axonal loss leading to a disruption of long- and short-range connections.[3] However, the brain is a complex network of structurally and functionally interconnected regions; thus, it is essential to study its topology to better understand pathology.[4] Diffusion tensor imaging (DTI) can map the structural connectivity (SC) between gray matter (GM) regions using white matter (WM) tractography, while functional connectivity (FC) examines synchronization in activity between different GM regions. Abnormalities in both modalities have been previously depicted in patients with both CIS and MS.[5] However, the lack of multimodal studies using structural and functional imaging in early MS makes it challenging to understand the pathophysiological processes occurring at this stage of the disease. A combination of these modalities may help bridge the gap between pathophysiological changes and clinical symptoms. SC and FC networks provide a different perspective of brain functioning. However, there is still a poor understanding of how each connectivity evolution relates to the other. Hence, simultaneously assessing SC and FC may provide complementary views of the brain and enhance our understanding of the disease evolution. Most network studies in patients with MS focus only on a single modality to explore the connectivity, and most have a cross-sectional design that may be insufficient to describe the pathological changes due to the disease. To that end, studies must combine structural and FC networks in a longitudinal setting to better understand pathological mechanisms in the brain. FC has been shown to be shaped and constrained by the underlying anatomy[6] and should provide information close to that obtained from SC. On the other hand, recent studies exploring neurological disorders other than MS have showed that the structural–functional (SC-FC) coupling, which represents the association between FC and SC, allows the detection of more subtle brain alterations than any single imaging modality.[7–9] Whether the SC-FC coupling could also be altered early in the course of MS is currently unknown.

The brain presents a modular structure with networks of densely interconnected regions, which are more sparsely connected with regions in other networks.[10,11] Recent studies have observed modular-specific alterations in patients with CIS and MS in both structural and functional networks,[12–16] suggesting that modular-related properties may be more sensitive than whole-brain

and nodal properties in reflecting brain abnormalities. We have previously reported functional reorganization, especially one year after CIS, by depicting a combination of underconnected and overconnected brain regions using the hub disruption index.[17] This allowed us to demonstrate global brain functional reorganization at this stage of the disease. However, the current study moves beyond the previous one, and intends to investigate both structural and functional connectivity evolution during the 1-year after CIS, especially at the modular-level, and more importantly how these two modalities relate to each other.

In this study, we combined FC and SC to investigate the longitudinal evolution of both global and modular-specific topology changes in the brain in the first year following CIS. We also hypothesized that due to the nature of MS, the disruption of connections may lead to SC-FC decoupling, which we investigated at both the modular and whole-brain levels.

Materials and methods

Standard protocol, approvals, registration, and patient consent

Each patient provided written informed consent. Patients were included in the prospective study without intervention, analyzing early brain damage in patients with CIS (SCICOG, ClinicalTrials.gov Identifier: NCT01865357). This study was approved by the local ethics committee.

Participants

The population used in this study has been described in a previous paper.[17] Briefly, we prospectively recruited 52 consecutive PwCIS less than 6 months after an initial neurological episode of the type seen in MS. They presented with at least two clinically silent cerebral lesions on fluid-attenuated inversion recovery (FLAIR) images that were characteristic of MS. These patients underwent MRI scan at baseline, and only 41 PwCIS were rescanned after one year of evolution, as 11 patients were lost to follow-up. The exclusion criteria included age below 18 years, inability to undergo MRI, history of other neurological or psychiatric disorders, MS relapse within 2 months prior to screening, corticosteroid pulse therapy within 2 months prior to screening, and severe depression (Beck Depression Inventory > 27). The patients underwent neurological examination by expert neurologists and were scored on the Kurtzke's Expanded Disability Status Scale (EDSS)[18] and the MS Functional Composite (MSFC) measure.[19]

Twenty healthy controls (HC) matched for age, sex, and educational level were also included in this study and underwent the same MRI protocol. Nineteen of these were rescanned one year after the first assessment.

To study the longitudinal evolution of structural and functional brain network topology, only participants with longitudinal follow-up were considered for the current analyses.

All participants were also evaluated using a comprehensive neuropsychological battery described in the supplementary material (**Supplementary Table 1**). Detailed neuropsychological results can be found in a previous paper.[17]

Information on the type of CIS can be found in **Table 1**. Additionally, in order to assess patients' lesions topography, we have computed a lesion frequency map for our CIS patients (**Supplementary Figure 1**). As it can be seen from this frequency map and from **Table 1**, our patients' lesion load is rather small, and the low lesion frequency indicates that lesion topography varies from one patient to another. In addition to that, since the number of patients per type of symptoms is small, it is not possible to interpret abnormalities in specific networks according to type of onsets.

MRI acquisition

MRI acquisition was performed on a 3T MRI system (Achieva TX system, Philips Healthcare, Best, The Netherlands; Sigma, GE Healthcare, Discovery MR 750w, Milwaukee, WI, USA). The acquisition protocol was harmonized between the magnets and consisted of a three-dimensional (3D) T1-weighted sequence using magnetization prepared rapid gradient echo imaging (repetition time [TR] = 8.2 ms, echo time [TE] = 3.5 ms, inversion time [TI] = 982 ms, $\alpha = 7°$, field of view [FOV] = 256 mm, voxel size = 1 mm^3, 180 slices), a 2D FLAIR sequence (TR = 11,000 ms, TE = 140 ms, TI = 2,800 ms, FOV = 230 mm, 45 axial slices, 3-mm slice thickness), a diffusion tensor echo-planar-imaging pulse sequence (TR = 11,676 ms, TE = 60 ms, FOV = 230 mm, an isotropic resolution of 1.6 × 1.6 × 1.6 mm^3 and b = 1000 s/mm^2) in 21 non-colinear directions, and one b = 0 s/mm^2. Resting-state functional MRI was obtained with an echo-planar-imaging sequence (250 volumes, 40 axial slices, TR = 2,200 ms, TE = 30 ms, 3 × 3-mm in-plane resolution, and 3-mm slice thickness).

Structural preprocessing and anatomical parcellation

Lesions were segmented on FLAIR data using the Lesion Segmentation Tool version 2.0.15 (http://www.applied-statistics.de/lst.html) in Statistical Parametric Mapping (SPM12;

www.fil.ion.ucl.ac.uk/spm). Then, they were manually corrected by two blinded experts. Using these maps, a lesion-filling algorithm[20] was applied to the T1-weighted images to avoid the lesions affecting brain tissue segmentation. Whole-brain, total-WM, GM, and CSF volumes were calculated using the volBrain system (http://volbrain.upv.es).[21]

Structural data were preprocessed with the FreeSurfer (v5.3) image analysis suite, which was documented and freely available online (http://surfer.nmr.mgh.harvard.edu).[22] The brain was separated into regions of interest using a custom-made atlas. The cortical atlas was derived from the Destrieux cortical atlas,[23] which was based on a parcellation scheme that first divided the neocortex into gyral and sulcal regions, with the limit between both being given by the curvature value of the surface. Other GM structures (thalamus, pallidus, accumbens, putamen, caudate, and amygdala, hippocampus), the cerebellar cortex, and the ventral diencephalon, as segmented by FreeSurfer, were also included as regions of interest. Finally, our custom-made atlas included 83 regions per hemisphere.

T1-weighted images were registered to diffusion images (B0 image as a reference) by a rigid registration followed by a non-rigid registration of the T1-weighted image to the subject's B0 space using ANTs software.[24] Registration between the functional MRI (fMRI) and the T1-weighted sequences was performed using boundary-based registration.

The complete atlas was then co-registered to each participant's fMRI and diffusion scans, and all registrations were visually checked.

DTI preprocessing

Diffusion data were preprocessed using the Oxford Centre for Functional MRI of the Brain Software Library (version 5.0.9; fsl.fmrib.ox.ac.uk/fsl). Eddy current distortions and motion artifacts were corrected, and brain tissue was extracted. Subsequently, MRtrix3 software[25] was used for diffusion-weighted tractography. First, a single-shell response function was estimated[26] to calculate the fiber orientation distributions using the constrained spherical-deconvolution algorithm.[27] Five-tissue-type segmented T1 image and anatomically-constrained tractography[25] were used to generate 10 million whole-brain tracts. These tracts were cropped at the GM–WM interface. Finally, these streamlines were filtered to 2 million using the spherical-deconvolution informed filtering of tractograms[28] to reduce reconstruction bias and improve biological plausibility.

Resting-state fMRI preprocessing

Using SPM12, we followed the same fMRI preprocessing that was used in a previous study.[17] Briefly, the constant offset and linear trend over each run were removed, a low-pass temporal filter with a 0.08-Hz cutoff was applied, and the data were slice time-corrected. Sources of spurious variance, as well as their temporal derivatives, were removed through linear regression, including the following: 1) six parameters obtained via correction of rigid body head motion, 2) the signal averaged over the whole brain, 3) the signal averaged over the ventricles, and 4) the signal averaged over the deep cerebral WM. This regression procedure contributed to the minimization of signal contributions of non-neuronal origin, including respiration-induced signal fluctuations.[29] The first four volumes of the functional run were discarded to achieve steady-state magnetization.

Brain network construction

Structural connectome construction

Streamlines previously obtained from tractography were mapped into the 166 atlas nodes to produce a 166 × 166 weighted SC matrix. Each element of the SC matrix represented the streamline counts normalized by the total number of tracts for each participant, to correct for seed region size.

Functional connectome construction

To construct the FC matrix, for each participant, the average BOLD (blood oxygen level-dependent imaging) time courses were extracted from each of the 166 regions defined by our final atlas. Then, Pearson's linear correlation coefficients were computed between the signals from all pairs of regions. A Fisher's Z-transformation was further applied to the correlation matrices to improve the normality of the correlation coefficient, leading to a 166 × 166-weighted FC matrix. Given the controversial nature of the physiological meaning of negative correlations,[30,31] the elements of significantly negative correlations were set to zero.

Network characteristics

We conducted graph theoretical network analysis to investigate the overall topological properties of whole-brain networks in PwCIS and HC. These analyses were carried out on the functional and SC networks of each participant using the Brain Connectivity Toolbox (http://www.brain-connectivity-toolbox.net).[32] We calculated segregation properties (clustering coefficient), centrality properties (degree, betweenness centrality), and integration properties (global efficiency). These measures were detailed in *Rubinov and Sporns (2010)*. Briefly, the clustering

coefficient represented the fraction of the node's neighbors that were also neighbors of each other. The degree of a node was the sum of all connections between this node and other nodes. Betweenness centrality was defined as the fraction of all the shortest paths in the network that pass through a given node. Global efficiency was the average inverse shortest path length and could estimate the efficiency with which brain regions communicated.

In order to verify the robustness of our brain parcellation to the network metrics, we have generated new parcellation schemes with approximately half the number of original regions by combining pairs of adjacent regions as in *Fagerholm et al. (2015)*.[33] Then, structural and functional connectivity matrices were computed again from these new parcellation and network measures were calculated. As a region may have more than one adjacent neighbor in the original parcellation, we randomly selected the neighboring region used to be combined. We repeated this process 30 times with different randomly selected adjacent regions to ensure stability.

Modularity

To identify brain functional modules (i.e., a set of densely intra-connected networks), we conducted a modularity analysis on the FC network. Given that the module membership varied between participants, we performed the modularity analysis at the group level by averaging FC matrices of all participants at baseline. Modular analysis aimed to find a specific module partition that yielded a maximum modularity Q^w.. Functional modules were detected using the Louvain modularity algorithm [34] combined with a fine-tuning algorithm.[35] Furthermore, to improve the reliability of the modular structure, this algorithm was repeated 250 times. Finally, we derived a consensus partition using the method described by *Lancichinetti et al. (2012)*.[36] The final consensus partition had a modularity of $Q^w = 0.41$ and contained five networks, including the fronto-parietal network (FPN), the salience network (SN), the default mode network (DMN), the visual network (VN), and the somatomotor network (SMN; **Fig. 1**). These networks were visually inspected and corresponded well with previously reported resting-state networks.[37–39]

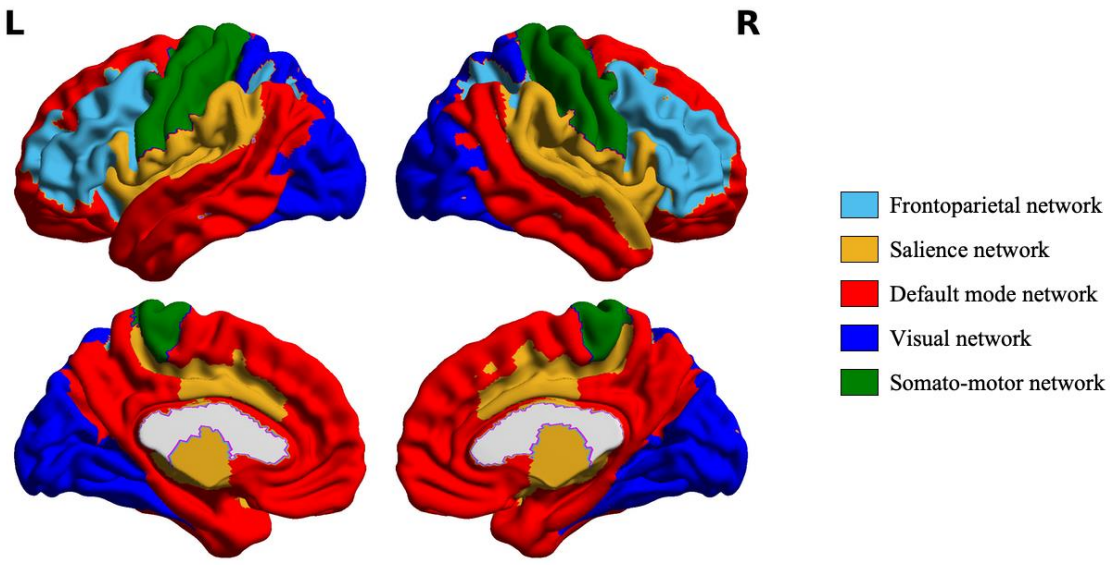

Figure 1. Identified resting-state functional networks

Modular characteristics

To characterize the modular-related topology at the nodal level, we calculated the participation coefficient (PC) that measured the inter-module connectivity of each node. For a node *i*, PC was calculated as:

$$PC_i = 1 - \sum_{s=1}^{N_M} \left(\frac{k_{is}}{k_i}\right)^2$$

where N_M is the total number of modules, k_{is} is the number of links of node *i* to nodes in module *s*, and k_i is the total degree of node *i*.

We also computed the within-module degree z-score (WD) that measured the intra-module connectivity of a node. For a node *i*, WD was calculated as:

$$WD_i = \frac{k_i - k_{s_i}}{\sigma_{k_{s_i}}}$$

where k_i is the number of links of the node *i*, k_{s_i} is the average of the degree over all nodes in s_i, and $\sigma_{k_{s_i}}$ is the standard deviation of the degree in s_i.

PC ranged from 0 to 1, where PC was close to 1 if node *i* had a homogeneous connection distribution with all the modules, and 0 if node *i* was exclusively linked to other nodes in its own module. WD, on the other hand, was large for a node *i* that had many intra-module connections

relative to other nodes in the same module. These modular parameters were computed for both structural and functional networks.

Structural–functional (SC-FC) coupling

We assessed SC-FC coupling as the correlation coefficient between strengths of the structural and functional networks. For each participant, this correlation was constrained by edges of non-zero SC. Specifically, non-zero SC edges were extracted to form a vector of structural connectivity values, which was further rescaled into a Gaussian distribution.[6] FC was then extracted to form a corresponding vector. Finally, SC-FC coupling was quantified by the Pearson's coefficient of correlation between the two previous vectors. We evaluated SC-FC coupling both at the whole-brain level and in each module.

Statistical analysis

Statistical analyses were performed using MATLAB 2016a (MathWorks, Natick, MA, USA) and SPSS 23.0 (SPSS, Chicago, IL, USA).

Normality of distribution was assessed by the Shapiro–Wilk test. Categorical variables were investigated with χ^2 tests, while continuous variables were investigated with two-sample *t*-tests. To examine between-group differences in network properties, a general linear model analysis was performed with age, gender, education level, and scanner as covariates at each time-point. For those network metrics showing significant group differences, a region-wise comparison of the corresponding metric was used to search for the major regions driving this modification. Region-wise comparison of global network metrics and modular metrics was performed using a randomized permutation testing (10,000 permutations) corrected for multiple comparisons[40,41] on age-, sex-, education-, and scanner-standardized residuals.

Finally, association between altered connectivity metrics and clinical/neuropsychological scores was analyzed using linear regression models where age, sex, and education level were considered as nuisance variables.

Data availability

The data that supported the findings of this study are available from the corresponding author upon reasonable request.

Results

Clinical, neuropsychological, and conventional MRI characteristics

The characteristics of both PwCIS and HC are summarized in **Table 1**. The two groups were matched for age, sex, and level of education at each time-point. In PwCIS, the EDSS and MSFC scores did not change significantly between baseline (median EDSS = 1, range = 0–3; mean MSFC = 0.32, standard deviation [SD] = 0.41) and year one (median EDSS = 1, range = 0–5; mean MSFC = 0.31, SD = 0.60), and T2 lesion volumes (T2 LV) did not differ significantly between baseline (median T2 LV = 0.98 mL, range = 0.02–63.12 mL) and year one (median T2 LV = 1.32 mL, range = 0.07–67.74 mL).

At baseline, PwCIS did not differ from HC in whole normalized brain, WM, GM, and total CSF volumes. However, after one year, PwCIS developed global brain atrophy with decreased whole-brain and WM volumes ($P < 0.05$) and increased total CSF volume ($P < 0.05$) compared to HC (**Table 1**).

Regarding cognition, PwCIS showed a moderate cognitive impairment at baseline with alterations on the Computerized Speed Cognitive Test (CSCT) and the Brief Visual Memory Test-Revised (BVMTR). At one year, this cognitive impairment was no longer observed.

Table 1. **Demographic, Clinical, and Conventional MRI Characteristics**

	Baseline		Year 1	
Clinical features	**HC** *(n = 19)*	**CIS** *(n = 41)*	**HC** *(n = 19)*	**CIS** *(n = 41)*
Mean age, years *(SD)*[a]	37.8 (8.6)	38.3 (11.2)	-	
Sex ratio *(F/M)*[b]	14/5	32/9		
Education level *(high/low*[c]*)*[b]	10/9	26/15		
Symptoms at clinical onset: *Brain* *Optic neuritis* *Brainstem/Cerebellar* *Spinal cord*		4 (10%) 7 (17%) 11 (27%) 19 (46%)	-	
Mean disease duration *(SD) in months*	-	4.12 (1.85)		
Median EDSS score *[range]*[d]	-	1.0 [0-3]	-	1.0 [0–5]
MSFC z-score *(SD)*[d]	-	0.32 (0.41)	-	0.31 (0.60)
Median T2 Lesion volume *(mL)*[d]	-	0.98 [0.02–63.12]	-	1.32 [0.07–67.74]
Normalized Brain fraction *(%)*[e,f]	86.41 ± 2.95	84.59 ± 4.08	86.39 ± 3.02	83.75 ± 4.11*
Normalized WM fraction *(%)*[g,e,f]	36.59 ± 2.42	35.52 ± 3.13	37.28 ± 3.14	34.51 ± 3.27**
Normalized GM fraction *(%)*[e,f]	49.82 ± 2.58	49.07 ± 2.85	49.11 ± 2.31	49.25 ± 2.86
Normalized CSF fraction *(%)*[e,f]	13.59 ± 2.95	15.41 ± 4.08	13.61 ± 3.02	16.25 ± 4.11*

[a] Mann–Whitney *U* test
[b] χ^2 test
[c] Education level was considered as high or low according to a French baccalaureate.
[d] Wilcoxon test to compare PwCIS at baseline and year one.
[e] GLM comparing PwCIS to HC with age, sex, level of education, and scanner as covariates.
[f] Percentage: (structure's volume/TIV) × 100.
Differences between PwCIS and HC: *: $p < 0.05$; **: $p < 0.01$.
SD, Standard Deviation; TIV, Total Intracranial Volume; EDSS, Expanded Disability Status Scale; MSFC, Multiple sclerosis functional composite score; WM, White Matter; GM, Grey Matter

Structural connectivity network

At baseline, the clustering coefficient was significantly increased in patients compared to HC (**Fig. 2A**), while the degree, betweenness centrality, and global efficiency were unaffected. At the nodal level, we found that these alterations were in the occipital, parietal, temporal, frontal, and central regions and in the right pallidum (**Fig. 2B**, **Supplementary Table 4**). At the modular level, the participation coefficient was significantly increased in the posterior part of the cingulate and the

inferior parietal lobe and decreased in the left central sulcus (**Fig. 2C**, **Supplementary Table 4**), while the within-module degree was significantly increased in the superior occipital, postcentral, and middle frontal gyrus (**Fig. 2D**, **Supplementary Table 4**).

At year one, there was no difference between PwCIS and HC in the overall network metrics (degree, betweenness centrality, clustering coefficient, and global efficiency). However, at the modular level, alterations were still present. The participation coefficient was significantly decreased in PwCIS compared to HC in the bilateral central sulcus and increased in the inferior parietal gyrus (**Fig. 2E**, **Supplementary Table 4**); on the other hand, the within-module degree was decreased in the cerebellum and inferior temporal sulcus and increased in the superior frontal sulcus (**Fig. 2F**, **Supplementary Table 4**). Using different parcellation schemes, clustering coefficient at baseline was still the only altered parameter as it was significantly increased in patients compared to controls in each case (**Supplementary Table 6**).

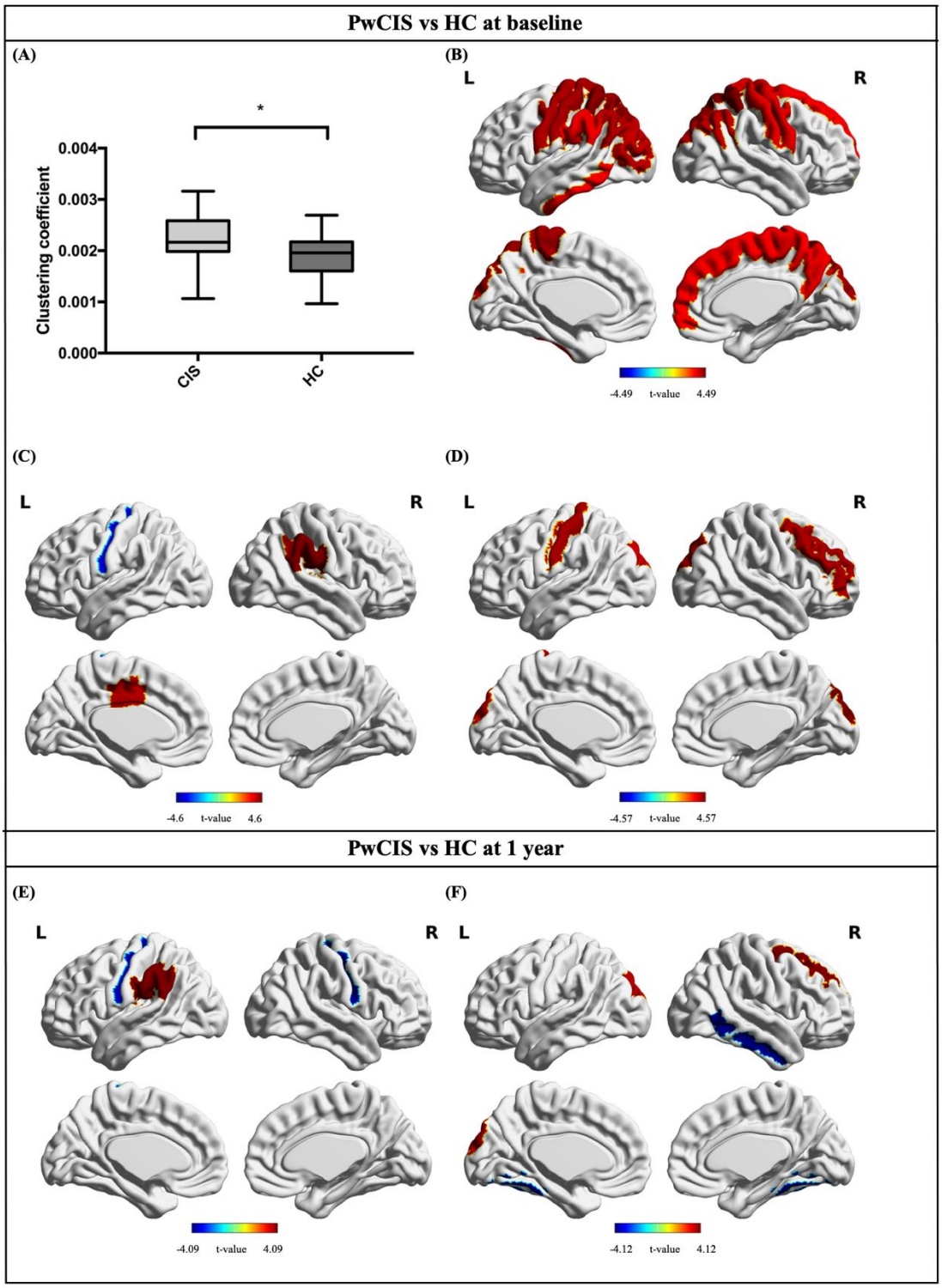

Figure 2. Structural connectivity alterations

(A) Overall clustering coefficient comparison, (B) Region-wise clustering coefficient comparison, (C) PC comparison between PwCIS and HC, (D) WD comparison between PwCIS and HC, (E) PC comparison between PwCIS and HC, and (F) WD comparison between PwCIS and HC.

PC, participation coefficient; WD, within-degree module z-score; PwCIS, patients with CIS; HC, healthy controls

FC network

At baseline, no differences were noted in the overall network metrics between PwCIS and HC. This was the same for modular-related metrics (participation coefficient and within-module degree) (**Fig. 3A**, **Fig. 3B**).

At year one, betweenness centrality was significantly increased in PwCIS compared to HC (0.023 ± 0.002 vs 0.021 ± 0.001; p = 0.006); however, no region survived after the multiple comparison correction for the nodal-level comparison. Regarding the modular-related metrics, the participation coefficient significantly increased in PwCIS compared to HC in the right anterior circular sulcus of the insula (**Fig. 3C**, **Supplementary Table 5**), while the within-module degree was increased in the right hippocampus and left post-ventral cingulate gyrus, and it was decreased in the bilateral frontomarginal gyrus and sulcus and left temporal pole (**Fig. 3D**, **Supplementary Table 5**). Using different parcellation schemes, betweenness centrality at 1-year was again the only altered parameter as it was significantly increased in patients compared to controls in each case (**Supplementary Table 7**).

SC-FC coupling

Both the PwCIS and HC groups showed significant correlations between regional SC and FC (all $P < 10^{-95}$, correlation coefficient ranging from 0.15 to 0.32). These correlations were still present when looking at the modular level (all $P < 10^{-4}$, ranging from 0.23 to 0.7).

At baseline, SC-FC coupling was preserved in patients compared to HC at both the whole-brain and the modular levels.

After one year of evolution, whole-brain coupling was still preserved; however, SC-FC decoupling was observed in three networks (SN, VN, and SMN) (**Fig. 4**).

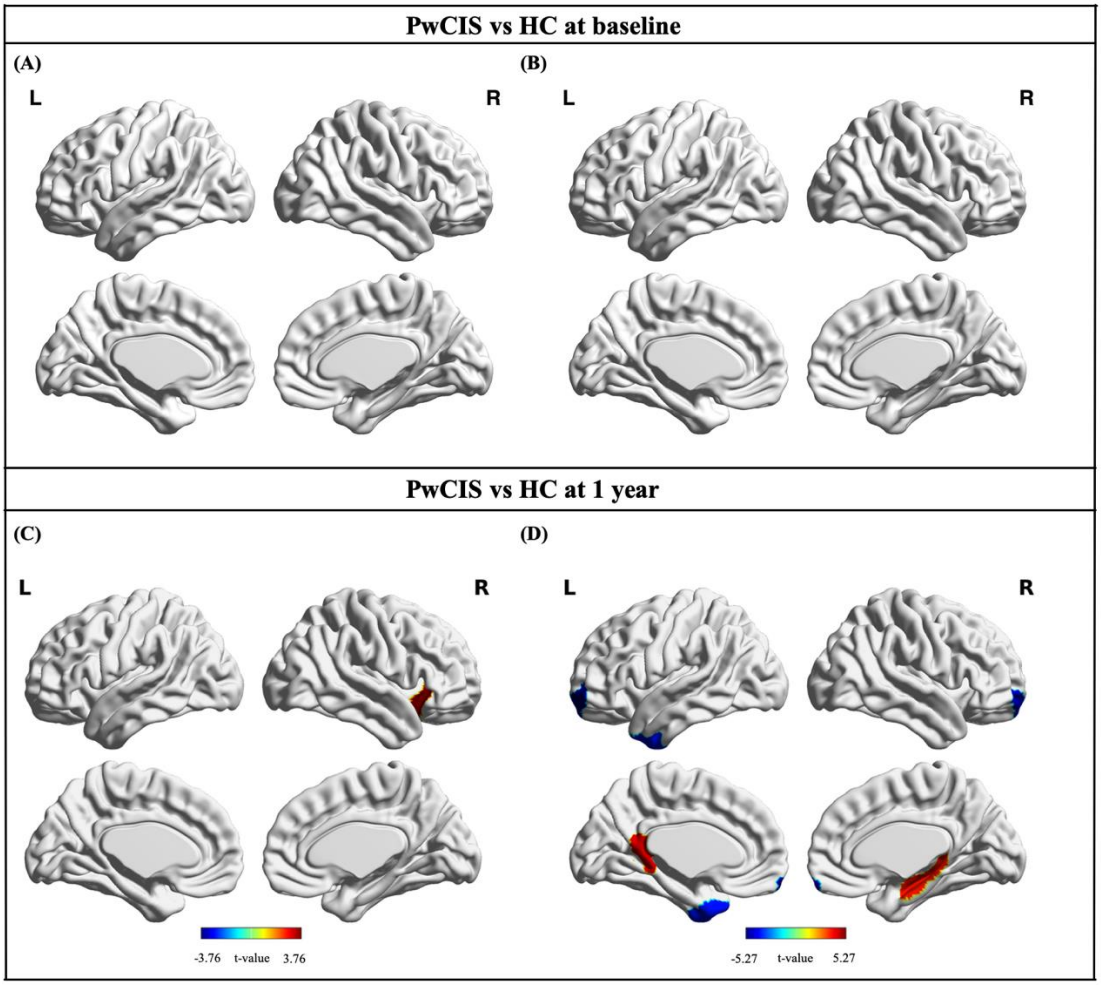

Figure 3. Functional connectivity alterations

(A) PC comparison between PwCIS and HC at baseline, (B) WD comparison between PwCIS and HC at baseline, (C) PC comparison between PwCIS and HC, and (D) WD comparison between PwCIS and HC.
PC, participation coefficient; WD, within-degree module z-score; PwCIS, patients with CIS; HC, healthy controls

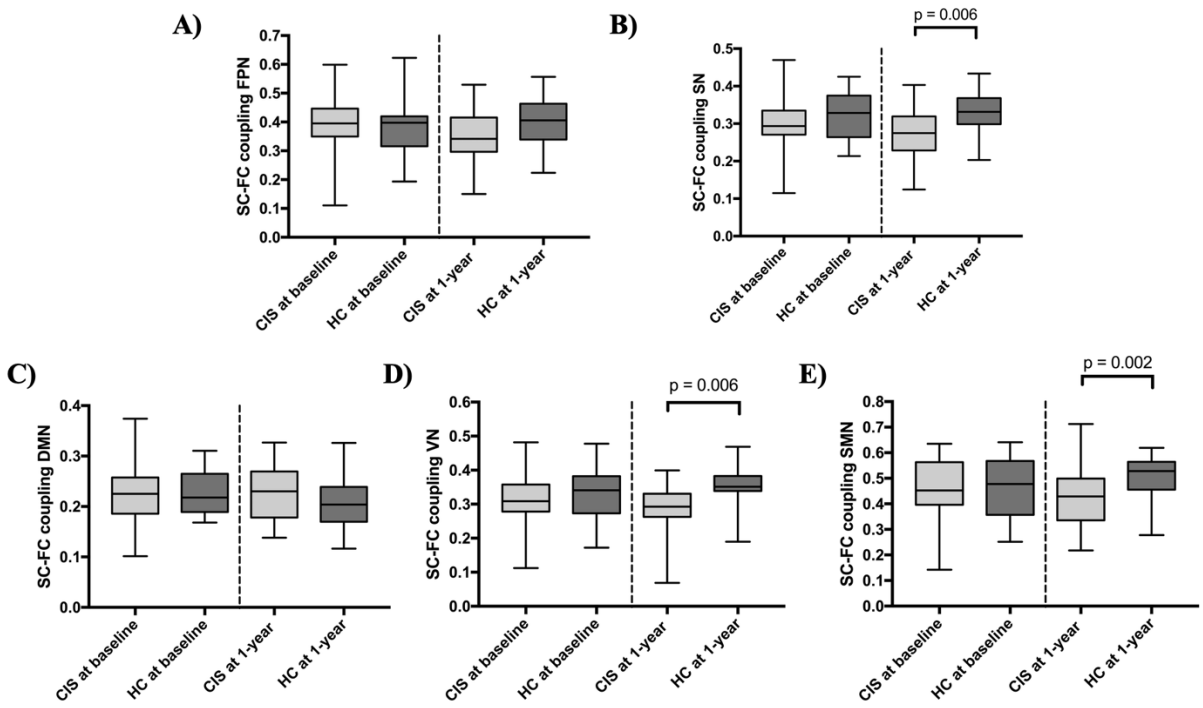

Figure 4. Structural–functional (SC-FC) decoupling at the network level at baseline and 1-year
FPN, frontoparietal network; SN, salience network; DMN, default mode network; VN, visual network; SMN, somatomotor network

Clinical and neuropsychological correlates

No association was found between SC-FC coupling and clinical/neuropsychological variables either at baseline or after one year of follow-up.

MSFC at baseline was associated with educational level ($\beta = -0.29$; $p = 0.049$) and DTI clustering coefficient at baseline ($\beta = -0.36$; $p = 0.017$) for a significant model ($p = 0.005$) explaining R^2_{adj} = 25% of the variance. Conversely, CSCT at baseline was associated with age ($\beta = -0.44$; $p = 0.003$) and DTI clustering coefficient at baseline ($\beta = -0.28$; $p = 0.049$) for a significant model ($p = 0.002$) explaining R^2_{adj} = 29% of the variance.

At year one, no clinical/neuropsychological variable was associated with altered network metrics at follow-up.

Discussion

In the present study, we investigated the longitudinal reorganization of both structural and functional brain networks in the first year following CIS. We showed that overall network

alterations were already present after the first clinical event, with structural damage as the clustering coefficient was increased in patients, and modular-related SC was altered. In particular, increased clustering coefficient was associated with clinical and cognitive deficit at baseline (MSFC and CSCT). After one year of evolution, both structural and functional reorganizations were observed with altered modular-related connectivity, and there was an increase of betweenness centrality in the functional network. At this stage, SC-FC decoupling in three modules was also noticed, together with the previous abnormalities.

Modularity has been considered as one of the main properties of brain network organization, leading to the functional specialization and segregation of the brain.[4] Specifically, we identified five densely intra-connected networks, which corresponded to the well-known functional modules frontoparietal, salience, default mode, visual, and motor/sensorimotor networks.[37–39]

At the clinical onset, structural damage was already present in patients with CIS, as we observed an increased clustering coefficient. Clustering coefficient, which has recently been shown to be increased in patients with early relapsing-remitting MS,[15] indicated the strengthening of short distance connections to preserve local information flow. This was also shown by the increased within-module degree inside FPN, VN, and SMN, which could be considered favorable for behaviors that required specialized processing.[42] In addition, the participation coefficient was increased in regions of the SN and decreased in some other region of the SMN. Alterations in these modular parameters in one direction or the other could inform on the ability of a region to recruit alternative routes. Ultimately, it is suggested that the brain is seeking the best trade-off with lower metabolic connection costs at the expense of losing integrative capacity by rerouting and reweighting its connections.[43] This type of reorganization has been observed in other neurological disorders such as Alzheimer's disease[44] or Parkinson's disease[45].

Importantly, the overall functional network was still preserved at this stage of the disease, although structural abnormalities were observed, which was in line with the recent results from *Liu and colleagues*.[16]

After one year of evolution, in addition to alterations within the structural network, functional reorganization appeared with an increased overall betweenness centrality and increased participation coefficient in the anterior insula sulcus, along with modifications of within-module degree within the DMN. These results supported the hypothesis that structural damage could

precede functional changes in MS and needed to achieve a certain threshold to cause these functional modifications.[46]

Structurally-connected GM regions showed stronger FC than structurally-unconnected regions, which led us to believe that SC could predict the functional connections.[6,47] However, FC was not constant, and it was continuously reconfigured around the underlying anatomy through plasticity.[48] Therefore, the SC-FC coupling could be informative and was found to be decreased in other neurological diseases, such as epilepsy,[7] stroke[8] or Alzheimer's disease.[9] Here, we investigated for the first time the SC-FC coupling in the early stages of MS. We observed a preserved coupling at the whole-brain level during follow-up; however, when looking at the modular level, SC-FC decoupling was noticed in the SN, VN, and SMN. These findings, along with the increased FC at year one, suggest that functional reorganization involves new functional connections, occurring across structurally-unconnected regions.

Only a moderate cognitive impairment was noted at baseline, as the CSCT and BVMTR scores were the only scores to be significantly decreased in PwCIS compared to HC. MS attacks have been known to impact cognitive performances, this is known as the post-relapse effect. However, this effect is no longer observed between 1 to 3 months after the attack.[49,50] Since our patients were included 2 to 6 months after their first episode, we postulate it is unlikely these early cognitive deficits depend on this effect. Additionally, worse CSCT performance and a lower MSFC score were associated with early structural damage (altered structural clustering coefficient). However, there was no more cognitive impairment at follow-up, and the global clinical state also did not worsen (MSFC and EDSS scores were not different from baseline).We have previously shown that functional reorganization occurring one year after CIS was associated to better cognitive performance.[17] Thus, it could be suggested that functional reorganization at this stage was able to compensate for the first deficits through indirect structural connections, and this compensation could fail once the structural damage was too widespread and functional rerouting was less efficient. One other explanation for normal cognitive performance at one year could come from the preserved SC-FC coupling in the DMN because connectivity alterations in the DMN were strongly associated with cognitive deficits at different stages of MS in previous papers.[51,52] However, a longer follow-up will be needed to confirm these statements.

The current study is not without limitations. First, SC-FC coupling is only computed for anatomically connected regions; however, FC can also result from indirect structural paths.[6] More

sophisticated computational models are needed to consider these pathways and their effect on the functional connectome. Additionally, since structural connectivity investigates white matter bundles and functional connectivity investigates synchronization between two GM regions, there is no anatomical overlay between these two modalities, making it impossible to use a voxel-wise approach, which explains our choice (and previous studies) to use a Pearson correlation coefficient between vectors representing each connectivity. Second, our DTI data covers only 21 directions in the whole sphere as a trade-off to the good resolution obtained. This could have an effect on our tractography estimation. However, this effect would be present in CIS patients and in HC controls as well which could limit its influence. Also, our data was acquired on two different scanners. To the best of our ability, we harmonized the protocols between the two magnets. For DTI, we have applied exactly the same directions to cover the whole sphere and obtained the same resolution. This was also the case for fMRI as we used the same acquisition parameters as well as the same number of runs. Recently, *An and colleagues*[53] tested the inter-vender reliability of the resting state fMRI and showed that this modality could be highly reliable among different scanners. In order to correct for this parameter even more, we have included the scanner variable as a covariable in all our analyses as we stated in the Statistical analysis part. Regarding the five modules we obtained in our analyses, they were detected using the Louvain algorithm which automatically detects regions synchronously connected to each other during the whole scan time and assigns them to the same network. Additionally, we repeated this algorithm 250 times and derived the consensus modules to improve our reliability. We have detailed this procedure in the Methods section. As a result, we do not control the number of modules, as well as the regions belonging to each one of them. We acknowledge the potential presence of more networks; however, we do not have the spatial or temporal resolution, nor a very high number of subjects to separate them from the obtained modules. Once our modules were obtained, we compared them with the literature and found a good correspondence.[37–39] Other papers investigating different neurological disorders have found similar number of modules in their analysis.[54–57] Finally, we only estimate FC as the mean of the entire recording. However, functional connectome has been shown to possess dynamic properties that may depend on the underlying anatomy.[58] Even though this is not the scope of our study, this question remains important for future understanding of the pathology.

In conclusion, the current study demonstrated structural damage preceding functional reorganization and possible compensation at both the whole-brain and network levels during the

first year following CIS. For the first time, we showed SC-FC decoupling in some brain networks in MS, suggesting that functional reorganization occurs along indirect anatomical pathways.

Acknowledgments: The authors thank the neurologists of the AQUISEP network for their involvement in recruiting patients. The authors thank Dr JC Ouallet, Dr A Moroso, and Dr P Louiset for referring patients to the study. This work has been performed with the help of the French Observatoire of Multiple Sclerosis (OFSEP), which is supported by a grant provided by the French State and handled by the "Agence Nationale de la Recherche," within the framework of the "Investments for the Future" program, under the reference no. ANR-10-COHO-002.

Funding: The authors disclose receipt of the following financial support for the research, authorship, and/or publication of this article: This study was supported by the Translational Research and Advanced Imaging Laboratory (TRAIL), laboratory of excellence (ANR- 10-LABX-57). The SCI-COG study was also supported by a grant from TEVA and ARSEP (Fondation ARSEP pour la recherche sur la sclérose en plaques).

Competing interests

I.K., P.B., M.D., J.C-M., A.S., and T.T. report no competing interests.

B.B. reports grants from the French Ministry of Health during the conduct of the study; personal fees and non-financial support from Biogen-idec, grants from Merck-serono, personal fees and non-financial support from Novartis, personal fees and non-financial support from Genzyme, grants, personal fees and non-financial support from TEVA, grants and non-financial support from Bayer, outside the submitted work.

A.R. reports grants from TEVA, during the conduct of the study; personal fees and non-financial support from Novartis, personal fees and non-financial support from Biogen, grants, personal fees and non-financial support from TEVA, grants and non-financial support from Roche, grants and non-financial support from Merck, grants and non-financial support from Genzyme, non-financial support from Medday, grants from Bayer, outside the submitted work.

Supplementary material

Supplementary material is available.

References

1. Miller DH, Chard DT, Ciccarelli O. *Clinically isolated syndromes*. Epub ahead of print 2012. DOI: 10.1016/S1474-4422(11)70274-5.
2. Polman CH, Reingold SC, Banwell B, et al. Diagnostic criteria for multiple sclerosis: 2010 Revisions to the McDonald criteria. *Ann Neurol* 2011; 69: 292–302.
3. Zipp F, Gold R, Wiendl H. Identification of Inflammatory Neuronal Injury and Prevention of Neuronal Damage in Multiple Sclerosis. *JAMA Neurol*. Epub ahead of print 21 October 2013. DOI: 10.1001/jamaneurol.2013.4391.
4. Bullmore E, Sporns O. Complex brain networks: graph theoretical analysis of structural and functional systems. *Nat Rev Neurosci* 2009; 10: 312–312.
5. Fleischer V, Radetz A, Ciolac D, et al. Graph theoretical framework of brain networks in multiple sclerosis: A review of concepts. *Neuroscience*. Epub ahead of print 2017. DOI: 10.1016/j.neuroscience.2017.10.033.
6. Honey CJ, Sporns O, Cammoun L, et al. Predicting human resting-state functional connectivity from structural connectivity. *Proc Natl Acad Sci* 2009; 106: 2035–2040.
7. Zhang Z, Liao W, Chen H, et al. Altered functional-structural coupling of large-scale brain networks in idiopathic generalized epilepsy. *Brain* 2011; 134: 2912–2928.
8. Zhang J, Zhang Y, Wang L, et al. Disrupted structural and functional connectivity networks in ischemic stroke patients. *Neuroscience* 2017; 364: 212–225.
9. Dai Z, Lin Q, Li T, et al. Disrupted Structural and Functional Brain Networks in Alzheimer's Disease. *Neurobiol Aging*. Epub ahead of print 2018. DOI: 10.1016/j.neurobiolaging.2018.11.005.
10. Newman MEJ, Girvan M. Finding and evaluating community structure in networks. *Phys Rev E* 2004; 69: 026113.
11. Newman MEJ. Modularity and community structure in networks. *Proc Natl Acad Sci* 2006; 103: 8577–8582.
12. Gamboa OL, Tagliazucchi E, Von Wegner F, et al. Working memory performance of early MS patients correlates inversely with modularity increases in resting state functional connectivity networks. *Neuroimage* 2014; 94: 385–395.
13. Kocevar G, Stamile C, Hannoun S, et al. Graph theory-based brain connectivity for automatic classification of multiple sclerosis clinical courses. *Front Neurosci* 2016; 10: 478.
14. Muthuraman M, Fleischer V, Kolber P, et al. Structural brain network characteristics can differentiate CIS from early RRMS. *Front Neurosci* 2016; 10: 14.
15. Fleischer V, Gröger A, Koirala N, et al. Increased structural white and grey matter network connectivity compensates for functional decline in early multiple sclerosis. *Mult Scler J* 2017; 23: 432–441.
16. Liu Y, Duan Y, Dong H, et al. Disrupted Module Efficiency of Structural and Functional Brain Connectomes in Clinically Isolated Syndrome and Multiple Sclerosis. *Front Hum Neurosci*. Epub ahead of print 2018. DOI: 10.3389/fnhum.2018.00138.
17. Koubiyr I, Deloire M, Besson P, et al. Longitudinal study of functional brain network reorganization in clinically isolated syndrome. 2018; 1–13.
18. Kurtzke JF. Rating neurologic impairment in multiple sclerosis: an expanded disability status scale (EDSS). *Neurology* 1983; 33: 1444–52.
19. Ontaneda D, Larocca N, Coetzee T, et al. Revisiting the multiple sclerosis functional composite: Proceedings from the National Multiple Sclerosis Society (NMSS) task force on

clinical disability measures. *Multiple Sclerosis Journal* 2012; 18: 1074–1080.
20. Prados F, Cardoso MJ, Kanber B, et al. A multi-time-point modality-agnostic patch-based method for lesion filling in multiple sclerosis. *Neuroimage* 2016; 139: 376–384.
21. Manjón J V, Coupé P. volBrain: An Online MRI Brain Volumetry System. *Front Neuroinform*; 10. Epub ahead of print 2016. DOI: 10.3389/fninf.2016.00030.
22. Dale AM, Fischl B, Sereno MI. Cortical surface-based analysis: I. Segmentation and surface reconstruction. *Neuroimage* 1999; 9: 179–194.
23. Destrieux C, Fischl B, Dale A, et al. Destrieux C, et al 2010 Automatic parcellation of human cortical gyri and sulci using standard anatomical nomenclature supplemental. *NeuroImage* 2010; 53: 1–15.
24. Avants BB, Tustison NJ, Song G, et al. A reproducible evaluation of ANTs similarity metric performance in brain image registration. *Neuroimage* 2011; 54: 2033–2044.
25. Tournier J-D, Calamante F, Connelly A. MRtrix: Diffusion tractography in crossing fiber regions. *Int J Imaging Syst Technol* 2012; 22: 53–66.
26. Tournier JD, Calamante F, Connelly A. Determination of the appropriate b value and number of gradient directions for high-angular-resolution diffusion-weighted imaging. *NMR Biomed* 2013; 26: 1775–1786.
27. Tournier JD, Calamante F, Connelly A. Robust determination of the fibre orientation distribution in diffusion MRI: Non-negativity constrained super-resolved spherical deconvolution. *Neuroimage* 2007; 35: 1459–1472.
28. Smith RE, Tournier JD, Calamante F, et al. SIFT: Spherical-deconvolution informed filtering of tractograms. *Neuroimage* 2013; 67: 298–312.
29. Van Dijk KRA, Hedden T, Venkataraman A, et al. Intrinsic Functional Connectivity As a Tool For Human Connectomics: Theory, Properties, and Optimization. *J Neurophysiol* 2010; 103: 297–321.
30. Chang C, Glover GH. Effects of model-based physiological noise correction on default mode network anti-correlations and correlations. *Neuroimage* 2009; 47: 1448–1459.
31. Anderson JS, Druzgal TJ, Lopez-Larson M, et al. Network anticorrelations, global regression, and phase-shifted soft tissue correction. *Hum Brain Mapp* 2011; 32: 919–934.
32. Rubinov M, Sporns O. Complex network measures of brain connectivity: Uses and interpretations. *Neuroimage* 2010; 52: 1059–1069.
33. Fagerholm ED, Hellyer PJ, Scott G, et al. Disconnection of network hubs and cognitive impairment after traumatic brain injury. *Brain* 2015; 138: 1696–1709.
34. Blondel VD, Guillaume JL, Lambiotte R, et al. *Fast unfolding of communities in large networks*. Epub ahead of print 2008. DOI: 10.1088/1742-5468/2008/10/P10008.
35. Sun Y, Danila B, Josić K, et al. *Improved community structure detection using a modified fine-tuning strategy*. Epub ahead of print 2009. DOI: 10.1209/0295-5075/86/28004.
36. Lancichinetti A, Fortunato S. Consensus clustering in complex networks. *Sci Rep*; 2. Epub ahead of print 2012. DOI: 10.1038/srep00336.
37. He Y, Wang J, Wang L, et al. Uncovering intrinsic modular organization of spontaneous brain activity in humans. *PLoS One* 2009; 4: 5226.
38. Power JD, Cohen AL, Nelson SM, et al. Functional Network Organization of the Human Brain. *Neuron* 2011; 72: 665–678.
39. Yeo BTT, Krienen FM, Sepulcre J, et al. The organization of the human cerebral cortex estimated by intrinsic functional connectivity. *J Neurophysiol* 2011; 106: 1125–65.
40. Blair RC, Karniski W. An alternative method for significance testing of waveform

difference potentials. *Psychophysiology* 1993; 30: 518–524.
41. Groppe DM, Urbach TP, Kutas M. Mass univariate analysis of event-related brain potentials/fields I: A critical tutorial review. *Psychophysiology* 2011; 48: 1711–1725.
42. Park HJ, Friston K. Structural and functional brain networks: From connections to cognition. *Science (80-)*; 342. Epub ahead of print 2013. DOI: 10.1126/science.1238411.
43. Bullmore E, Sporns O. The economy of brain network organization. *Nat Rev Neurosci* 2012; 13: 336–349.
44. Lo C-Y, Wang P-N, Chou K-H, et al. Diffusion Tensor Tractography Reveals Abnormal Topological Organization in Structural Cortical Networks in Alzheimer's Disease. *J Neurosci* 2010; 30: 16876–16885.
45. Hall JM, Shine JM, Ehgoetz Martens KA, et al. Alterations in white matter network topology contribute to freezing of gait in Parkinson's disease. *J Neurol* 2018; 265: 1353–1364.
46. Schoonheim MM, Meijer KA, Geurts JJG. Network collapse and cognitive impairment in multiple sclerosis. *Front Neurol*; 6. Epub ahead of print 2015. DOI: 10.3389/fneur.2015.00082.
47. Hagmann P, Cammoun L, Gigandet X, et al. Mapping the structural core of human cerebral cortex. *PLoS Biol* 2008; 6: 1479–1493.
48. Hagmann P, Sporns O, Madan N, et al. White matter maturation reshapes structural connectivity in the late developing human brain. *Proc Natl Acad Sci* 2010; 107: 19067–19072.
49. Benedict RHB, Morrow S, Rodgers J, et al. Characterizing cognitive function during relapse in multiple sclerosis. *Mult Scler J* 2014; 20: 1745–1752.
50. Giedraitiene N, Kaubrys G, Kizlaitiene R. Cognition During and After Multiple Sclerosis Relapse as Assessed With the Brief International Cognitive Assessment for Multiple Sclerosis. *Sci Rep* 2018; 8: 8169.
51. Louapre C, Perlbarg V, García-Lorenzo D, et al. Brain networks disconnection in early multiple sclerosis cognitive deficits: An anatomofunctional study. *Hum Brain Mapp* 2014; 35: 4706–4717.
52. Eijlers AJC, Meijer KA, Wassenaar TM, et al. Increased default-mode network centrality in cognitively impaired multiple sclerosis patients. *Neurology* 2017; 88: 952–960.
53. An HS, Moon WJ, Ryu JK, et al. Inter-vender and test-retest reliabilities of resting-state functional magnetic resonance imaging: Implications for multi-center imaging studies. *Magn Reson Imaging* 2017; 44: 125–130.
54. Rudie JD, Brown JA, Beck-Pancer D, et al. Altered functional and structural brain network organization in autism. *NeuroImage Clin* 2013; 2: 79–94.
55. Sun Y, Dai Z, Li J, et al. Modular-level alterations of structure–function coupling in schizophrenia connectome. *Hum Brain Mapp* 2017; 38: 2008–2025.
56. Shin DJ, Jung WH, He Y, et al. The effects of pharmacological treatment on functional brain connectome in obsessive-compulsive disorder. *Biol Psychiatry* 2014; 75: 606–614.
57. Dai Z, Lin Q, Li T, et al. Disrupted Structural and Functional Brain Networks in Alzheimer's Disease. *Neurobiol Aging* 2018; 75: 71–82.
58. Shen K, Mišić B, Cipollini BN, et al. Stable long-range interhemispheric coordination is supported by direct anatomical projections. *Proc Natl Acad Sci* 2015; 112: 6473–6478.

Supplementary material

Neuropsychological assessment

Here is a brief summary of the neuropsychological battery used in this study. For a more detailed description, please refer to Koubiyr et al. 2018.

Table S1: Summary of the neuropsychological tests

Domain	Test	Subtests
Attention	Test of attentional performance (TAP)	RT of visual scanning
		RT of auditory attention
		RT of visual and auditory divided attention
Working memory	Paced-Auditory Serial Addition Test-3s (PASAT)	-
Episodic memory	Selective reminding test (SRT)	LTS
		CLTR
		SRT-DR
	Brief Visual Memory Test Revised (BVMTR)	Learning
		Delay recall
Executive functions	Stroop test	Inhibition task scores
	Word list generation (WLG)	-
Information processing speed	Computerised Speed Cognitive Test (CSCT)	-
	Alertness	With warning
		Without warning

RT: reaction time; LTS: long-term storage; CLTR: consistent long-term retrieval; DR: delay recall.

Table S2: Cognitive performances of clinically isolated syndrome patients and healthy controls at baseline

	HC	% of CI	CIS	% of CI	P-value
CSCT	**0.25 (0.87)**	**1.8 %**	**-0.25 (1.1)**	**9.8 %**	**0.04**
BVMTR	**0.53 (0.8)**	**1.8 %**	**0.01 (0.97)**	**2.4 %**	**0.006**
BVMTR-DR	**0.53 (0.53)**	**0 %**	**-0.11 (1.04)**	**7.3 %**	**0.003**
PASAT	0.16 (0.94)	3.7 %	0.12 (1.05)	7.3 %	0.93
SRT-LTS	0.42 (1.02)	3.7 %	0.29 (0.93)	4.9 %	0.48
SRT-CLTR	0.34 (1.05)	5.6 %	0.23 (1.07)	4.9 %	0.59
SRT-DR	0.32 (0.69)	1.8 %	0.20 (0.92)	7.3 %	0.95
WLG	-0.30 (0.73)	3.6 %	-0.58 (0.76)	7.3 %	0.07
Alertness	0.49 (0.69)	0 %	0.21 (2.55)	4.9 %	0.29
RT_Simple_Visual_Attention	0.24 (0.97)	1.8 %	-0.13 (1.21)	14.6 %	0.43
RT_Simple_Auditory_Attention	0.15 (1.03)	0 %	0.16 (1.04)	5 %	0.52
RT_Divided_Visual_Attention	-0.51 (1.54)	14.5 %	-0.15 (1.18)	7.5 %	0.28
RT_Divided_Auditory_Attention	-0.04 (1.26)	9.1 %	-0.26 (1.23)	12.5 %	0.31
Stroop	0.03 (0.88)	3.6 %	0.23 (0.84)	2.6 %	0.28

Cognitive impairment at each test is determined at the 5th percentile (z-score < -1.64).
HC: healthy controls; CIS: clinically isolated syndrome; CI: cognitive impairment; CT: computerized speed cognitive test; BVMTR: brief visual memory test revised; DR: delay recall; PASAT: paced auditory serial addition test; SRT: selective reminding test; LTS: long-term storage; CLTR: consistent long-term retrieval; WLG: word list generation; RT: reaction time.

Table S3: Cognitive performances of clinically isolated syndrome patients and healthy controls at 1-year

	HC	% of CI	CIS	% of CI	P-value
CSCT	0.43 (1.18)	1.9 %	0.02 (1.04)	7.3 %	0.09
BVMTR	0.44 (0.72)	0 %	0.39 (0.89)	4.9 %	0.91
BVMTR-DR	0.22 (0.77)	3.8 %	0.15 (0.89)	4.9 %	0.69
PASAT	0.39 (0.8)	1.9 %	0.36 (0.91)	2.4 %	0.94
SRT-LTS	0.38 (0.75)	1.9 %	0.26 (1.16)	7.3 %	0.65
SRT-CLTR	0.27 (0.98)	1.9 %	0.31 (1.1)	4.9 %	0.85
SRT-DR	0.15 (0.88)	7.5 %	-0.04 (1.06)	9.8 %	0.84
WLG	-0.24 (0.96)	1.9 %	-0.19 (0.98)	7.3 %	0.81
Alertness	0.68 (0.61)	0 %	0.25 (1.2)	7.3 %	0.17
RT_Simple_Visual_Attention	0.27 (1.01)	3.8 %	-0.05 (1.1)	12.2 %	0.16
RT_Simple_Auditory_Attention	0.30 (0.91)	1.9 %	-0.07 (1.16)	9.8 %	0.13
RT_Divided_Visual_Attention	0.08 (1.22)	1.9 %	-0.09 (1.27)	7.3 %	0.80
RT_Divided_Auditory_Attention	-0.11 (1.17)	13.2 %	-0.003 (1.33)	7.3 %	0.96
Stroop	0.19 (0.99)	3.8 %	0.35 (1.1)	7.5 %	0.46

Cognitive impairment at each test is determined at the 5th percentile (z-score < -1.64).
HC: healthy controls; CIS: clinically isolated syndrome; CI: cognitive impairment; CSCT: computerized speed cognitive test; BVMTR: brief visual memory test revised; DR: delay recall; PASAT: paced auditory serial addition

test; SRT: selective reminding test; LTS: long-term storage; CLTR: consistent long-term retrieval; WLG: word list generation; RT: reaction time.

Figure S1: Lesion frequency map of CIS patients

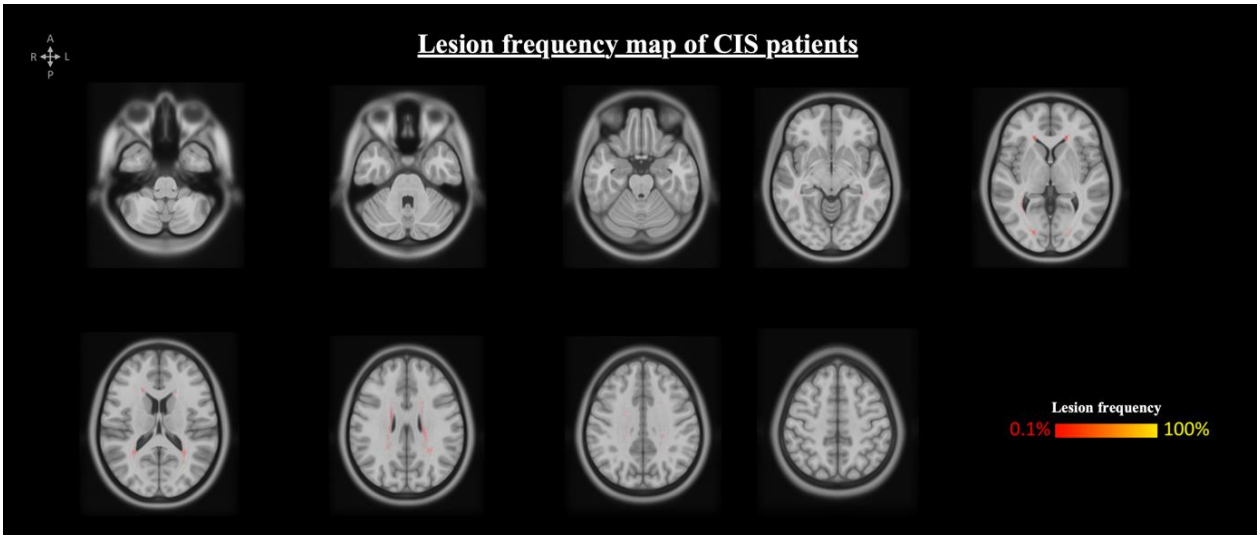

Table S4: Location of regional alterations in structural network metrics

Brain region	Network	Patients vs controls at baseline	Patients vs controls at year 1
Clustering coefficient			
Pallidum	SN	+(R)	
Paracentral G and S	SMN	+(L/R)	
Middle occipital G	VN	+(L)	
Superior occipital G	VN	+(L/R)	
Inferior angular parietal G	DMN	+(L/R)	
Inferior supramarginal parietal G	SN	+(L)	
Superior parietal G	VN	+(L/R)	
Postcentral G	SMN	+(L/R)	
Precentral G	SMN	+(L/R)	
Inferior temporal G	DMN	+(L)	
Superior frontal G	DMN	+(R)	
Precuneus G	DMN	+(R)	
Participation coefficient			
Mid-posterior cingulate G and S	SN	+(L)	
Central S	SMN	-(L)	-(L/R)
Inferior supramarginal parietal G	SN	+(R)	+(L)
Within-degree module z-score			
Superior occipital G	VN	+(L/R)	+(L)
Postcentral G	SMN	+(L)	
Middle frontal G	FPN	+(R)	
Cerebellum	FPN		-(L/R)
Superior frontal S	DMN		+(R)
Inferior temporal S	DMN		-(R)

G: gyrus; S: sulcus; L: left; R: right; +: increase in patients compared to controls; -: decrease in patients compared to controls; FPN: frontoparietal network; SN: salience network; DMN: default mode network; VN: visual network; SMN: somato-motor network.

Table S5: Location of regional alterations in functional network metrics

Brain region	Network	Patients vs controls at baseline	Patients vs controls at year 1
Betweenness centrality			
-	-	-	-
Participation coefficient			
Insula anterior circular S	FPN		+(R)
Within-degree module z-score			
Hippocampus	DMN		+(R)
Frontomarginal G and S	DMN		-(L/R)
Post-ventral cingulate G	DMN		+(L)
Temporal pole	DMN		-(L)

G: gyrus; S: sulcus; L: left; R: right; +: increase in patients compared to controls; -: decrease in patients compared to controls; FPN: frontoparietal network; DMN: default mode network.

Table S6: Baseline DTI clustering coefficient differences between patients and controls for each parcellation scheme

Parcellation scheme n°	Patients		Controls		p-value
	Mean	Std	Mean	Std	
1	0.00314	0.00133	0.00240	0.00134	0.049
2	0.00316	0.00116	0.00249	0.00129	0.048
3	0.00304	0.00102	0.00235	0.00105	0.018
4	0.00302	0.00114	0.00232	0.00118	0.032
5	0.00321	0.00134	0.00238	0.00118	0.023
6	0.00289	0.00094	0.00224	0.00102	0.018
7	0.00310	0.00114	0.00239	0.00118	0.030
8	0.00316	0.00130	0.00242	0.00137	0.047
9	0.00309	0.00113	0.00238	0.00118	0.029
10	0.00313	0.00113	0.00243	0.00124	0.037
11	0.00309	0.00115	0.00235	0.00122	0.026
12	0.00298	0.00111	0.00231	0.00119	0.035
13	0.00302	0.00114	0.00230	0.00116	0.026
14	0.00315	0.00128	0.00237	0.00122	0.030
15	0.00322	0.00134	0.00245	0.00137	0.044
16	0.00316	0.00130	0.00236	0.00117	0.026
17	0.00304	0.00114	0.00236	0.00127	0.041
18	0.00310	0.00120	0.00239	0.00127	0.039
19	0.00312	0.00119	0.00242	0.00128	0.041
20	0.00293	0.00099	0.00221	0.00091	0.009
21	0.00313	0.00119	0.00242	0.00139	0.048
22	0.00303	0.00111	0.00235	0.00122	0.036
23	0.00304	0.00112	0.00234	0.00121	0.034
24	0.00312	0.00120	0.00233	0.00112	0.019
25	0.00303	0.00127	0.00231	0.00132	0.048
26	0.00298	0.00101	0.00231	0.00109	0.023
27	0.00308	0.00115	0.00238	0.00125	0.038
28	0.00314	0.00118	0.00239	0.00120	0.026
29	0.00312	0.00126	0.00235	0.00121	0.028
30	0.00319	0.00125	0.00243	0.00132	0.037

Table S7: 1-year fMRI betweenness centrality differences between patients and controls for each parcellation scheme

Parcellation scheme n°	Patients		Controls		p-value
	Mean	Std	Mean	Std	
1	0.03196	0.00248	0.00872	0.01505	$p < 0.0001$
2	0.03203	0.00221	0.00832	0.01435	$p < 0.0001$
3	0.03180	0.00205	0.00848	0.01463	$p < 0.0001$
4	0.03261	0.00227	0.00859	0.01482	$p < 0.0001$
5	0.03262	0.00258	0.00845	0.01456	$p < 0.0001$
6	0.03156	0.00184	0.00895	0.01547	$p < 0.0001$
7	0.03189	0.00255	0.00848	0.01461	$p < 0.0001$
8	0.03107	0.00227	0.00778	0.01340	$p < 0.0001$
9	0.03224	0.00259	0.00828	0.01434	$p < 0.0001$
10	0.03186	0.00233	0.00883	0.01519	$p < 0.0001$
11	0.03250	0.00255	0.00850	0.01468	$p < 0.0001$
12	0.03172	0.00233	0.00832	0.01438	$p < 0.0001$
13	0.03251	0.00262	0.00868	0.01495	$p < 0.0001$
14	0.03178	0.00234	0.00828	0.01426	$p < 0.0001$
15	0.03115	0.00188	0.00821	0.01413	$p < 0.0001$
16	0.03243	0.00266	0.00848	0.01462	$p < 0.0001$
17	0.03248	0.00229	0.00844	0.01453	$p < 0.0001$
18	0.03200	0.00247	0.00797	0.01374	$p < 0.0001$
19	0.03165	0.00259	0.00806	0.01388	$p < 0.0001$
20	0.03198	0.00270	0.00823	0.01417	$p < 0.0001$
21	0.03258	0.00230	0.00841	0.01449	$p < 0.0001$
22	0.03184	0.00253	0.00801	0.01380	$p < 0.0001$
23	0.03201	0.00226	0.00794	0.01366	$p < 0.0001$
24	0.03286	0.00248	0.00841	0.01450	$p < 0.0001$
25	0.03315	0.00270	0.00905	0.01561	$p < 0.0001$
26	0.03188	0.00241	0.00833	0.01445	$p < 0.0001$
27	0.03297	0.00249	0.00893	0.01538	$p < 0.0001$
28	0.03294	0.00255	0.00844	0.01451	$p < 0.0001$
29	0.03166	0.00216	0.00825	0.01421	$p < 0.0001$
30	0.03218	0.00259	0.00881	0.01522	$p < 0.0001$

References

Koubiyr, Ismail, Mathilde Deloire, Pierre Besson, Pierrick Coupé, Cécile Dulau, Jean Pelletier, Thomas Tourdias, et al. 2018. “Longitudinal Study of Functional Brain Network Reorganization in Clinically Isolated Syndrome,” 1–13. https://doi.org/10.1177/1352458518813108.

Chapter 5

General discussion

In the present chapter, I will summarize the main findings of this thesis, then I will state the limitations of our study. I will also present our perspectives and introduce the future work we intend to do.

Main findings

In **chapter 2**, we showed that:

Gray matter is differentially vulnerable at the beginning of MS as only hippocampus showed microstructural alterations at the CIS stage, while no deep gray matter or cortical atrophy was noticed.

After one year of evolution, the pathology was spreading towards the cortex and gray matter volume loss was depicted in the hippocampus, the putamen and different parts of the cortex.

Hippocampus mean diffusivity at baseline is independently able to predict its volume loss over one year.

In **chapter 3**, we showed that:

Regional functional brain reorganization starts from the beginning of the disease and becomes more pronounced after one year of evolution.

There was no difference in the brain's functional global efficiency between CIS patients and healthy controls, along with preserved cognitive performances in patients.

Functional reorganization was correlated to the brief visuospatial memory test, indicating a more pronounced brain network reorganization as the cognitive performances are getting better.

These results suggest a compensation mechanism at the first year after a CIS.

In **chapter 4**, we showed that:

Structural damage precedes functional reorganization at a global and modular level during the first year following a CIS.

Structural-functional decoupling is only present after one year of the disease onset, specifically in the salience, visual and somatomotor networks, along with preserved cognitive performances.

These results suggest that functional reorganization, that may be responsible for the preservation of cognitive performances, occurs along indirect anatomical pathways.

Mechanisms of cognitive impairment in MS

Even though the exact mechanisms underlying the onset and progression of cognitive impairment in MS are still unclear, we have tried to shed some light into the neural correlates of cognitive functioning in the early stage of MS.

Focal white matter lesions may play a key role in the interruption of neuronal pathways supporting physiological cognitive functioning.[1] Previous MRI studies showed that cognitive performances correlate better with measures of diffuse brain damage than lesion load.[2,3] This led to the hypothesis that MS-related cognitive deficits derive from a **disconnection syndrome** mainly affecting white matter.[4] MRI surrogates of diffuse damage of apparently normal brain tissue, such as the mean magnetization transfer ratio (MTR), correlate well with cognitive deterioration overtime.[5] Although many studies investigated the association between white matter lesion load/diffuse damage and cognitive performance in MS,[1] the origin of cognitive impairment in MS seems to be more complex and multifactorial combining both white matter and gray matter pathology. GM pathology in key areas like the cerebellum, the thalami and the cerebral cortex could play a major role in these mechanisms particularly early on before diffuse damage. For example, cerebellum has been associated with cognitive processes both in healthy subjects and MS patients.[6,7] Anatomically, the cortico-cerebellar loop connects cerebellar posterior hemispheres and dentate nuclei to prefrontal, superior temporal and lateral parietal cortices, via the thalamus and the pons. An association between cognitive impairment and atrophy in specific cerebellar lobules was shown in MS patients,[8] while a decrease in cerebellar activation was considered to be a failure of the cerebellum in its role facilitating rapid cognitive performances. This failure of cerebellum facilitation on cognitive processes paralleled the activation of frontal compensatory mechanisms which is associated with the extent of diffuse brain damage.[9] The loss of the facilitating role of the cerebellum on information processing speed (IPS) due to damage to the posterior cerebellar lobules could contribute significantly to the slowness of IPS.[6] The thalamus is considered as a central node playing an important role in many cognitive functions such as IPS, episodic memory, working memory, and attention with its cortical, subcortical, and cerebellar connections.[10] It could be considered as a central hub in several networks including those particularly involved in IPS through the cortico-cerebellar loops. Thalamic involvement in cognitive deficits in MS has been previously highlighted.[11-13] Neuronal loss and demyelination were observed in thalamic tissue of MS patients and MRI revealed thalamic atrophy and abnormal

microstructural integrity using DTI metrics.[14,15] It has been proposed that thalamic involvement in cognitive impairment in MS is related to GM rather than WM damage in thalamic nuclei.[16] Consequently, early GM or diffuse WM damage within the relevant WM tracts between these key eloquent GM areas could explain the emergence of cognitive deficits. Compensatory mechanisms have been found mainly at the early stage of MS and could explain the paradox of the heterogeneous cognitive performances with the same visible brain damage.[9,17] In this context, we have investigated the differential vulnerability of gray matter involvement in the early stage of MS (**Chapter 2**). We showed that hippocampus was the first altered structure with microstructural abnormalities appearing from the onset of the disease and predicting its future volume loss, and that the pathology was spreading towards the cortex after one year of evolution. This result indicates the importance of early neurodegeneration, especially in the hippocampus. Using the experimental autoimmune encephalomyelitis (EAE) model (one of the most utilized models in MS research), it was recently shown that synaptic plasticity deficits in the dentate gyrus were associated with dendritic degeneration, neuronal apoptosis, microglial activation and diffusion tensor imaging abnormalities, causing early memory impairment.[18] This reinforces the idea that **synaptic failure** may play an important role in the pathogenesis of MS-related cognitive impairment.

Another important approach to use to better understand the neural correlates of cognitive performance in MS is the investigation of functional networks reorganization. In MS, increased functional connectivity was detected as a possible compensatory mechanism,[19-24] while decreased functional connectivity as a probable consequence of maladaptive reorganization due to acute or chronic inflammation was also detected.[20,22,23] These previous studies suggested network alterations predominantly in the sensorimotor cortex, cingulate, and fronto-temporal regions, as well as in the thalamus.[20-23] These heterogeneous findings of connectivity may be due to the inclusion of different sample sizes, phenotypes, disease durations, or disability levels. Also, most studies have been performed cross-sectionally, which limits the understanding of the dynamics of brain network reorganization in MS and, thus cannot infer about the role of these connectivity changes. While at rest, the brain presents several large-scale cerebral networks called resting-state networks.[24] These networks included the sensorimotor and visual networks, primarily involved in the processing of sensorimotor and visual information, respectively, as well as the frontoparietal network, which is involved in different types of cognitive processes.[25,26] The most widely studied

resting state network is the default mode network (DMN), encompassing precuneus/posterior cingulate cortex (PCC), mesiofrontal/anterior cingulate cortex (ACC), and temporoparietal junction areas. This network has been associated to different cognitive functions, such as stimulus-independent thoughts,[27] mind-wandering,[28] social cognition,[29] introspection,[30] monitoring of the mental self,[31] and integration of cognitive processes.[32] Importantly, functional changes were noticed in MS patients' DMN with both increased[21,33] and decreased[34-36] connectivity both related to poorer cognitive performances. It was even shown that during the disease, cognitively impaired patients present a shift in the hierarchy of the entire brain network, where the DMN becomes more important.[23] However, most of these studies considered functional connectivities as stationary by averaging the signal over the entire scan. More recent evidence points towards the nonstationarity of brain functional connections and how they alternate between periods of low and high functional coupling over time.[37,38] The dynamics of these fluctuations have been shown to be reduced in cognitively impaired MS patients in default-mode, frontoparietal, and visual networks, in addition to a loss of the interplay between default-mode and visual networks.[39] In order to detect the potential brain functional reorganization at the onset of the disease, (**Chapter 3**), we used a longitudinal cohort of CIS patients and showed that regional functional brain reorganization starts from the beginning of the disease and becomes more pronounced after one year of evolution, with a combination of overconnected and underconnected brain regions. This functional reorganization was present along with preserved cognitive performances, and more importantly, these cognitive performances were getting better as brain network reorganization was more pronounced, suggesting a compensation mechanism at this early stage of the disease. Currently, it is still a matter of debate whether functional reorganization is a maladaptive or compensative mechanism to the disease.[40-42] However, using longitudinal studies combining neuropsychological assessments and MRI data, we can untangle these processes and better model the evolution of the pathology.

Moreover, functional connectivity (FC) can be shaped and constrained by the structural connectivity (SC).[43] Nevertheless, the consequences of structural brain damage on the change of connectivity are still poorly understood.[20,40] It is then important to look at the evolution of both modalities and how they relate to each other to get a better sense of the underlying mechanisms of the disease. This was the aim of **Chapter 4**, where we investigated a novel parameter called the structural-functional coupling, representing the direct association between FC and SC. We then

noticed a structural-functional decoupling in some brain networks, along with functional reorganization and preserved cognitive performances, suggesting that the functional reorganization responsible for the early compensation mechanism occurs along indirect anatomical pathways.

Finally, we highlight the importance of combining both structural and functional connectivity along with neuropsychological assessments in a longitudinal set-up to investigate the neural mechanisms of cognitive impairment in MS and move towards the confirmation of the network collapse hypothesis (discussed in **Chapter 1**).[46] Hence, studying our cohort some years later (see **Perspectives**) may confirm this hypothesis and elucidate the process behind network collapse and cognitive impairment.

Limitations

We have to keep in mind that our work is not without limitations. First, when assessing gray matter integrity, our patients did not have double inversion recovery (DIR) sequences, thus we could have missed some cortical lesions and included them in the cortical gray matter mask. Second, we are aware that the follow-up time (one year) is too short to observe more brain damage or worst cognitive functioning in our patients, this is why we intend to follow them at a longer period of time (see **Perspectives**). However, this short follow-up period was used to detect very early changes occurring at the onset of MS.

Also, regarding functional networks, we only considered the most robust effects in the steady state (i.e. averaging the whole scan). This leaves unknown transient states in network connectivity that may better explain how functional brain networks adapt to challenge and disruption, and how they relate to structural networks.

Additionally, our DTI data covers only 21 directions in the whole sphere as a trade-off to the good resolution obtained at the time of the study set-up. This could have affected our tractography estimation. However, this effect would be present in CIS patients and in healthy controls as well which could limit its influence. We intend to perform a more sophisticated diffusion sequence in a future study investigating CIS (see **Perspectives**). This would allow us to confirm our current results.

Perspectives

5-year follow-up of the CIS-COG study

As previously stated, we intend to further follow-up this current cohort, and we are currently calling them back for their 5-year visit. After 5 years of follow-up, we expect a more global structural-functional decoupling in MS patients. Whether this decoupling could be a compensative or maladaptive mechanism in terms of cognition would be an interesting and innovative result to look at, especially with the potential extent of their cognitive deficits at that stage. Additionally, by combining both modalities along with an extensive neuropsychological battery, we will be able to address with sufficient information the proposed model for MS evolution from the onset of the disease. It will also allow us to better understand the network's behavior during neurodegenerative and neuroinflammatory combined processes. Thus, these network measures will add reliable and quantifiable value in monitoring patients' disease progression and could have an impact on treatment decisions and management.

The GM-COG study

The GM-COG study is a translational project aiming to identify the mechanisms that trigger grey matter alterations at the early stage of MS and their impact on cognition. Part of this project includes a clinical study enrolling patients after their first clinical attack (i.e. CIS patients) scanned with state-of-the-art MRI techniques and tested with neuropsychological tests. With this cohort, we intend to better investigate the microstructural integrity using multi-shell diffusion data. Then, we are interested in analyzing subfields of important gray matter regions (e.g. hippocampus, thalamus). Here is a more detailed description of our future work:

Hippocampal subfields in the early stage of MS

We have previously demonstrated a regional vulnerability within the hippocampus in CIS patients, as the hippocampal degeneration spread from the dentate gyrus to CA1 in terms of atrophy (see **Annex**).[31] However, we did not yet investigate the microstructural integrity nor the functional changes within these subfields. By taking advantage of the multi-shell diffusion sequence included in the GM-COG study, we aim to have a better look at what is happening inside these subfields.

Neurite orientation dispersion and density imaging (NODDI)

Quantitative measures can be extracted from DTI data reflecting microstructural integrity, cellular organization and anatomical connectivity.[32] Multiple studies showed diffusion alterations in MS patients, whether in T2-lesions, normal appearing white matter or even gray matter.[33] However in MS, demyelination, axonal loss and fiber orientation dispersion have similar impact on DTI measures, and thus cannot be differentiated.[34] Advanced multi-shell diffusion-weighted imaging methods like the Neurite Orientation Dispersion and Density Imaging (NODDI) address some of these limitations by modeling the signal as the sum of three components: the cerebrospinal fluid (CSF) compartment with isotropic diffusion; the intra neurite compartment, which represents the space bounded by the membrane of neurites and is modeled as a set of cylinders of zero radius to capture the highly restricted nature of diffusion perpendicular to neurites and unhindered diffusion along them; and the extra neurite compartment, which refers to the space around the neurites occupied by cell bodies and glial cells (**Figure 1**).[35]

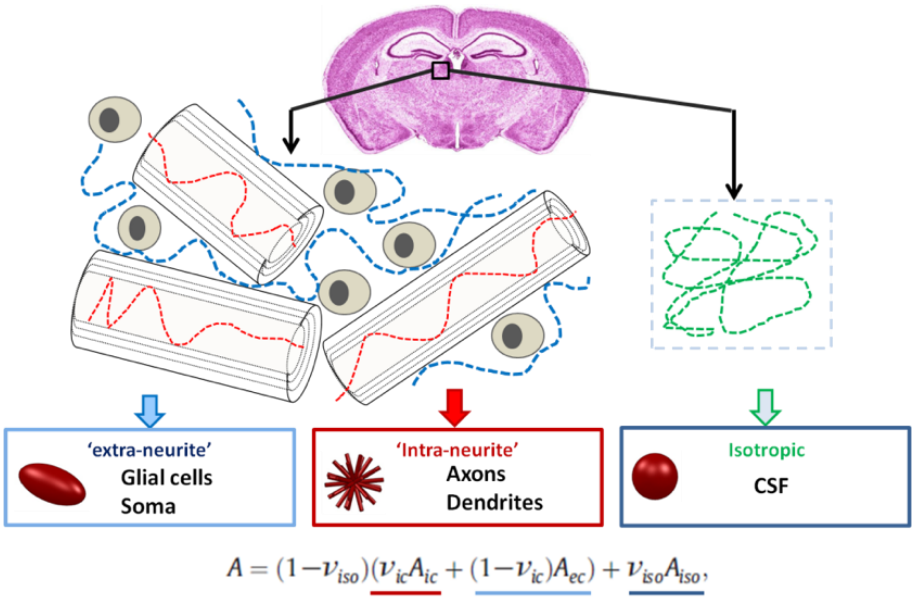

Figure 1. Principle of NODDI

NODDI is based on identification of 3 compartments at each voxel which account for the signal attenuation: 1) hindered reflecting the "extra-cellular" space and the glial environment, 2) restricted/intraneurites (axons and dendrites) that is described through the normalized parameter intra neurite volume fraction (also called "intra-cellular" vic) and that reflects the neurite density (ND) and 3) isotropic for CSF water molecules. The dispersion of sticks (representing neurites) is represented by the orientation dispersion (OD) index.

In a pilot study investigating 5 MS patients, Schneider and colleagues demonstrated the viability of NODDI in MS as it improved sensitivity and specificity by distinguishing orientation dispersion and fiber density better than classical DTI measures (**Figure 2**).[36]

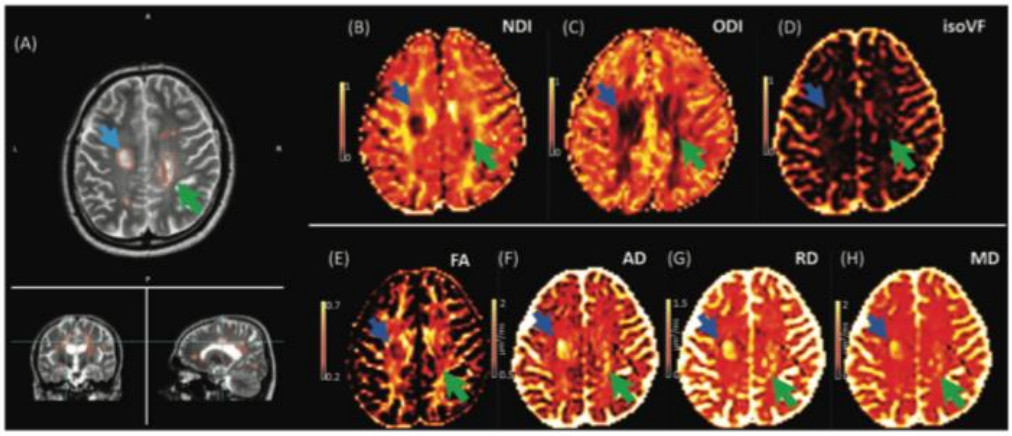

Figure 2. Neurite orientation dispersion density imaging (NODDI) and diffusion tensor imaging (DTI) maps from one multiple sclerosis patient

The blue arrow points the MS lesion within white matter associated to pronounced abnormalities in the axial diffusivity, mean diffusivity, radial diffusivity, and neurite density index (NDI) maps. The green arrow highlights the superiority of NDI compared to DTI metrics in periventricular lesion in particular in regions with cerebrospinal fluid partial volume and fiber crossings (Adapted from Schneider et al., 2017).

Besides, some studies showed the importance of NODDI as it correlated with myelin density in the corpus callosum in both healthy mouse and human brains and was not affected by crossing, fanning or kissing fiber.[37] In Parkinson's disease where NODDI was able to reflect a decrease in the length of dendrites and loss of dendritic spines in the substantia nigra pars compacta.[38] In that sense, our aim is to use this technique to assess the potential ability of NODDI to highlight early damage in MS, and to provide innovative and relevant information on the microstructural alterations in both white matter and gray matter regions. This will be the first study using NODDI technique to investigate microstructural damage in CIS patients. At this early stage of the disease, these results could represent an important and relevant tool for monitoring treatment (e.g. following neurites density in neuroprotective treatments).

Thalamic subfields

Recent works have highlighted the role of thalamus in cognition in MS.[12,13] It is known that thalamic pathology is frequently present in MS patients. Neuronal loss and demyelination were observed in thalamic tissue of MS patients and MRI revealed thalamic atrophy and abnormal DTI

metrics.[14,15] It has been proposed that thalamic involvement in cognitive impairment in MS is related to GM rather than WM damage in thalamic nuclei.[16] By analogy with the hippocampus in which some subfields could be more relevant than others, it is important to depict the thalamic nuclei directly involved in the cognitive networks and most prominent to damage in MS.

Our group in collaboration with Stanford University has pioneered the use of a particular regime of MR contrast with a sequence that we called white matter nulled MPRAGE (WMn-MPRAGE) and that generates a high contrast within the thalamus that it permits the delineation of its internal anatomy in close relation with the nuclei described in histological atlas (**Figure 3**).[39] This sequence is now available and included in our GM-COG protocol. It offers the unique opportunity to pinpoint specific nucleus to look for its contribution to a particular cognitive domain. In collaboration with Stanford, our group has developed an automatic segmentation method called THOMAS (Thalamus Optimized Multi-Atlas Segmentation) to make such a delineation fully automatically with high reproducibility.[40] We obtain higher resolution and better segmentation performance than current state of the art DTI and multi-modal techniques. We have therefore all the method to address the regional contribution of the thalamus (in terms of volume, microstructure or functional activity) in relation with cognitive performances at the early stage of MS.

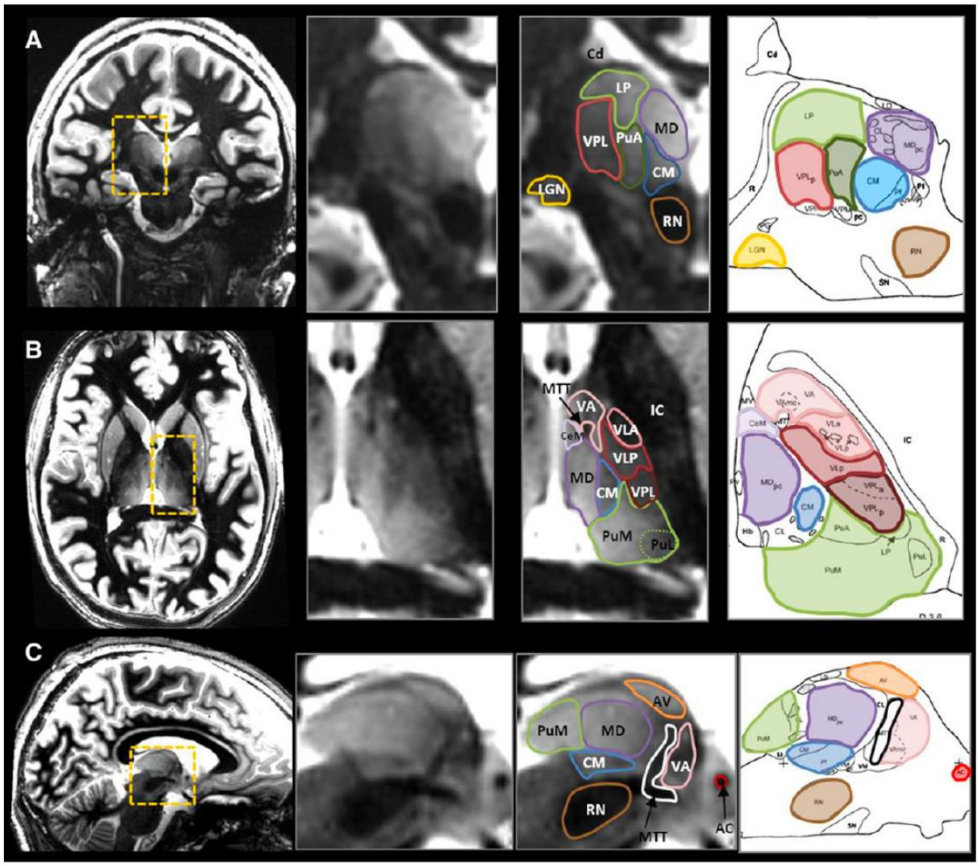

Figure 3. Visualization of thalamic nuclei compared with histological plates

Representative examples of MR scans in the 3 orthogonal orientations (each orientation shown in a different volunteer) and presented with the corresponding histological plates. Several nuclei can be identified thanks to enhanced intrinsic contrast between adjacent structures. Also, thin hypointense bands helped to isolate structures with otherwise close signal. For example, see the thin boundaries around the pulvinar anterior (PuA, green) in coronal (A), around the ventral anterior nucleus (VA, pink) in axial (B), and around the anterior ventral nucleus (AV, orange) in sagittal (C). Good correspondence between MR boundaries and the atlas can be observed. (Adapted from Tourdias et al., NeuroImage, 2013).

References

1. Rocca MA, Amato MP, De Stefano N, et al. Clinical and imaging assessment of cognitive dysfunction in multiple sclerosis. *Lancet Neurol* 2015; 14: 302–317.
2. Rocca MA, Amato MP, De Stefano N, Enzinger C, Geurts JJ, Penner IK, et al. Clinical and imaging assessment of cognitive dysfunction in multiple sclerosis. *Lancet Neurol*. 2015;14:302-317
3. Filippi M, Rocca MA, Benedict RH, DeLuca J, Geurts JJ, Rombouts SA, et al. The contribution of mri in assessing cognitive impairment in multiple sclerosis. *Neurology*. 2010;75:2121-2128
4. Dineen RA, Vilisaar J, Hlinka J, et al. Disconnection as a mechanism for cognitive dysfunction in multiple sclerosis. *Brain* 2009; 132: 239–249.
5. Deloire MS, Ruet A, Hamel D, Bonnet M, Dousset V, Brochet B. Mri predictors of cognitive outcome in early multiple sclerosis. *Neurology*. 2011;76:1161-1167
6. Buckner RL. The cerebellum and cognitive function: 25 years of insight from anatomy and neuroimaging. *Neuron*. 2013;80:807-815
7. Schmahmann JD. From movement to thought: Anatomic substrates of the cerebellar contribution to cognitive processing. *Hum Brain Mapp*. 1996;4:174-198
8. Moroso A, Ruet A, Lamargue-Hamel D, et al. Posterior lobules of the cerebellum and information processing speed at various stages of multiple sclerosis. *J Neurol Neurosurg Psychiatry* 2017; 88: 146–151.
9. Bonnet MC, Allard M, Dilharreguy B, Deloire M, Petry KG, Brochet B. Cognitive compensation failure in multiple sclerosis. *Neurology*. 2010;75:1241-1248
10. Kern KC, Gold SM, Lee B, Montag M, Horsfall J, O'Connor MF, et al. Thalamic-hippocampal-prefrontal disruption in relapsing-remitting multiple sclerosis. *Neuroimage Clin*. 2015;8:440-447
11. Batista S, Zivadinov R, Hoogs M, Bergsland N, Heininen-Brown M, Dwyer MG, et al. Basal ganglia, thalamus and neocortical atrophy predicting slowed cognitive processing in multiple sclerosis. *J Neurol*. 2012;259:139-146
12. Benedict RH, Hulst HE, Bergsland N, Schoonheim MM, Dwyer MG, Weinstock-Guttman B, et al. Clinical significance of atrophy and white matter mean diffusivity within the thalamus of multiple sclerosis patients. *Mult Scler*. 2013;19:1478-1484
13. Schoonheim MM, Hulst HE, Brandt RB, Strik M, Wink AM, Uitdehaag BM, et al. Thalamus structure and function determine severity of cognitive impairment in multiple sclerosis. *Neurology*. 2015;84:776-783
14. Cifelli A, Arridge M, Jezzard P, Esiri MM, Palace J, Matthews PM. Thalamic neurodegeneration in multiple sclerosis. *Ann Neurol*. 2002;52:650-653
15. Houtchens MK, Benedict RH, Killiany R, Sharma J, Jaisani Z, Singh B, et al. Thalamic atrophy and cognition in multiple sclerosis. *Neurology*. 2007;69:1213-1223
16. Bisecco A, Rocca MA, Pagani E, Mancini L, Enzinger C, Gallo A, et al. Connectivity-based parcellation of the thalamus in multiple sclerosis and its implications for cognitive impairment: A multicenter study. *Hum Brain Mapp*. 2015;36:2809-2825
17. Audoin B, Au Duong MV, Ranjeva JP, Ibarrola D, Malikova I, Confort-Gouny S, et al. Magnetic resonance study of the influence of tissue damage and cortical reorganization on pasat performance at the earliest stage of multiple sclerosis. *Hum Brain Mapp*. 2005;24:216-228

18. Planche V, Panatier A, Hiba B, et al. Selective dentate gyrus disruption causes memory impairment at the early stage of experimental multiple sclerosis. *Brain Behav Immun* 2017; 60: 240–254.
19. Dogonowski AM, Siebner HR, SoelbergSorensen P, et al. Resting-state connectivity of pre-motor cortex reflects disability in multiple sclerosis. *Acta Neurol Scand* 2013; 128(5): 328–335.
20. Rocca MA, Valsasina P, Meani A, et al. Impaired functional integration in multiple sclerosis: A graph theory study. *Brain Struct Funct* 2016; 221(1): 115–131.
21. Faivre A, Rico A, Zaaraoui W, et al. Assessing brain connectivity at rest is clinically relevant in early multiple sclerosis. *Mult Scler* 2012; 18(9): 1251–1258.
22. Schoonheim MM, Geurts JJG, Wiebenga OT, et al. Changes in functional network centrality underlie cognitive dysfunction and physical disability in multiple sclerosis. *Mult Scler* 2014; 20(8): 1058–1065.
23. Eijlers AJC, Meijer KA, Wassenaar TM, et al. Increased default-mode network centrality in cognitively impaired multiple sclerosis patients. *Neurology* 2017; 88(10): 952–960.
24. Damoiseaux JS, Rombouts SA, Barkhof F, Scheltens P, Stam CJ, Smith SM, Beckmann CF. Consistent resting-state networks across healthy subjects. *Proc Natl Acad Sci* U S A. 2006 Sep 12; 103(37):13848-53.
25. Dodds CM, Morein-Zamir S, Robbins TW. Dissociating inhibition, attention, and response control in the frontoparietal network using functional magnetic resonance imaging. *Cereb Cortex* 2011;21(5):1155–1165.
26. Scolari M, Seidl-Rathkopf KN, Kastner S. Functions of the human frontoparietal at- tention network: evidence from neuroimaging. *Curr Opin Behav Sci* 2015;1:32–39.
27. McKiernan KA, D'Angelo BR, Kaufman JN, Binder JR. Interrupting the "stream of consciousness": an fMRI investigation. *Neuroimage*. 2006 Feb 15; 29(4):1185-91.
28. Mason MF, Norton MI, Van Horn JD, Wegner DM, Grafton ST, Macrae CN. Wandering minds: the default network and stimulus-independent thought. *Science*. 2007 Jan 19; 315(5810):393-5.
29. Schilbach L, Eickhoff SB, Rotarska-Jagiela A, Fink GR, Vogeley K. Minds at rest? Social cognition as the default mode of cognizing and its putative relationship to the "default system" of the brain. *Conscious Cogn*. 2008 Jun; 17(2):457-67.
30. Goldberg II, Harel M, Malach R. When the brain loses its self: prefrontal inactivation during sensorimotor processing. *Neuron*. 2006 Apr 20; 50(2):329-39.
31. Lou HC, Luber B, Crupain M, Keenan JP, Nowak M, Kjaer TW, Sackeim HA, Lisanby SH. Parietal cortex and representation of the mental Self. *Proc Natl Acad Sci* U S A. 2004 Apr 27; 101(17):6827-32.
32. Greicius MD, Krasnow B, Reiss AL, Menon V. Functional connectivity in the resting brain: a network analysis of the default mode hypothesis. *Proc Natl Acad Sci* U S A. 2003 Jan 7; 100(1):253-8.
33. Hawellek DJ, Hipp JF, Lewis CM, Corbetta M, Engel AK. Increased functional connectivity indicates the severity of cognitive impairment in multiple sclerosis. *Proc Natl Acad Sci* USA 2011;108:19066–19071.
34. Louapre C, Perlbarg V, Garcia-Lorenzo D, et al. Brain networks disconnection in early multiple sclerosis cognitive deficits: an anatomofunctional study. *Hum Brain Mapp* 2014;35:4706–4717.

35. Rocca MA, Valsasina P, Absinta M, et al. Default-mode network dysfunction and cognitive impairment in progressive MS. *Neurology* 2010;74:1252–1259.
36. Leavitt VM, Paxton J, Sumowski JF. Default network connectivity is linked to memory status in multiple scle- rosis. *J Int Neuropsychol Soc* 2014;20:937–944.
37. Bassett DS, Sporns O. Network neuroscience. *Nat Neurosci* 2017;20(3):353–364.
38. Hutchison RM, Womelsdorf T, Allen EA, et al. Dynamic functional connectivity: promise, issues, and interpretations. *Neuroimage* 2013;80:360–378.
39. Eijlers AJC, Wink AM, Meijer KA, et al. Reduced Network Dynamics on Functional MRI Signals Cognitive Impairment in Multiple Sclerosis. *Radiology* 2019; 182623.
40. Tewarie P, Schoonheim MM, Schouten DI, et al. Functional brain networks: Linking thalamic atrophy to clinical disability in multiple sclerosis, a multimodal fMRI and MEG study. *Hum Brain Mapp* 2015; 36(2): 603–618.
41. Penner IK, Aktas O. Functional reorganization is a maladaptive response to injury - NO. *Multiple Sclerosis Journal* 2017; 23: 194–196.
42. Rocca MA, Filippi M. Functional reorganization is a maladaptive response to injury – YES. *Mult Scler J* 2017; 23: 191–193.
43. Schoonheim MM. Functional reorganization is a maladaptive response to injury – Commentary. *Mult Scler J* 2017; 23: 194–196.
44. Honey CJ, Sporns O, Cammoun L, et al. Predicting human resting-state functional connectivity from structural connectivity. *Proc Natl Acad Sci* 2009; 106: 2035–2040.
45. Zhou F, Zhuang Y, Wang L, Zhang Y, Wu L, Zeng X, et al. Disconnection of the hippocampus and amygdala associated with lesion load in relapsing-remitting multiple sclerosis: A structural and functional connectivity study. *Neuropsychiatr Dis Treat*. 2015;11:1749-1765
46. Schoonheim MM, Meijer KA, Geurts JJG. Network collapse and cognitive impairment in multiple sclerosis. *Front Neurol*; 6. Epub ahead of print 2015. DOI: 10.3389/fneur.2015.00082.
47. Planche V, Koubiyr I, Romero JE, et al. Regional hippocampal vulnerability in early multiple sclerosis: Dynamic pathological spreading from dentate gyrus to CA1. *Hum Brain Mapp* 2018; 39: 1814–1824.
48. Le Bihan D. Apparent Diffusion Coefficient and Beyond: What Diffusion MR Imaging Can Tell Us about Tissue Structure. *Radiology* 2013; 268: 318–322.
49. Rovaris, M. and Filippi, M. (2007) 'Diffusion tensor MRI in multiple sclerosis', *Journal of Neuroimaging*, 17(SUPPL. 1), pp. 27–30. doi: 10.1111/j.1552-6569.2007.00133.x.
50. Wheeler-Kingshott, C. A. M. and Cercignani, M. (2009) 'About "axial" and "radial" diffusivities', *Magnetic Resonance in Medicine*. Wiley-Blackwell, 61(5), pp. 1255–1260. doi: 10.1002/mrm.21965.
51. Zhang, H., Schneider, T., Wheeler-Kingshott, C. A. and Alexander, D. C. (2012) 'NODDI: Practical in vivo neurite orientation dispersion and density imaging of the human brain', *NeuroImage*, 61(4), pp. 1000–1016. doi: 10.1016/j.neuroimage.2012.03.072.
52. Schneider, T., Brownlee, W., Zhang, H., Ciccarelli, O., Miller, D. H. and Wheeler-Kingshott, C. G. (2017) Sensitivity of multi-shell NODDI to multiple sclerosis white matter changes: A pilot study, *Functional Neurology*. doi: 10.11138/FNeur/2017.32.2.097.
53. Sepehrband, F., Clark, K. A., Ullmann, J. F. P., Kurniawan, N. D., Leanage, G., Reutens, D. C. and Yang, Z. (2015) 'Brain tissue compartment density estimated using diffusion-

weighted MRI yields tissue parameters consistent with histology', *Human Brain Mapping*. John Wiley & Sons, Ltd, 36(9), pp. 3687–3702. doi: 10.1002/hbm.22872.
54. Kamagata, K., Hatano, T., Okuzumi, A., Motoi, Y., Abe, O., Shimoji, K., Kamiya, K., Suzuki, M., Hori, M., Kumamaru, K. K., Hattori, N. and Aoki, S. (2016) 'Neurite orientation dispersion and density imaging in the substantia nigra in idiopathic Parkinson disease'. *Eur Radiol*. doi: 10.1007/s00330-015-4066-8.
55. Tourdias T, Saranathan M, Levesque IR, Su J, Rutt BK. Visualization of intra-thalamic nuclei with optimized white-matter-nulled mprage at 7t. *Neuroimage*. 2013;84C:534-545.
56. Su JH, Thomas FT, Kasoff WS, et al. Thalamus Optimized Multi Atlas Segmentation (THOMAS): fast, fully automated segmentation of thalamic nuclei from structural MRI. *Neuroimage* 2019; 194: 272–282.

Annex

Regional hippocampal vulnerability in early multiple sclerosis: dynamic pathological spreading from dentate gyrus to CA1

Vincent Planche[1,2,3], Ismail Koubiyr[1,2], José E. Romero[4], José V. Manjon[4], Pierrick Coupé[5], Mathilde Deloire[3], Vincent Dousset[1,2,3], Bruno Brochet[1,2,3] , Aurélie Ruet[1,2,3,#] and Thomas Tourdias[1,2,3,#]

[1] Univ. Bordeaux, F-33000 Bordeaux, France

[2] Inserm U1215 - Neurocentre Magendie, F-33000 Bordeaux, France

[3] CHU de Bordeaux, F-33000 Bordeaux, France

[4] Instituto Universitario de Tecnologías de la Información y Comunicaciones (ITACA), Universitat Politècnica de València, Camino de Vera s/n, 46022 Valencia, España

[5] Laboratoire Bordelais de Recherche en Informatique, UMR CNRS 5800, PICTURA, F-33405 Talence, France

# Both authors contributed equally to this work

Human Brain Mapping. (2018) doi: 10.1002/hbm.23970

Abstract

Background*:* Whether hippocampal subfields are differentially vulnerable at the earliest stages of multiple sclerosis (MS) and how this impacts memory performances is a current topic of debate.

Methods*:* We prospectively included 56 persons with clinically isolated syndrome (CIS) suggestive of MS in a 1-year longitudinal study, together with 55 matched healthy controls at baseline. Participants were tested for memory performance and scanned with 3T MRI to assess the volume of 5 distinct hippocampal subfields using automatic segmentation techniques.

Results*:* At baseline, CA4/dentate gyrus was the only hippocampal subfield with a volume significantly smaller than controls ($p<0.01$) compared to controls. After one year, CA4/dentate gyrus atrophy worsened (-6.4%, $p<0.0001$) and significant CA1 atrophy appeared (both in the stratum-pyramidale and the stratum radiatum-lacunosum-moleculare, -5.6%, $p<0.001$ and -6.2%, $p<0.01$) respectively. CA4/dentate gyrus volume at baseline predicted CA1 volume one year after CIS (R^2=0.44 to 0.47, $p<0.001$, with age, T2 lesion-load and global brain atrophy as covariates). The volume of CA4/dentate gyrus at baseline was associated with MS diagnosis during follow-up, independently of T2-lesion load and demographic variables ($p<0.05$). Whereas CA4/dentate gyrus volume was not correlated with memory scores at baseline, CA1 atrophy was an independent correlate of episodic verbal memory performance one year after CIS (ß=0.87, $p<0.05$).

Conclusion*:* The hippocampal degenerative process spread from dentate gyrus to CA1 at the earliest stage of MS. This dynamic vulnerability is associated with MS diagnosis after CIS and will ultimately impact hippocampal-dependant memory performances.

Introduction

Patients with multiple sclerosis (MS) are often afflicted with episodic memory impairment and, over the past decade, a growing number of studies have investigated how hippocampal abnormalities might be related to this deficit.[1-4] Post-mortem anatomopathological analyses of MS brains, together with studies on animal models of MS, have described early microglial activation, neuronal loss, synaptic dysfunction and demyelination within different regions of the hippocampus.[2,5,6] However, the time course of these alterations and the inter-relations between the different types of cellular modifications during the evolution of the disease remain largely unknown.

One way to isolate pathogenic mechanisms within the hippocampal circuit is to study its regional vulnerability.[7] Indeed, the hippocampus is composed of distinct subfields whose morphological, cellular, molecular, functional and connectivity profiles are very different: the dentate gyrus, the cornu ammonis (CA, with subdivisions from CA1 to CA4) and the subiculum. Initially used to study Alzheimer's disease and physiological aging,[8] this approach of interrogating differentially the malfunctioning hippocampal circuit has been adapted more recently to investigate MS.[1,9-11]

Regarding MRI studies, the differential vulnerability of one hippocampal subfield compared to the others during the course of MS remains controversial. Indeed, some authors have highlighted the differential vulnerability of CA1[1,10] and others the vulnerability of CA3/CA4/dentate gyrus.[9,11] The reasons for discrepancies between studies remain speculative but they might be explained by the heterogeneity of the measurement methods used (surface-based mesh modelling and volumetric analyses) and/or by the heterogeneity of the populations studied (relapsing MS with different disease durations and/or progressive MS). This latter point seems crucial if we postulate that the pattern of atrophy of hippocampal subfields changes according to disease progression. Previous studies have so far been unable to test such timing and the dynamics of differential hippocampal subfield damage because of cross-sectional design. It is also important to note that none of these works investigated clinically isolated syndrome (CIS), which is required to address the question of the differential vulnerability of hippocampal subfields to the earliest pathophysiological mechanisms in MS. Indeed, CIS is the first demyelinating event suggestive of a future relapsing-remitting MS, that will be formally defined later on by the dissemination in time

and space of demyelinating lesions.[12,13] Thus, studying persons with CIS offers a unique opportunity to understand the "first steps" of the pathophysiological mechanisms leading to MS.

By analogy with other neurodegenerative diseases,[14,15] we hypothesize here that hippocampal degeneration in persons with CIS and early MS is not uniform and that pathological alterations will spread from one hippocampal subfield to the others in a process leading to diffuse hippocampal atrophy. To test this hypothesis, we measured the volumes of five distinct hippocampal subfields longitudinally, using advanced 3T MRI-based automatic segmentation techniques, and analysed the dynamics of atrophy of these subfields together with their clinical and neuropsychological correlates.

Methods

Participants

Fifty-six persons with CIS (PwCIS) were prospectively enrolled between 2 to 6 months after an initial clinical event compatible with a demyelinating inflammatory syndrome: a monofocal and monophasic neurological symptom that can be related to an optic nerve, spinal cord, brainstem or cerebellum lesion.[13] Patients were assessed by neuropsychological testing and MRI at baseline and at 1-year follow up. At baseline, at least two clinically silent lesions with a minimum diameter of 3mm were required for inclusion. One of these lesions had to be cerebral (ovoid or periventricular), while the other could be located in the spine or brain. None of the patients were treated with disease-modifying therapy at inclusion. Contraindications to MRI, the presence of other neurological, psychiatric or systemic diseases, steroid treatment within one month, starting or stopping antidepressants or anxiolytic treatments within 2 months of MRI and neuropsychological examination, were considered as exclusion criteria. During the follow-up period of one year, the diagnosis of multiple sclerosis was confirmed (or not) by the treating physician according to the 2010 McDonald criteria.[12]

Fifty-five healthy controls (HC), free of neurological, psychiatric, or systemic diseases, and drug or alcohol abuse, were also included. They were tightly matched for age, gender and educational level to PwCIS, to calculate cognitive z-scores both at baseline and one year after (see below). Among these 55 controls, a subgroup of 38 HC (still matched with the CIS group, see Table 1) underwent MRI at baseline but they were not re-scanned at year 1.

All subjects were prospectively enrolled from 2012 to 2015 at our MS centre. Written informed consent was obtained prior to participation. This study was approved by the local institutional ethics review board and registered in Clinicaltrial.gov (NCT01865357).

Neuropsychological testing

In order to assess hippocampal functions, PwCIS and HC performed the Selective Reminding Test (SRT) for episodic verbal memory performances and the Brief Visuospatial Memory Test (BVMT-R) to test episodic visuospatial memory performances. Each PwCIS was compared with the HC group at the appropriate time point to calculate a z-score for each test at each time point. To take into account practice effects, the scores of PwCIS at baseline were compared with the mean score of the HC group obtained at baseline, while the scores of PwCIS at 1 year were compared with the mean score of the HC group obtained during their second session of neuropsychological testing at 1 year. The z-scores of each SRT and BVMT-R subtest were averaged in order to calculate one composite verbal memory score and one composite visuospatial memory score. Lower z-scores indicate lower performances. A patient was considered impaired in a given cognitive domain if his/her score was below the fifth percentile (*i.e.* z-score < -1.64).

MRI acquisition and analyses

Participants were scanned on a 3T MRI system at our MS centre (either Philips Achieva or GE Medical Systems Discovery MR 750w). The imaging protocol was harmonized between magnets and included the same 3D gradient-echo T1-weighted sequence (TR/TE/TI/flip angle=8.2ms/3.5ms/982ms/7°, resolution 1x1x1mm, 256mm FOV) and a 2D axial Fluid Attenuated Inversion Recovery (FLAIR) sequence (TR/TE/TI=11000ms/140ms/2800ms, resolution 1x1.1x3mm, 230mm FOV).

Lesion load was determined by the lesion growth algorithm as implemented in the Lesion Segmentation Tool (LST) version 2.0.15 (http://www.applied-statistics.de/lst.html) in Statistical Parametric Mapping (SPM12).[16] To do this, T1 images were co-registered with FLAIR images to calculate lesion belief maps thresholded with the same parameters for each patient (kappa=0.3). Binary maps of lesions were reviewed and corrected manually by two blinded experts (MR engineer and neurologist), using 3D Slicer 4.4.0 (www.slicer.org).

For the volumetric analyses of brain structures, T1-weighted images were processed using the volBrain system (http://volbrain.upv.es).[17] After denoising with an adaptive non-local mean filter,[18] images were affine-registered in the Montreal Neurological Institute (MNI) space using ANTS software,[19] corrected for image inhomogeneities using N4[20] and finally intensity-normalized.[21] Then, the hippocampal subfields were segmented based on a multi-atlas framework combining nonlinear registration and patch-based label fusion.[22,23] This method uses a training library composed of 5 high resolution T1-weighted images labelled manually according to the protocol proposed by Winterburn and colleagues[24] which is one of the rare freely available atlases that specifically separate CA4/DG from CA2/3 on the one hand and CA1 neuritic and pyramidal layers on the other hand.[25] The 3D-T1-weighted images of the subjects considered in this study ($1x1x1mm^3$) were up-sampled to the image resolution of the training library ($0.5x0.5x0.5mm^3$) using the local adaptive super-resolution (LASR) method.[26] The method finally provided automatic segmentation of hippocampal subfields gathered into 5 labels: Subiculum, CA1-SP (stratum pyramidale), CA1-SRLM (stratum radiatum-lacunosum-moleculare), CA2/3 and CA4/dentate gyrus (**Fig. 1**), allowing us to test our *a priori* hypotheses regarding the selective vulnerability of the dentate gyrus or CA1, as suggested in the literature from animal, neuropsychological (using pattern separation tasks) and MRI studies.[1,6,11,27] Every up-sampled image and every subfield label were quality-controlled and then blindly checked and manually corrected by a blinded neurologist if needed (in the case of inappropriate inclusion of para-hippocampal T1-hypointense lesions (**Suppl. Fig. 1**), choroidal plexus and/or CSF "pockets", using 3D Slicer 4.4.0 (www.slicer.org)). To control for variations in head size, the volumes of hippocampal subfields were normalized using the intracranial cavity volume of each subject.[28] Normalized brain volume (NBV) was also calculated as the sum of cerebral white and grey matters, divided by the intracranial cavity volume of each subject.

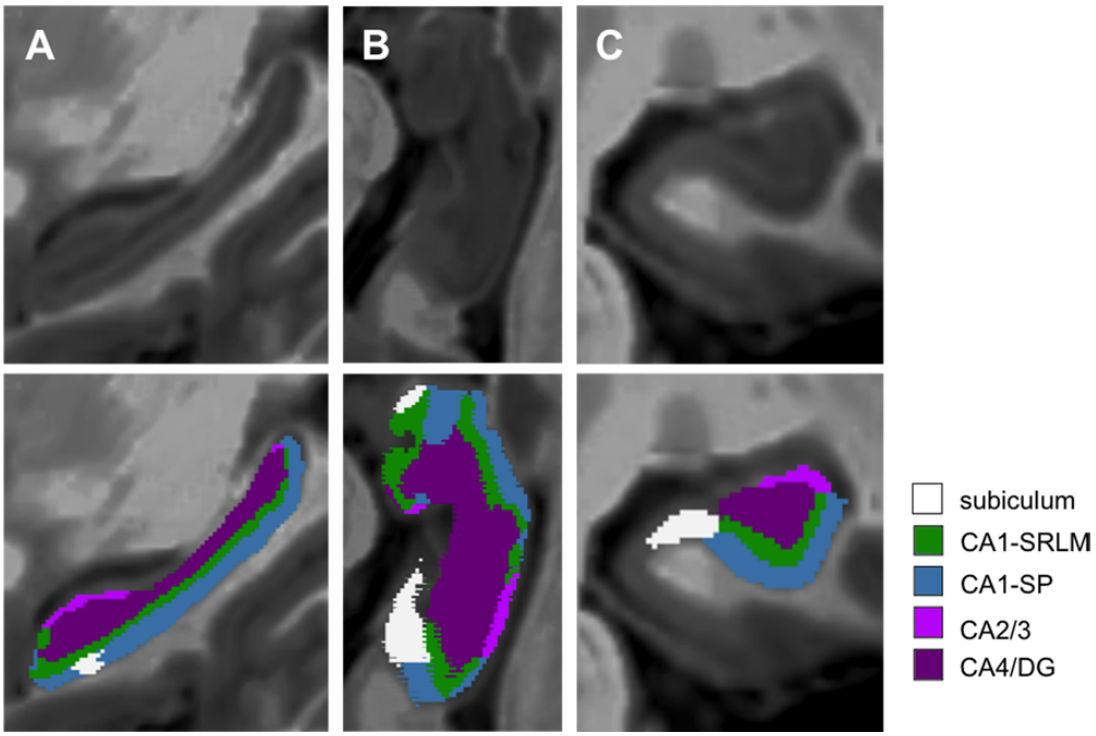

Figure 1: Segmentation of the five hippocampal subfields.
Super-resolution T1-weighted images (0.5x0.5x0.5mm^3) centred on the left hippocampus of a patient with clinically isolated syndrome (PwCIS) in the sagittal plane (A), in an oblique axial cut parallel to the plane of the hippocampus (B) and in the coronal plane (C). Five hippocampal subfields were automatically segmented (and manually corrected if needed) according to the atlas of Winterburn *et al*.: the subiculum, the stratum pyramidale of CA1 (CA1-SP), the stratum-lacunosum-moleculare of CA1 (CA1-SRLM), CA2/3 and CA/4dentate gyrus (CA4/DG).

Statistical Analyses

Statistical analyses were performed with Prism software 6 (Graphpad) and XLstats 19.4 (Addinsoft). The distribution of all continuous data was tested with the Shapiro-Wilk normality test. We first compared clinical, neuropsychological and imaging characteristics between HC and PwCIS at baseline by using Fisher's exact tests for categorical variables, and unpaired t-tests or Mann-Whitney tests for ordinal variables. The comparisons of baseline and 1-year characteristics of PwCIS were done with paired t-tests or Wilcoxon tests, as appropriate.

To compare the volumes of the 5 hippocampal subfields between groups, we first performed an analysis of variance, followed by a Sidak multiple comparisons test. Cohen's d was used to measure the effect size of atrophy between patients and HC whereas annualized rate of atrophy was used to compare PwCIS at year 1 and baseline.

Then, because the decreases in subfield volumes were consistent between right and left hippocampi, further statistical analyses were performed on the sum of right and left subfield volumes to avoid multiple comparisons. Relationships between neuropsychological scores, demographic, clinical and imaging variables were assessed using correlation coefficients (Pearson or Spearman according to statistical distribution). The associations were further tested in multivariate context. To this end, *(i)* hippocampal subfields volumes at year 1, *(ii)* conversion to MS and *(iii)* memory performances (dependent variables) were predicted with hierarchical regression models, including two hierarchical blocks. In the first block, relevant demographical, clinical and general MRI features known as nuisance variables were systematically forced into the model. In the second block, the volumes of hippocampal subfields were added to the variables of the first block. To evaluate the added prognostic value of CA4/DG baseline volume, the predictive power of the two blocks was compared by using the Akaike information criterion (AIC). A linear regression model was used whenever possible while logistic regression was seen as the appropriate alternative for categorical/binary outcome variables. All tests were two-tailed, with a global type I error set at $\alpha=0.05$.

Results

Demographic, clinical and general MRI features of participants

A total of 56 PwCIS and 55 HC were included. At baseline, all PwCIS and HC were tested with the neuropsychological battery while all PwCIS but only a subgroup 38 HCs were assessed with MRI. At year 1, because 10 patients were lost to follow-up, 46 PwCIS were re-tested with the same neuropsychological battery and re-scanned with the same imaging protocol. All the 55 HCs were re-tested with the same neuropsychological battery but they were not re-scanned at year 1.

The CIS and HC groups were comparable for age, sex and educational level (**Table 1**). In this cohort of patients, after one year, 65.2% of PwCIS were diagnosed with MS according to the 2010 McDonald criteria.

In PwCIS, there was no significant difference between baseline and 1-year follow-up regarding disability (Expanded Disability Status Scale, EDSS) and T2-lesion load. Neuropsychological testing was also rather stable between baseline and 1-year follow-up, except for the episodic visuospatial memory score that had even slightly increased (p=0.02) (**Table 1**). Normalized brain

volume (NBV) significantly decreased during this period (-1.4%, p=0.012).

Table 1: Clinical, neuropsychological and general MRI features of the studied populations

	Controls with MRI *(n=38)*	**CIS baseline** *(n=56)*	**CIS 1-year** *(n=46)*	***p-value***
Demographic and clinical features				
Mean age, years [SD]	36.6 [10.7]	36.5 [11.2]	-	0.94
Sex ratio (F/M)	26/12	46/10	-	0.14
Education level, (High/Low§)	27/11	39/17	-	0.88
Median EDSS score [range]	-	1.0 [1.0 to 6.0]	1.0 [1.0 to 6.0]	0.63
Conversion to MS	-	-	30/46 (65.2%)	-
Neuropsychological features				
Median verbal memory z-score [range] {% impaired}		0.10 [-4.9 to 1.0] {7.4%}	-0.13 [-3.7 to 1.2] {10.7%}	0.91
Median visuospatial memory z-score [range] {% impaired}		-0.20 [-5.2 to 0.82] {17.9%}	0.10 [-3.5 to 1.0] {6.5%}	0.02
Imaging features				
Median T2 lesion volume, mL [range]	-	0.73 [0.02-63.12]	1.08 [0.06-67.74]	0.67
Mean normalized brain volume, % [SD]	86.4 [3.2]	85.1 [3.9]	83.9 [4.1]	0.21#/0.012†

CIS = Clinically Isolated Syndrome; EDSS = Expanded Disability Status Scale; MS: Multiple Sclerosis; SD = Standard Deviation. § Education level was considered as high or low according to French baccalaureate (equivalent to A-level). # Controls vs CIS baseline. † CIS baseline vs CIS 1-year.

Dynamics of regional hippocampal vulnerability

At baseline, hippocampal volumes were significantly lower in PwCIS compared to controls only in the CA4/dentate gyrus subfield (**Fig. 2**). This was consistently true for the left (-6.5%, d=0.53, p<0.05) and for the right hippocampus (-7.7%, d=0.54, p<0.01) and when both sides were pooled together (-7.2%, d=0.58, p<0.01). In PwCIS, this atrophy of CA4/dentate gyrus was not correlated with age, disability or T2 lesion-load at baseline.

Follow-up data after one year compared to baseline measures showed that the normalized volumes of CA4/dentate gyrus (-6.4%, p<0.001), CA1-SP (-5,6%, p<0.01) and CA1-SRLM (-6,2%, p<0.05) significantly decreased in both sides. No significant atrophy was found in the subiculum or CA2/3 subfields (**Fig. 3**).

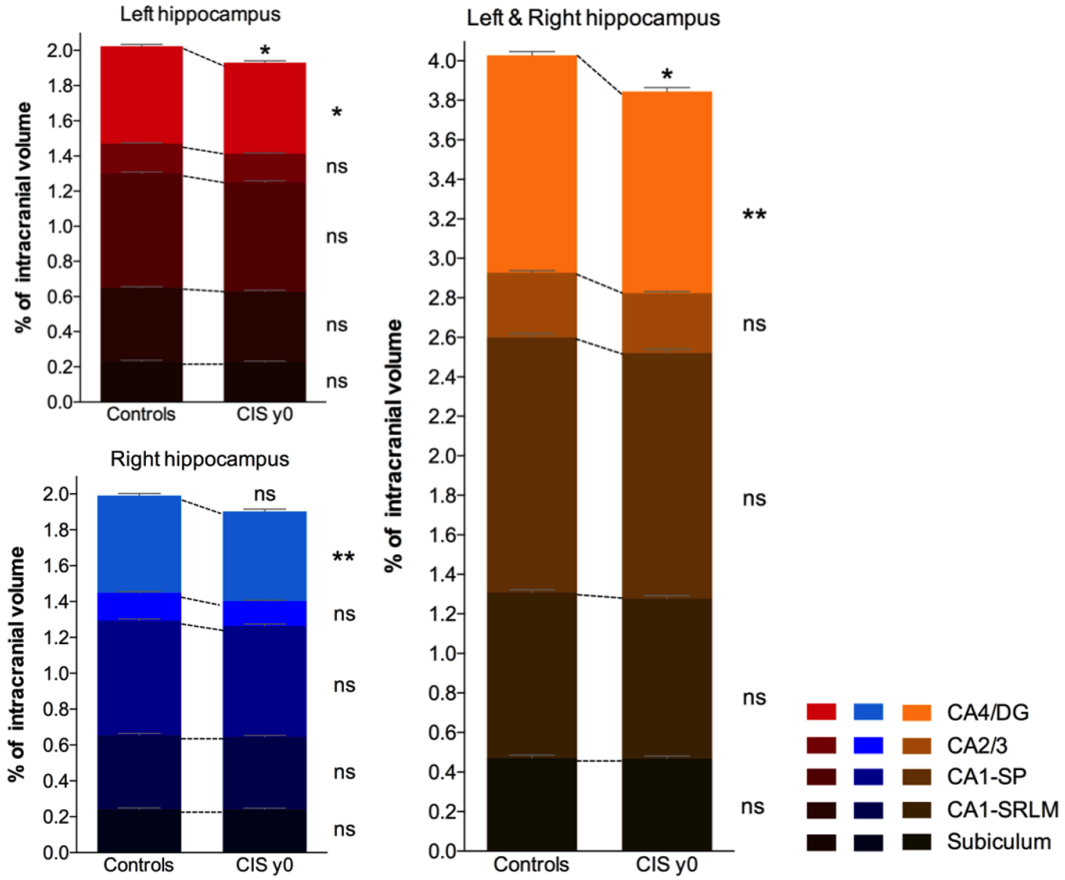

Figure 2: Comparison of the normalized volumes of hippocampal subfields between healthy controls and persons with clinically isolated syndrome (CIS) at baseline (y0).

Histograms represent the cumulative volumes of all the left hippocampal subfields (in red), of all the right hippocampal subfields (in blue) and of all right & left hippocampal subfields (in orange). The colour gradient represents individual hippocampal subfields. ns = non-significant, *p<0.05, **p<0.01 (corrected for multiple comparisons).

As the atrophy of CA1 subfield chronologically succeeded the atrophy of CA4/dentate gyrus, this suggests that the same pathophysiological process spreads from CA4/dentate gyrus to CA1 in individual patients. To test this hypothesis, we designed a hierarchical linear regression model to test how CA1-SP, CA1–SRLM and whole hippocampus volumes at year 1 (dependent variables) can be predicted by the volume of CA4/dentate gyrus at baseline (while first taking into account

confounders such as age, T2 lesion-load and NBV in the model). We found that CA4/dentate gyrus at baseline improved the statistical prediction of CA1 volumes at year 1 from R^2=0.19 (when considering usual factors such as age, T2 lesions and NBV) to R^2=0.44 ($AIC_{block2} < AIC_{block1}$). It also predicted the whole hippocampal volume one year afterwards independently of age, T2 lesions or NBV (**Table 2**). CA4/DG remained a significant and independent correlate of CA1 and whole hippocampal volumes at year 1, although other hippocampal subfields (subiculum and CA2/3) were introduced in the model (ß=0.34, p=0.018 for CA1-SP and ß=0.39, p<0.001 for the whole hippocampus, respectively). Altogether, a smaller focal volume at baseline predicted smaller global volumes at year 1, which points to a pathological continuum starting within CA4/dentate gyrus and spreading progressively and more globally to CA1.

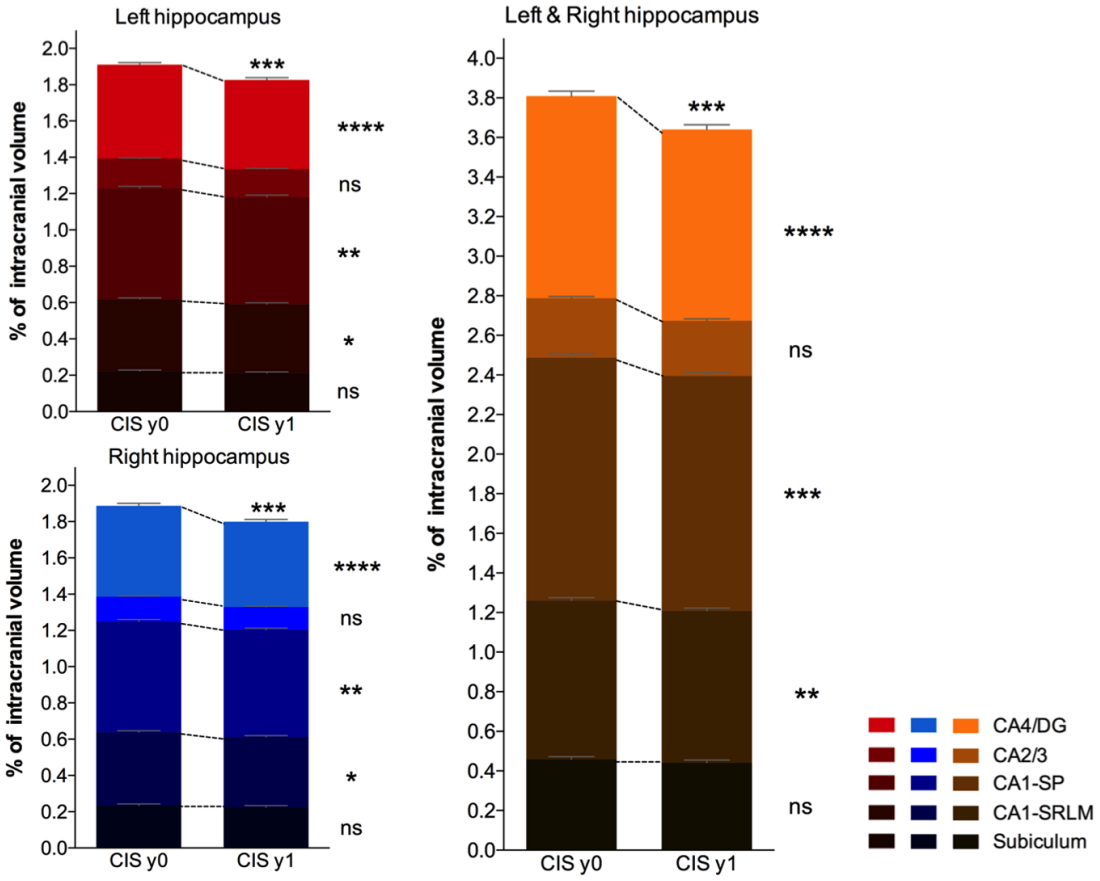

Figure 3: Comparison of the normalized volumes of hippocampal subfields between persons with clinically isolated syndrome (CIS) at baseline (y0) and 1-year follow-up (y1).

The histograms represent the cumulative volumes of all the left hippocampal subfields (in red), of all the right hippocampal subfields (in blue) and of all right&left hippocampal subfields (in orange). The colour gradient represents individual hippocampal subfields. ns = non-significant, *p<0.05, **p<0.01, ***p<0.001, ****p<0.0001 (corrected for multiple comparisons).

Table 2: Univariate correlations and hierarchical linear regression models between volumes of CA1 subfields or whole hippocampal volume at year 1 (dependent variables) and volume of CA4/dentate gyrus at baseline

1 year volume		Explanatory variables (at baseline)	Univariate analysis (*r*)	Multivriate analysis (ß)	Adjusted multivariate model (R^2)
CA1-SP	*Block 1*	Age	-0.16	ns	0.19*
		T2LL	-0.21	ns	
		NBV	0.44**	0.47*	
	Block 2	Age	-0.16	ns	0.44***#
		T2LL	-0.21	ns	
		NBV	0.44**	ns	
		CA4/DG	0.63***	0.40***	
CA1-SRLM	*Block 1*	Age	-0.06	ns	0.27**
		T2LL	-0.16	ns	
		NBV	0.48***	0.64***	
	Block 2	Age	-0.06	ns	0.47***#
		T2LL	-0.16	ns	
		NBV	0.48***	0.40*	
		CA4/DG	0.62***	0.47***	
Hippocampus	*Block 1*	Age	-0.16	ns	0.32**
		T2LL	-0.26	ns	
		NBV	0.56***	0.65***	
	Block 2	Age	-0.16	ns	0.61***#
		T2LL	-0.26	ns	
		NBV	0.56***	0.37*	
		CA4/DG	0.71***	0.58***	

Age, T2LL and NBV were entered into an initial model (block 1) as nuisance variables. CA1-SP = CA1-stratum pyramidale, CA1-SRLM = CA1-stratum radiatum-lacunosum-moleculare, CA4/DG = CA4/dentate gyrus, NBV = Normalized Brain Volume, T2LL = T2 Lesion-Load. ns = non-significant, *p<0.05, **p<0.01, ***p<0.001. # $AIC_{block2} < AIC_{block1}$.

Relationship between the atrophy of hippocampal subfields and clinical outcomes

In order to study the link between the early vulnerability of CA4/dentate gyrus and the pathophysiological process specific to MS, we first investigated whether CA4/dentate gyrus volume at baseline would be able to predict MS diagnosis at year 1. Using univariate analyses, we found that both T2-lesion load and CA4/dentate gyrus volume were significantly associated with conversion to MS (p=0.002 and p=0.014, respectively). A multiple logistic regression model showed that the volume of CA4/dentate gyrus at baseline was the only factor independently associated with conversion to MS (ß=0.57, p=0.025 and R^2=0.28, p=0.016) while age, gender, EDSS, T2-lesion load and NBV were not predictive.

Finally, we investigated whether early hippocampal regional vulnerability had a clinical impact on episodic memory performances. The results of univariate correlations and regression models between memory scores and demographic, clinical and imaging data at baseline and year 1 are presented in **Table 3**. According to multivariate analyses, no model was able to explain memory performance at baseline. The volume of CA1-SP and the educational level of patients were independent predictors of the episodic verbal memory composite score at year 1 (ß=0.87, p=0.042 and ß=0.51, p=0.031, respectively).

Table 3: Univariate correlations and hierarchical regression models between memory composite scores at baseline or after 1-year follow-up (dependent variables) and demographical, clinical and MRI features

		Explanatory variables	Univariate analysis (r)	Multivriate analysis (ß)	Adjusted multivariate model (R^2)
Baseline					
Episodic verbal memory	*Block 1*	Age	-0.04	ns	ns
		T2LL	-0.20	ns	
		NBV	0.12	ns	
		Education level	0.32*	0.38*	
	Block 2[§]	-	-	-	-
Episodic spatial memory	*Block 1*	Age	-0.18	ns	ns
		T2LL	-0.18	ns	
		NBV	0.17	ns	
		Education level	0.32*	ns	
	Block 2[§]	-	-	-	-
1 year					
Episodic verbal memory	*Block 1*	Age	-0.15	ns	ns
		T2LL	-0.14	ns	
		NBV	0.17	ns	
		Education level	0.24	ns	
	Block 2	Age	-0.15	ns	0.26*
		T2LL	-0.14	ns	
		NBV	0.17	ns	
		Education level	0.24	0.51*	
		CA1-SP	0.30*	0.87*	
		CA1-SRLM	0.24	ns	
Episodic spatial memory	*Block 1*	Age	-0.35*	ns	ns
		T2LL	-0.17	ns	
		NBV	-0.03	ns	
		Education level	0.14	ns	
	Block 2[§]	-	-	-	-

Age, T2LL, NBV and educational level were entered into an initial model (block 1) as nuisance variables. Covariables related to hippocampal subfields were added in a second model (block 2) according to univariate correlations (p-value <0.2) to predict memory scores. CA1-SP = CA1-stratum pyramidale, CA1-SRLM = CA1-stratum radiatum-lacunosum-moleculare, T2LL = T2 Lesion-Load. NBV = Normalized Brain Volume. ns = non-significant, *p<0.05. [§]: Block 2 was equivalent to Block 1 because no correlation (p<0.2) was found between the volume of any hippocampal subfields and the memory score.

Discussion

We demonstrated in this study that the CA4/dentate gyrus subfield of the hippocampus is the first subfield to be atrophied across the course of MS, at the stage of CIS. This pattern of regional hippocampal atrophy worsens during the first year of disease evolution and spreads within CA1 (both in the cell bodies layer CA1-SP and the neuritic layers CA1-SRLM). CA4/dentate gyrus volume at baseline was associated with the diagnosis of MS one year afterwards. Whereas isolated CA4/dentate gyrus atrophy at the stage of CIS failed to correlate with memory scores, it predicted the extension of the pathological process within CA1 one year later, which was in turn correlated with episodic verbal memory performances, independently of usual confounders.

Our main finding of a "natural history" of hippocampal subfield degeneration in MS, from dentate gyrus to CA1, is supported by anatomical and functional studies in both human and animal models of the disease. First, we previously reported that pattern separation performance - a cognitive task critically dependant on dentate gyrus function[29] - was decreased in patients with CIS and early MS, when conventional visuospatial episodic memory tests (BVMT-R) were not yet altered, suggesting an early and isolated dentate gyrus dysfunction during the course of the disease.[27] Such functional alterations suggested by the pattern separation task are therefore consolidated by the anatomical alterations observed in the present MRI study. Second, our findings are also supported by a previous work showing that dentate gyrus structure and function are selectively disrupted by microglial activation at the early stage of experimental autoimmune encephalomyelitis (EAE, the animal model of MS).[6] The independent association we found here between CA4/dentate gyrus volume at the stage of CIS and the diagnosis of MS one year after CIS also suggests this link between dentate gyrus damage and the early diffuse pathophysiological process specific to MS. Third, the vulnerability of the dentate gyrus, prior to other hippocampal subfields at the early stage of MS, could be explained by its particular anatomical location. Indeed, it is adjacent to cerebrospinal fluid (CSF) spaces (third ventricle in rodents and choroidal fissure in humans) where cytokines and immune cells preferentially penetrate the hippocampus, as suggested experimentally in EAE.[30] We postulate that the hierarchical vulnerability of hippocampal subfields in MS might be better explained by their anatomical contiguity rather than by a network-dependent disposition, as in Alzheimer's disease for instance.[31] A gradient of infiltrating immune cells and cytokines would diffuse progressively from the CSF to the dentate gyrus, then to CA1, and probably to the

whole medial temporal lobe. In this model, the progression of the disease from the dentate gyrus to CA1 might be slowed down by the presence of the vestigial intrahippocampal sulcus, potentially explaining the delay between dentate gyrus and CA1 atrophy reported in this study. Additional experiments will be needed to test these mechanistic hypotheses.

From the anatomopathological point of view, our study also highlights the striking vulnerability of the hippocampus to neurodegeneration in the context of neuroinflammation. Indeed, the annualized rate of atrophy during the first year of the disease's evolution ranged from -5.6% to -6.4%, respectively for CA1 and CA4/dentate gyrus, whereas it was 'only' -1.4% for the whole-brain parenchymal fraction in our population of PwCIS (which was in the upper range of what was usually observed in the literature on CIS and relapsing MS, *i.e.* from -0.5% to -1.35%).[32,33] This selective and disproportionate hippocampal volume loss, in excess to global brain atrophy, has already been observed in a seminal cross-sectional study on patients with relapsing and progressive MS.[1] The annualized rate of hippocampal atrophy we report here (-5.9%) is even in the upper range of what has been reported for patients with Alzheimer's disease or mild cognitive impairment (-3.5% to -6%/year)[34-36] and far beyond what has been reported for physiological aging (-0.8% to -2.3%/year).[37]

Besides these anatomical considerations, we also questioned the link between the early regional vulnerability of the hippocampus and memory impairment in MS. On the one hand, the CA4/dentate gyrus atrophy observed at baseline was not correlated with episodic memory performance in our cohort. Although we have to take into account that the memory abilities of the PwCIS included in this study were not severely affected (regarding the median z-score and the percentage of impaired patients), we postulate that CA4/dentate gyrus atrophy at the stage of CIS is "not enough" to explain the memory decline observed in "global" episodic memory tests such as the SRT or the BVMT-R. Perhaps more specific tests such as the behavioural pattern separation task[38] would have allowed us to pinpoint such a subtle memory decline related to CA4/dentate gyrus damage[27] and future studies should address this point. On the other hand, we found that CA1 atrophy explained part of the "global" episodic verbal memory decline one year after inclusion, when diagnosis of MS was finally observed in 65.2% of the patients. This suggests that CA1 atrophy is the best anatomical correlate of memory performance in MS, as previously described in cross-sectional studies including patients with relapsing and progressive MS.[1,10]

A recent cross-sectional study found an "expansion" of the dentate gyrus during MS.[11] The divergences between our findings and this previous work may be attributed to various points. Indeed, contrary to our work, this study investigated patients at a later stage of the disease, with relapsing and progressive MS, and it used a surface-based mesh modelling technique to study the shape of the hippocampus.[39] Using this technique, the authors found an outward displacement of the supero-medial hippocampal surface and concluded on a larger radial distance of the dentate gyrus in patients with MS. However, it should be borne in mind that when using such a method, measuring external surface modifications does not enable the direct characterization of the inner alterations of a particular subfield. It is not clear how the atrophy of the deepest regions of the hippocampus (such as the dentate gyrus, which is curled inside the Cornu Ammonis) would impact the outer surface of the structure. For instance, the expansion of CSF pockets due to atrophy within the hippocampal fissure/sulcus might result in tissue "expansion" on the supero-medial side of the hippocampus despite there being no real dentate gyrus "hypertrophy". We also hypothesized that a shift of rotation of the hippocampus due to atrophy would induce an outward displacement of part of the surface, introducing contradictory results. Thus, radial mapping provides valuable information on hippocampal surface change (*i.e.* CA1 and the subiculum) but should be interpreted with caution for inner structures such as the dentate gyrus.[40] The limits of these surface-based modelling strategies to assess hippocampal subfield anatomy have been discussed extensively in the field of Alzheimer's disease and aging,[15,41] even by the authors who pioneered the method.[39,42] Therefore, proper volumetric analyses with manual or automatic segmentation are now considered more relevant than radial mapping to investigate hippocampal regional vulnerability, although they have their own limitations and require protocol harmonization to clearly define subfield boundaries.[43] For instance, we acknowledge that the Winterburn protocol we used here mainly delineates CA2/3 in its dorsal portion to increase segmentation reliability, although it can lead to volume underestimations. Therefore, our results might have differed by using other definitions of the hippocampal subfields boundaries.

The main limitation of our study is the lack of MRI follow-up for our healthy control group to clearly disentangle the contribution of time-dependant *versus* disease-dependant processes in our longitudinal measures of atrophy in the CIS group. However, our results on the dynamics of progressive hippocampal subfield atrophy are likely related to the disease process because they are specific (*i.e.* CA4/dentate gyrus and CA1 but not CA2/3 and the subiculum) and because the

annualized rate of hippocampal atrophy measured (-5.9%/year) is clearly above what can be observed on average in the healthy population (-0.4%/year in people less than 55 years old).[44] Another limitation is the short follow-up period (1-year), which was nonetheless long enough to capture the sequential progression of hippocampal subfield atrophy. We also acknowledge that we did not assess the potential microstructural damage that underlies or precedes hippocampal regional atrophy, with sequences such as diffusion-tensor imaging or magnetization transfer MRI, but these technics are difficult to implement at the spatial resolution required to study hippocampal subfields. The final limitation was that, although no area of T2-hypersignal or T1-black hole was clearly detected within the hippocampus on our conventional sequences, we did not assess potential subtle demyelinating hippocampal lesions with specific double inversion recovery sequences.

Conclusion

We demonstrated that CA4/dentate gyrus is the first subfield of the hippocampus to be atrophied during the course of MS, from the stage of CIS. This regional pattern of hippocampal atrophy rapidly spread to CA1. This dynamic vulnerability is associated with future diagnosis of MS and contributes to hippocampal-dependant memory performances.

Study funding

This study was funded by the ARSEP Foundation, Bordeaux University Hospital and TEVA laboratories. The work was further supported by public grants from the French Agence Nationale de la Recherche within the context of the Investments for the Future program referenced ANR-10-LABX-57, named TRAIL (project IBIO-NI, GM-COG and HR-DTI), ANR-10-LABX-43, named BRAIN (Project MEMO-MS), ANR-10-IDEX-03-02, named IdEx Bordeaux – CPU, ANR-10-COHO-002, named French Observatoire for multiple sclerosis (OFSEP) and the CNRS multidisciplinary project "Défi ImagIn" HL-MRI. This research was also funded by Spanish UPV2016-0099 and TIN2013-43457-R grants from UPV and the Ministerio de Economia y competitividad. The sponsors did not participate in any aspect of the design or performance of the study, including data collection, management, analysis, and the interpretation or preparation, review, and approval of the manuscript.

Disclosures

VP received a research grant from the ARSEP Foundation to conduct this study; he received travel expenses and/or consulting fees from Biogen, Teva-Lundbeck and Merk-Serono unrelated to the submitted work. BB serves on scientific advisory boards on behalf of his institution and has received honoraria or research support from Biogen-Idec, Merck-Serono, Novartis, Genzyme, Teva, Roche, Medday and Bayer unrelated to the submitted work. AR received research grants and/or consulting fees from Novartis, Biogen, Merck-Serono, Bayer Healthcare, Roche, Teva, and Genzyme unrelated to the submitted work.

Acknowledgments

The authors thank Julie Charré-Morin and Aurore Saubusse (Bordeaux University Hospital) for neuropsychological testing and the ARSEP Foundation for its support.

References

1. Sicotte NL, Kern KC, Giesser BS, Arshanapalli A, Schultz A, Montag M, Wang H, Bookheimer SY (2008): Regional hippocampal atrophy in multiple sclerosis. Brain 131:1134–1141.
2. Dutta R, Chang A, Doud MK, Kidd GJ, Ribaudo MV, Young EA, Fox RJ, Staugaitis SM, Trapp BD (2011): Demyelination causes synaptic alterations in hippocampi from multiple sclerosis patients. Ann Neurol 69:445–454.
3. Hulst HE, Schoonheim MM, Van Geest Q, Uitdehaag BMJ, Barkhof F, Geurts JJG (2015): Memory impairment in multiple sclerosis: Relevance of hippocampal activation and hippocampal connectivity. Mult Scler 21:1705–1712.
4. Planche V, Ruet A, Coupé P, Lamargue-Hamel D, Deloire M, Pereira B, Manjon JV, Munsch F, Moscufo N, Meier DS, Guttmann CR, Dousset V, Brochet B, Tourdias T (2017a): Hippocampal microstructural damage correlates with memory impairment in clinically isolated syndrome suggestive of multiple sclerosis. Mult Scler 23:1214–1224.
5. Papadopoulos D, Dukes S, Patel R, Nicholas R, Vora A, Reynolds R (2009): Substantial archaeocortical atrophy and neuronal loss in multiple sclerosis. Brain Pathol 19:238–253.
6. Planche V, Panatier A, Hiba B, Ducourneau E-G, Raffard G, Dubourdieu N, Maitre M, Lesté-Lasserre T, Brochet B, Dousset V, Desmedt A, Oliet SH, Tourdias T (2017b): Selective dentate gyrus disruption causes memory impairment at the early stage of experimental multiple sclerosis. Brain Behav Immun 60:240–254.
7. Small SA (2014): Isolating pathogenic mechanisms embedded within the hippocampal circuit through regional vulnerability. Neuron 84:32–39.
8. West MJ, Coleman PD, Flood DG, Troncoso JC (1994): Differences in the pattern of hippocampal neuronal loss in normal ageing and Alzheimer's disease. Lancet 344:769–772.
9. Gold SM, Kern KC, O'Connor M-F, Montag MJ, Kim A, Yoo YS, Giesser BS, Sicotte NL (2010): Smaller cornu ammonis 2-3/dentate gyrus volumes and elevated cortisol in multiple sclerosis patients with depressive symptoms. Biol Psychiatry 68:553–559.
10. Longoni G, Rocca MA, Pagani E, Riccitelli GC, Colombo B, Rodegher M, Falini A, Comi G, Filippi M (2015): Deficits in memory and visuospatial learning correlate with regional hippocampal atrophy in MS. Brain Struct Funct 220:435–444.
11. Rocca MA, Longoni G, Pagani E, Boffa G, Colombo B, Rodegher M, Martino G, Falini A, Comi G, Filippi M (2015): In vivo evidence of hippocampal dentate gyrus expansion in multiple sclerosis. Hum Brain Mapp 36:4702–4713.
12. Polman CH, Reingold SC, Banwell B, Clanet M, Cohen JA, Filippi M, Fujihara K, Havrdova E, Hutchinson M, Kappos L, Lublin FD, Montalban X, O'Connor P, Sandberg-Wollheim M, Thompson AJ, Waubant E, Weinshenker B, Wolinsky JS (2011): Diagnostic criteria for multiple sclerosis: 2010 revisions to the McDonald criteria. Ann Neurol 69:292–302.
13. Miller DH, Chard DT, Ciccarelli O (2012): Clinically isolated syndromes. Lancet Neurol 11:157–169.
14. Maruszak A, Thuret S (2014): Why looking at the whole hippocampus is not enough-a critical role for anteroposterior axis, subfield and activation analyses to enhance predictive value of hippocampal changes for Alzheimer's disease diagnosis. Front Cell Neurosci 8:95.

15. de Flores R, La Joie R, Chételat G (2015): Structural imaging of hippocampal subfields in healthy aging and Alzheimer's disease. Neuroscience 309:29–50.
16. Schmidt P, Gaser C, Arsic M, Buck D, Förschler A, Berthele A, Hoshi M, Ilg R, Schmid VJ, Zimmer C, Hemmer B, Mühlau M (2012): An automated tool for detection of FLAIR-hyperintense white-matter lesions in Multiple Sclerosis. NeuroImage 59:3774–3783.
17. Manjón JV, Coupé P (2016): volBrain: An Online MRI Brain Volumetry System. Front Neuroinformatics 10:30.
18. Manjón JV, Coupé P, Martí-Bonmatí L, Collins DL, Robles M (2010): Adaptive non-local means denoising of MR images with spatially varying noise levels. J Magn Reson Imaging JMRI 31:192–203.
19. Avants BB, Tustison NJ, Song G, Cook PA, Klein A, Gee JC (2011): A reproducible evaluation of ANTs similarity metric performance in brain image registration. NeuroImage 54:2033–2044.
20. Tustison NJ, Avants BB, Cook PA, Zheng Y, Egan A, Yushkevich PA, Gee JC (2010): N4ITK: improved N3 bias correction. IEEE Trans Med Imaging 29:1310–1320.
21. Nyúl LG, Udupa JK (1999): On standardizing the MR image intensity scale. Magn Reson Med 42:1072–1081.
22. Romero JE, Coupe P, Manjón JV (2016): High Resolution Hippocampus Subfield Segmentation Using Multispectral Multiatlas Patch-Based Label Fusion. In: Patch-Based Techniques in Medical Imaging. Springer, Cham. Lecture Notes in Computer Science pp 117–124.
23. Romero JE, Coupé P, Manjón JV (2017): HIPS: A new hippocampus subfield segmentation method. NeuroImage 163:286–295.
24. Winterburn JL, Pruessner JC, Chavez S, Schira MM, Lobaugh NJ, Voineskos AN, Chakravarty MM (2013): A novel in vivo atlas of human hippocampal subfields using high-resolution 3 T magnetic resonance imaging. NeuroImage 74:254–265.
25. Yushkevich PA, Amaral RSC, Augustinack JC, Bender AR, Bernstein JD, Boccardi M, Bocchetta M, Burggren AC, Carr VA, Chakravarty MM, Chételat G, Daugherty AM, Davachi L, Ding S-L, Ekstrom A, Geerlings MI, Hassan A, Huang Y, Iglesias JE, La Joie R, Kerchner GA, LaRocque KF, Libby LA, Malykhin N, Mueller SG, Olsen RK, Palombo DJ, Parekh MB, Pluta JB, Preston AR, Pruessner JC, Ranganath C, Raz N, Schlichting ML, Schoemaker D, Singh S, Stark CEL, Suthana N, Tompary A, Turowski MM, Van Leemput K, Wagner AD, Wang L, Winterburn JL, Wisse LEM, Yassa MA, Zeineh MM, Hippocampal Subfields Group (HSG) (2015): Quantitative comparison of 21 protocols for labeling hippocampal subfields and parahippocampal subregions in in vivo MRI: towards a harmonized segmentation protocol. NeuroImage 111:526–541.
26. Coupé P, Manjón JV, Chamberland M, Descoteaux M, Hiba B (2013): Collaborative patch-based super-resolution for diffusion-weighted images. NeuroImage 83:245–261.
27. Planche V, Ruet A, Charré-Morin J, Deloire M, Brochet B, Tourdias T (2017c): Pattern separation performance is decreased in patients with early multiple sclerosis. Brain Behav 7(8):e00739.
28. Manjón JV, Eskildsen SF, Coupé P, Romero JE, Collins DL, Robles M (2014): Nonlocal intracranial cavity extraction. Int J Biomed Imaging 2014:820205.
29. Bakker A, Kirwan CB, Miller M, Stark CEL (2008): Pattern separation in the human hippocampal CA3 and dentate gyrus. Science 319:1640–1642.

30. Habbas S, Santello M, Becker D, Stubbe H, Zappia G, Liaudet N, Klaus FR, Kollias G, Fontana A, Pryce CR, Suter T, Volterra A (2015): Neuroinflammatory TNFα Impairs Memory via Astrocyte Signaling. Cell 163:1730–1741.
31. Kerchner GA, Bernstein JD, Fenesy MC, Deutsch GK, Saranathan M, Zeineh MM, Rutt BK (2013): Shared vulnerability of two synaptically-connected medial temporal lobe areas to age and cognitive decline: a seven tesla magnetic resonance imaging study. J Neurosci 33:16666–16672.
32. Pérez-Miralles F, Sastre-Garriga J, Tintoré M, Arrambide G, Nos C, Perkal H, Río J, Edo MC, Horga A, Castilló J, Auger C, Huerga E, Rovira A, Montalban X (2013): Clinical impact of early brain atrophy in clinically isolated syndromes. Mult Scler 19:1878–1886.
33. De Stefano N, Airas L, Grigoriadis N, Mattle HP, O'Riordan J, Oreja-Guevara C, Sellebjerg F, Stankoff B, Walczak A, Wiendl H, Kieseier BC (2014): Clinical relevance of brain volume measures in multiple sclerosis. CNS Drugs 28:147–156.
34. Jack CR, Petersen RC, Xu Y, O'Brien PC, Smith GE, Ivnik RJ, Boeve BF, Tangalos EG, Kokmen E (2000): Rates of hippocampal atrophy correlate with change in clinical status in aging and AD. Neurology 55:484–489.
35. Wang L, Swank JS, Glick IE, Gado MH, Miller MI, Morris JC, Csernansky JG (2003): Changes in hippocampal volume and shape across time distinguish dementia of the Alzheimer type from healthy aging. NeuroImage 20:667–682.
36. Du AT, Schuff N, Kramer JH, Ganzer S, Zhu XP, Jagust WJ, Miller BL, Reed BR, Mungas D, Yaffe K, Chui HC, Weiner MW (2004): Higher atrophy rate of entorhinal cortex than hippocampus in AD. Neurology 62:422–427.
37. Jack CR, Barkhof F, Bernstein MA, Cantillon M, Cole PE, Decarli C, Dubois B, Duchesne S, Fox NC, Frisoni GB, Hampel H, Hill DLG, Johnson K, Mangin J-F, Scheltens P, Schwarz AJ, Sperling R, Suhy J, Thompson PM, Weiner M, Foster NL (2011): Steps to standardization and validation of hippocampal volumetry as a biomarker in clinical trials and diagnostic criterion for Alzheimer's disease. Alzheimers Dement 7:474–485.e4.
38. Stark SM, Yassa MA, Lacy JW, Stark CEL (2013): A task to assess behavioral pattern separation (BPS) in humans: Data from healthy aging and mild cognitive impairment. Neuropsychologia 51:2442–2449.
39. Thompson PM, Hayashi KM, De Zubicaray GI, Janke AL, Rose SE, Semple J, Hong MS, Herman DH, Gravano D, Doddrell DM, Toga AW (2004): Mapping hippocampal and ventricular change in Alzheimer disease. NeuroImage 22:1754–1766.
40. La Joie R, Fouquet M, Mézenge F, Landeau B, Villain N, Mevel K, Pélerin A, Eustache F, Desgranges B, Chételat G (2010): Differential effect of age on hippocampal subfields assessed using a new high-resolution 3T MR sequence. NeuroImage 53:506–514.
41. Morra JH, Tu Z, Apostolova LG, Green AE, Avedissian C, Madsen SK, Parikshak N, Hua X, Toga AW, Jack CR, Schuff N, Weiner MW, Thompson PM, Alzheimer's Disease Neuroimaging Initiative (2009): Automated 3D mapping of hippocampal atrophy and its clinical correlates in 400 subjects with Alzheimer's disease, mild cognitive impairment, and elderly controls. Hum Brain Mapp 30:2766–2788.
42. Frisoni GB, Ganzola R, Canu E, Rüb U, Pizzini FB, Alessandrini F, Zoccatelli G, Beltramello A, Caltagirone C, Thompson PM (2008): Mapping local hippocampal changes in Alzheimer's disease and normal ageing with MRI at 3 Tesla. Brain 131:3266–3276.
43. Wisse LEM, Daugherty AM, Olsen RK, Berron D, Carr VA, Stark CEL, Amaral RSC, Amunts K, Augustinack JC, Bender AR, Bernstein JD, Boccardi M, Bocchetta M,

Burggren A, Chakravarty MM, Chupin M, Ekstrom A, de Flores R, Insausti R, Kanel P, Kedo O, Kennedy KM, Kerchner GA, LaRocque KF, Liu X, Maass A, Malykhin N, Mueller SG, Ofen N, Palombo DJ, Parekh MB, Pluta JB, Pruessner JC, Raz N, Rodrigue KM, Schoemaker D, Shafer AT, Steve TA, Suthana N, Wang L, Winterburn JL, Yassa MA, Yushkevich PA, la Joie R, Hippocampal Subfields Group (2017): A harmonized segmentation protocol for hippocampal and parahippocampal subregions: Why do we need one and what are the key goals? Hippocampus 27:3–11.

44. Fraser MA, Shaw ME, Cherbuin N (2015): A systematic review and meta-analysis of longitudinal hippocampal atrophy in healthy human ageing. NeuroImage 112:364–374.

Supplementary material

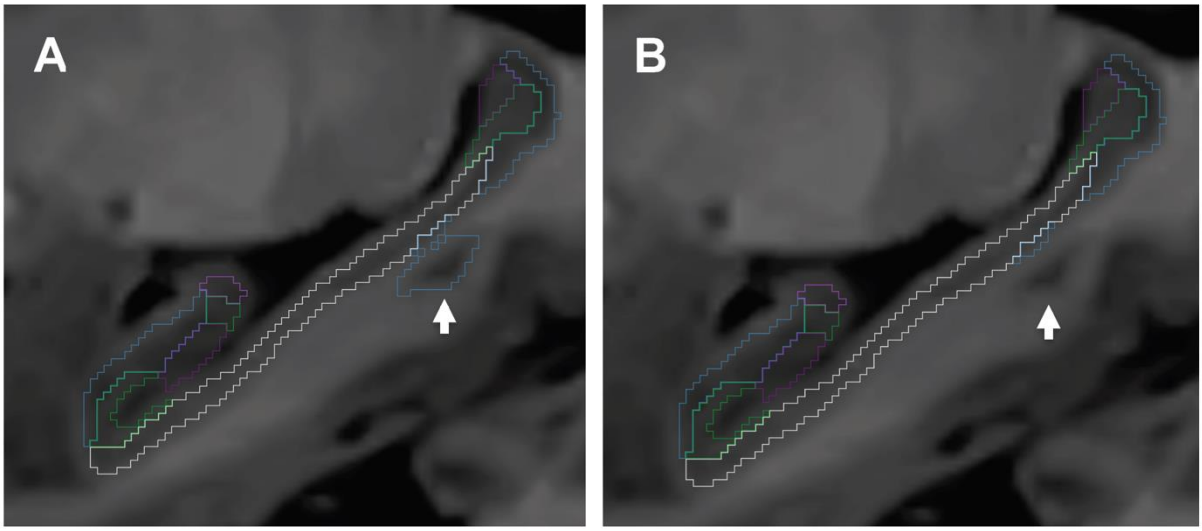

Supplementary figure 1: *Example of manual correction of the automated segmentation (A: automated segmentation; B: edited segmentation). The error was due to a MS parahippocampal "black hole" that was mistaken for a part of the CA1-SP (in blue).*